What is below the water masses?

Multibeam studies of Öskjuvatn, Thingvallavatn and Kleifarvatn

Árni Friðriksson

Faculty of Earth Sciences

University of Iceland

2014

What is below the water masses?

Multibeam studies of Öskjuvatn, Thingvallavatn and Kleifarvatn, Iceland

Árni Friðriksson

60 ECTS thesis submitted in partial fulfilment of a
Magister Scientiarum degree in Geology

Supervisor
Ármann Höskuldsson

MS-Committee
Ingibjörg Jónsdóttir
Magnús Tumi Guðmundsson

Examiner
Guðrún Helgadóttir

Faculty of Earth Sciences
School of Engineering and Natural Sciences
University of Iceland
Reykjavik, May 2014

What is below the water masses? – Multibeam studies of Öskjuvatn, Thingvallavatn and Kleifarvatn
What is below the water masses? Multibeam studies
60 ECTS thesis submitted in partial fulfilment of a *Magister Scientiarum* degree in geology

Faculty of Earth Sciences
School of Engineering and Natural Sciences
University of Iceland
Sturlugata 7
101, Reykjavik
Iceland

Telephone: 525 4000

Bibliographic information:
Árni Friðriksson, 2014, What is below the water masses? – Multibeam studies of Öskjuvatn, Thingvallavatn and Kleifarvatn, Master's thesis, Faculty of Earth Sciences, University of Iceland, pp. 76.

Printing: Háskólaprent
Reykjavik, Iceland, May 2014

Abstract

Multibeam echo sounding systems are used worldwide to survey ocean floors, ship canals and lake floors. They transmit pulses of acoustic waves at various frequencies into the water and listen to the returning echoes. Most systems record both bathymetry and the strength of the returning echoes (backscatter intensity). Three Icelandic lakes, Öskjuvatn, Kleifarvatn and Thingvallavatn, are all situated in volcanological environment. Their surroundings have been studied extensively but lack of high-resolution bathymetric data has limited the possibility of studying the lake floors. In June and September 2012 and November 2013 Kleifarvatn, Öskjuvatn and the SW-part of Thingvallavatn respectively, were surveyed with a Simrad EM3002 high-resolution multibeam echo sounder from Kongsberg Maritime. The results of these surveys are three bathymetric maps with 2 m horizontal resolution and 10 m contours, three backscatter intensity maps with 2 m horizontal resolution and three generalized geologic maps of the surveyed areas. Three craters, or cones, five lava flows, six solfataras and massive landslides were observed underwater in the Öskjuvatn caldera. Numerous faults, volcanic deposits and lava flow fronts were observed in SW-Thingvallavatn. However, no geothermal activity was recorded in the survey area. Four volcanic ridges, six solfataras and numerous faults, all of which aligned in a similar manner to regional topography, were observed on the lake floor of Kleifarvatn.

Útdráttur

Fjölgeisla bergmálsdýptarmælar eru notaðir út um allan heim til mælinga á höfum, í skipaskurðum og á stöðuvötnum. Þeir senda hljóðbylgjur niður í vatnið og hlusta svo eftir endurköstum frá botninum eða hlutum í vatninu. Flestir fjölgeisla bergmálsdýptarmælar safna og vista bæði dýptarmælingar og styrk endurkastanna frá hljóðbylgjunum. Rannsóknarsvæðin voru þrjú vötn í eldvirku umhverfi, Öskjuvatn, Kleifarvatn og suðvesturhluti Þingvallavatns. Mælingar fóru fram á Kleifarvatni í júní 2012, Öskjuvatni í september 2012 og Þingvallavatni í nóvember 2013. Simrad EM3002 fjölgeisla bergmálsdýptarmælir frá Kongsberg Maritime var notaður við mælingarnar. Niðurstöður mælinganna eru þrjú dýptarkort með tveggja metra nákvæmni ásamt 10 metra dýptarlínum, þrjú kort sem sýna endurkaststyrk hljóðbylgnanna með tveggja metra nákvæmni og þrjú jarðfræðikort af vötnunum. Þrjár eldkeilur og gígar, fimm hraun, sex jarðhitasvæði og nokkur jarðföll eru meðal þeirra fyrirbæra sem kortlögð voru á botni Öskjuvatns. Á botni Þingvallavatns sást meðal annars fjöldi jarðskjálftasprungna, hraunjaðar Þingvallahrauns og merki um eldvirkni á síðjökultíma. Í Kleifarvatni fundust einnig merki um eldvirkni, svipuð og í Þingvallavatni, sex jarðhitasvæði og nokkrar jarðskjálftasprungur, en flest hefur þetta stefnu svipaða og sprungur og hryggir í nágrenninu.

Table of Contents

List of Figures

List of Tables

Acknowledgements

I would like to thank my wife Heiðrún for her constant support and encouragement during the time of this research and for always being there for me. I also want to thank my supervisor, Ármann Höskuldsson, for all his help on this project, for believing in me for the whole time and giving me the opportunity to work on this project. Also thanks to Ármann for teaching me how to use all the necessary software and equipment during the data processing. Special thanks to Þorsteinn Jónsson, mechanic in Askja, for countless hours surveying Öskjuvatn, Thingvallavatn and Kleifarvatn and being a good mate. Thanks to Ragnar Þórhallsson, instrumentation engineer at Landsvirkjun, for all his help with the surveying equipment and always being ready to assist with anything. Thanks to Vatnajökull National Park for letting us survey Öskjuvatn, one of the most spectacular places in Iceland. Also thanks to Thingvellir National Park, and specially Einar Sæmundsen, director of education at Thingvellir National Park, for his assistance and help during the surveying of Thingvallavatn. Many thanks to the people of the Meteorological office in Iceland for letting me use old bathymetric data from Öskjuvatn, Thingvallavatn and Kleifarvatn. Thanks to Karolina Banul for her help on backscatter images and valuable discussion throughout this process.

Financial support is crucial for a project like this one. Many thanks to Landsvirkjun Research Fund (Orkurannsóknasjóður Landsvirkjunar), Friends of Vatnajökull (Vinir Vatnajökuls), University of Iceland and Thingvellir National Park.

Special thanks to the Icelandic Coast Guard for making it possible to survey Öskjuvatn.

Last but not least, thanks to my colleagues for showing interest in my work and providing vital assessment in the form of coffee and chatting.

1 Introduction

The main goal of this work was to acquire bathymetric and backscatter intensity data from Lake Öskjuvatn, Lake Thingvallavatn and Lake Kleifarvatn in Iceland. The data was used to make bathymetric maps, backscatter intensity maps and geologic maps of the three lakes. These maps were all produced using the ArcGIS software but the processing of the data was done using Hips & Sips 8.1 from CARIS. All these maps can be used as a basic guide to the formation of the three lakes.

Unsurprisingly, all three lakes were formed by different forces based around their geologic environment. Öskjuvatn is situated in the Northern Volcanic Zone (NVZ), surrounded by a central volcano, indicating a mostly volcanic origin. Thingvallavatn is located in the Western Rift Zone (WRZ), just north of the Hengill central volcano, immediately south of Thingvellir and occupying the Thingvellir graben, which indicates a primarily tectonic origin. Kleifarvatn is located on the Reykjanes Peninsula just north of the Krýsuvík geothermal fields, surrounded by lavas, hyaloclastite ridges and Table Mountains. It is elongated NNE-SSW indicating both tectonic and volcanic origin. The geologic maps of Öskjuvatn, Thingvallavatn and Kleifarvatn provided valuable information about the structure and types of bottom material in the lakes, which could be used to determine if the predictions above were correct.

The following two chapters give a review of the physics of sound in water and multibeam theory and application, and background information about Crater Lake, Öskjuvatn, Thingvallavatn and Kleifarvatn. Crater Lake was used as a case study for a lake formed in a caldera-collapse event, similar to Öskjuvatn. Chapter four illustrates the data gathering processes and the methods used to process the data. The bathymetric maps, backscatter intensity maps and geologic maps of the three lakes are presented in chapter five with explanations of the features on the maps. Then, chapter six will give a general discussion about the geologic maps and the forces responsible for their formation. Chapter seven summarises the conclusions of the work.

Terminology: Sigurður Þórarinsson used the name “Askja” as a term for caldera (askja) in Icelandic (Sæmundsson, 1982). Here “Askja” refers to the Askja central volcano whereas “Askja caldera” refers to the early Holocene caldera inside the Askja central volcano. “Lake Öskjuvatn” refers to the amount of water that partly fills the 1875 caldera formed in the southeast corner of the Askja caldera and “Öskjuvatn caldera” refers to the

total volume of caldera collapse. “Öskjuvatn” always refers to the lake, not the caldera. Similarly “Thingvallavatn” refers to “Lake Thingvallavatn” and “Kleifarvatn” refers to “Lake Kleifarvatn”.

The island in Öskjuvatn has several names such as Askur and Hornfirðingahólmi, but here it will be referred to as “Askur”.

2 Theory of multibeam echo sounder

This chapter gives a general introduction to echo sounders, or sonars, both single- and multibeam, and the physics behind this technology. Backscatter intensity will also be introduced and explained. Note: Multibeam echo sounder will be referred to as MBES and singlebeam echo sounder as SBES.

2.1 Physics of sound in water

When an acoustic pulse of energy is released into a water column it propagates through the water at the velocity of sound in water. The sound velocity can be described by the following equation:

$$Speed\ of\ sound = Frequency * Wavelength$$

The wavelength is the physical distance between travelling pressure fronts in a wave and is measured in meters. Frequency is the count of pressure fronts generated per second, measured in Hertz (1/s). The velocity can vary between water bodies and even between areas in the same body of water. Not only does the velocity of sound in water vary horizontally but also vertically. Sound travels at about 1497 m/s in freshwater at 25°C and the main factors influencing the velocity are: Conductivity (salinity), Temperature and Depth (pressure). The changes due to these factors are listed in Table 1. Many things can influence these factors such as evaporation and precipitation (salinity), solar heating and rain/run off (temperature) along with some others (Brennan, 2009).

Table 1. Factors that influence changes of sound velocity in water (Brennan, 2009).

Factor	*Change in velocity*
+1°C change in Temperature	+4.0 m/s
+1 ppt change in Salinity	+1.4 m/s
+100 m change in Depth	+1.7 m/s

Ping refers to the transmission of an acoustic through a body of water. Factors which influence the speed of sound in water (listed above) operate on the pulse as it travels to the bottom and also on its return to the receiver. Other factors influence the acoustic energy in the water, these are called *transmission losses*. These transmission losses can be separated into a few categories, *spreading loss, absorption, and reverberation and scattering* (Brennan, 2009).

2.1.1 Spreading loss

Spreading loss does not mean loss of energy but rather states the fact that the acoustic energy is constantly spread over a larger surface as the wave propagates through the medium. The energy density is thus reduced although the reduction is not frequency dependent. Spreading loss is described in decibels (dB). *Spherical spreading loss* (acoustic energy spreads out evenly in all directions from the source) is the case if there are no boundaries to the medium in which the acoustic energy travels. The transmission loss (described in dB) is given as: $\boldsymbol{TL = 20 * \log R}$, where R is the range. *Cylindrical spreading loss* is more realistic as the acoustic energy hits upper and lower boundaries, much like the water surface and bottom, and is trapped between them. The transmission loss (described in dB) is given as: $\boldsymbol{TL = 10 * \log R}$, where R is the range. Acoustic energy decreases at much slower rate due to cylindrical spreading loss than spherical spreading loss (Brennan, 2009).

2.1.2 Absorption

Conversion of acoustic energy into heat as it strikes molecules in the water column can be referred to as *absorption*. It is frequency dependent, i.e. higher frequency means more of the energy is absorbed by the water column. This happens because as the operating frequency gets higher, the vibration of the particles in the water increases which leads to greater transference of acoustic energy. All this leads to more attenuation of acoustic waves. This is why lower operating frequencies are used to obtain data at deeper levels. Absorption is considerably greater in seawater because of higher number of molecules (salinity of ~35 ppt) than in freshwater (salinity of <0.5 ppt). Temperature can influence absorption of acoustic waves. Increasing temperature in sea water results in greater absorption, however the opposite is true of freshwater (Brennan, 2009; Instruments, 2000).

2.1.3 Reverberation and scattering

Everything in the water column from suspended dust to large fish will scatter, that is redirect, acoustic energy. Scattering from many individual objects together is referred to as reverberation and decreases the acoustic energy and increases transmission losses. Reverberation is divided into three categories: water surface reverberation, bottom reverberation and volume reverberation (Brennan, 2009).

Both the water surface and bottom reflect and scatter sound waves. Reflections from the water's surface can lead to second and even in some cases tertiary bottom returns. Volume of air bubbles in the surface layer is directly related to wind speed, these air bubbles scatter sound waves and produce errors in depth measurements. The strength of the scattering of sound waves from the bottom depends on the bottom type (roughness, hardness and composition), angle of incidence of the acoustic wave and the operating frequency of the echo sounder. Soft bottom reflects weaker signal than hard bottom, meaning that soft bottom absorbs more energy than hard bottom. The bottom absorption is also dependent on the operating frequency, acoustic pulses at higher frequencies are more easily absorbed by the bottom than lower frequencies (Brennan, 2009). This kind of scattering is also referred to as "noise" in the echo sounder data. If this noise becomes too high, the echo sounder operator can increase the transmit power or pulse length to accommodate for the losses (Brennan, 2009).

2.2 Principles of an echo sounder

Echo sounder, also termed sonar, is an instrument which uses sound waves to remotely detect and locate objects in water. It is also used to detect the ocean floor and lake floors and give information about their composition. Echo sounders can be either *passive* or *active*, depending on their nature of operation. *Passive* echo sounders "listen" for sound waves coming from other objects in the water, such as seismic waves, ships, submarines and marine creatures. *Active* echo sounders produce pulses of sound waves, or *pings*, of specific frequencies and listen for the echoes of these sound waves returned from objects in the water (Instruments, 2000). From this point all echo sounders mentioned are considered active.

A ping generated by an echo sounder must travel to the lake/ocean bottom and then its echoes travel back to the surface. The time between the transmission and the return of the echoes is the *travel time* of the sound waves. This time, along with the sound speed in water, is used to calculate the *range* to the bottom using the following equation:

$$Range = \frac{1}{2} * velocity * echo\ time \qquad \text{Equation (1)}$$

In a bathymetric echo sounder a ping is generated via *projector*. The projector repeatedly produces acoustic pulses with precise characteristics such as frequency and power. The projector is generally constructed of piezo-electric ceramic which changes in size momentarily when voltage is applied to it. A projector uses particular voltages for transmitting sound waves with specific frequencies into the water. The transmitted acoustic pulses encounter several processes which affect the amount of echoes returning back to the surface (Instruments, 2000). These processes, spreading loss, absorption, and reverberation and scattering (Brennan, 2009), were listed in chapters 2.1.1 through 2.1.3. Another part, *hydrophone*, listens for the returning echoes and converts the oscillating energy into voltage. The hydrophone only listens to echoes with roughly the same characteristics as the acoustic pulses transmitted by the projector. Projectors and hydrophones are often the same piece of hardware because of the similarities of their functions. In such cases the term *transducer* is used when referring to a hydrophone, projector or both (Instruments, 2000).

The *Control and Display system* controls the ping cycle, i.e. when the transducer transmits a ping, the frequency and power of the ping etc. When an echo of a ping returns to the transducer it sends all electrical signals to the *Receiver system* which records the time of arrival and computes the dept. The *Control and Display system* records the depth and then triggers the next ping (Instruments, 2000).

To keep track of all factors influencing the sound waves and their echoes in water, the *Sonar Equation* (Equation 2) is used:

$$SE = SL - 2TL + BS - NL + TA \qquad \text{Equation (2)}$$

where SE is the *Signal Excess*, the strength of the measured echo, SL is *transmitted Source Level*, the original amount of acoustic energy transmitted into the water, TL is *transmission loss*, explained in chapter 2.1, BS is *Backscatter Strength*, the strength/intensity of the backscatter from the bottom, NL is *Noise Level*, amount of other sounds in the water

column, and TA is the *Target Area*. All quantities, except for *Target Area*, are described in decibels (dB) (Instruments, 2000). Figure 1 explains the Sonar Equation as it works in the water.

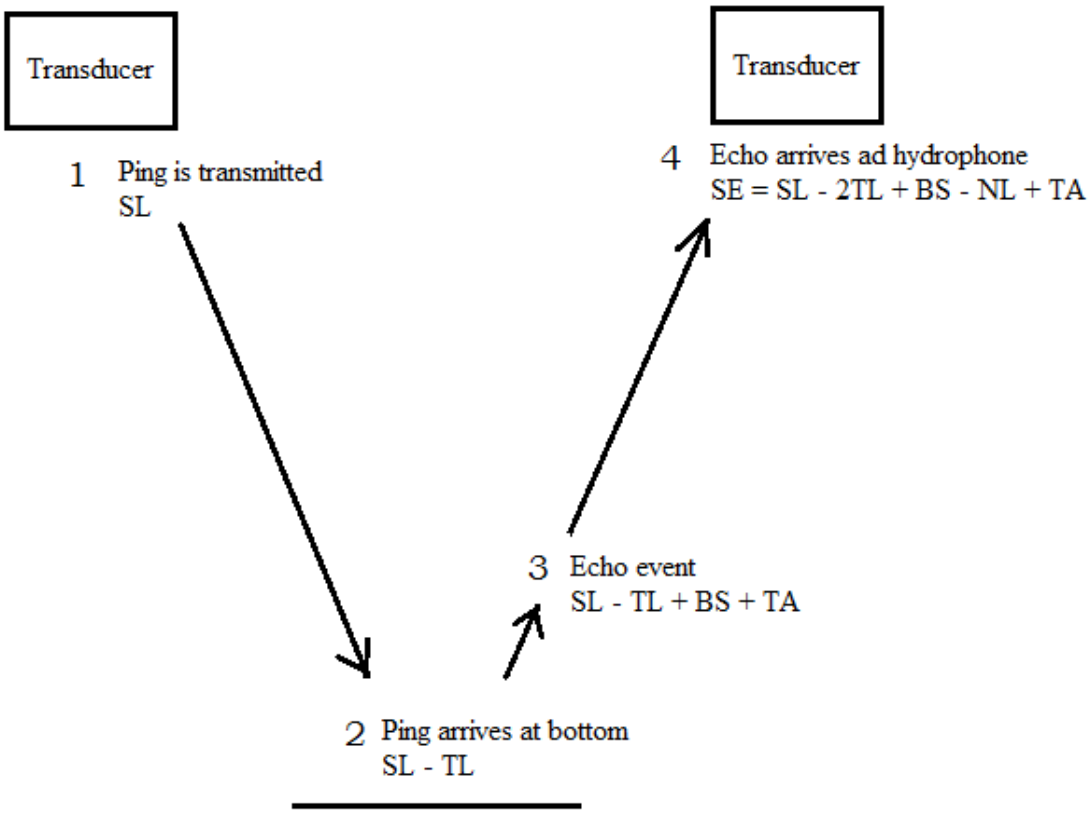

Figure 1. Path of a single ping. Noise Level is continuously increasing throughout the whole process in the water column. Image redrawn by Árni Friðriksson, originally by (Instruments, 2000).

Research vessels do not always operate in perfect weather conditions, the main weather factor is the wind speed which can greatly affect the precision of the depth measurements. Most echo sounders are fitted with motion compensation equipment, *Vertical Reference Unit*, and precise GPS system to compensate for roll, pitch and heave motions of the vessel. The Vertical Reference Unit records roll, pitch and heave information which is applied to the data when used to calculate the precise bottom locations for each beam (Instruments, 2000).

2.2.1 Multibeam vs Singlebeam echo sounder

Singlebeam echo sounders (SBES) are the most widely used and basic echo sounding devices. They make one-at-a-time depth measurements below the vessel. In a way, a SBES insonifies a narrow strip on the bottom below the vessel. These strips can then be joined

together to make a bathymetric map of the bottom. The shortcomings of SBESs are great compared to the MBESs, both in accuracy of the depth measurements and amount of measurements within a given time frame (Instruments, 2000).

Most SBESs send out a ping, listen to the first echo and then calculate the depth below the vessel. But the bottom is not always homogenous so the first echo may not have originated from directly below the vessel. To accommodate for this most devices introduce some directivity to the ping, meaning that they only listen to echoes coming from a specific area. Weather can also greatly influence the uncertainty of SBES measurements. Since most transducers are mounted to the hull of a vessel, large waves can be problematic and result in the narrow beam illuminating scattered areas of the bottom. Survey time is very important when bathymetric mapping is performed, the survey must be cost-effective. A SBES survey is not very cost-effective since it only makes one depth measurement at a time. And if the depth is great each ping cycle takes longer to complete since the last echo must reach the transducer before the next ping can be produced. The area on the bottom measured by the SBES can be increased by increasing the width of the beam. That, however, causes poorer bottom resolution (Instruments, 2000).

Multibeam echo sounder (MBES) is an instrument which maps more than one location on the bottom in a single ping and with higher resolution than SBESs. A MBES maps a wide strip perpendicular to the direction of the vessel, referred to as *swath*. The strip is narrow in the direction of the vessel but the width can be altered depending on the needs of the survey. The surveyed swath width depends greatly on the depth, greater depth means wider swath and less survey time. To produce this narrow strip the system uses the so called *Mills Cross* technique, where the projectors and hydrophones are arranged perpendicular to each other (Figure 2).

A single ping cycle is roughly the time it takes for the echoes from the farthest beams to arrive back to the transducer. It is about twice as long as for a SBES, but a MBES usually makes over 100 soundings in a single ping cycle, thus reducing the operating time considerably. MBESs are much more complicated than SBESs so they cost much more but the reduction in running time more than compensates for the extra cost (Instruments, 2000).

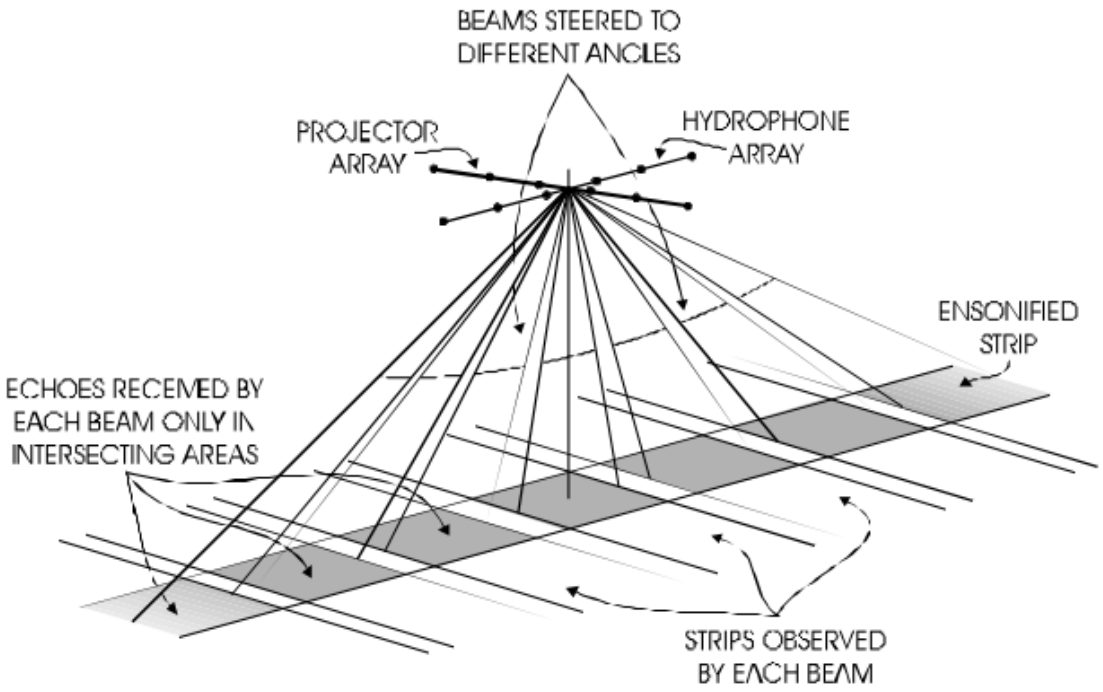

Figure 2. Projector and hydrophone arrays with multiple beams arranged in a Mills Cross (Instruments, 2000).

2.3 Principles of acoustic backscatter

Acoustic backscatter images reveal information about the composition of the bottom by taking advantage of the difference in sound reflectivity and absorption characteristics of different materials (Fonseca & Calder, 2005; Instruments, 2000). Acoustic backscatter can be linked to several different things such as bottom roughness, physical properties of the bottom, angle of incidence and abrupt changes in bathymetry (Medialdea et al., 2008). Many MBESs record both bathymetry and backscatter intensity and use the same hardware and processes for both applications. The main difference between the backscatter intensity application and a conventional depth-sounding system is the way the returning echoes are processed. Acoustic backscatter detects the strength of incoming echoes from each beam and displays them as a plot of amplitude versus time. Due to attenuation in the water column with time, time-varying gain must be applied to the amplitude values so that features with similar reflectivity characteristics have similar amplitudes (Instruments, 2000; Moustier & Matsumoto, 1993). Some systems have automatic multibeam correction routines, such as automated gain corrections and automatic slope correction using inherent multibeam bathymetry (Caris, 2013; Fonseca & Calder, 2007). The greatest obstacle in

acoustic backscatter processing is the correction for the angle of incidence on the bottom. If no correction is made the resulting mosaic will not be uniform across the swath. High values appear near nadir and lower values to the sides (Figure 3). The most common technique to get rid of these artifacts is the Angle Varying Gain (AVG) correction. The AVG correction normalizes the backscatter intensity across the swath and therefore allows for better visualization and interpretation of the research area (Fonseca & Calder, 2007). Greyscale is normally used where dark displays low amplitude and light displays high amplitude, or vice-versa, depending on the observer.

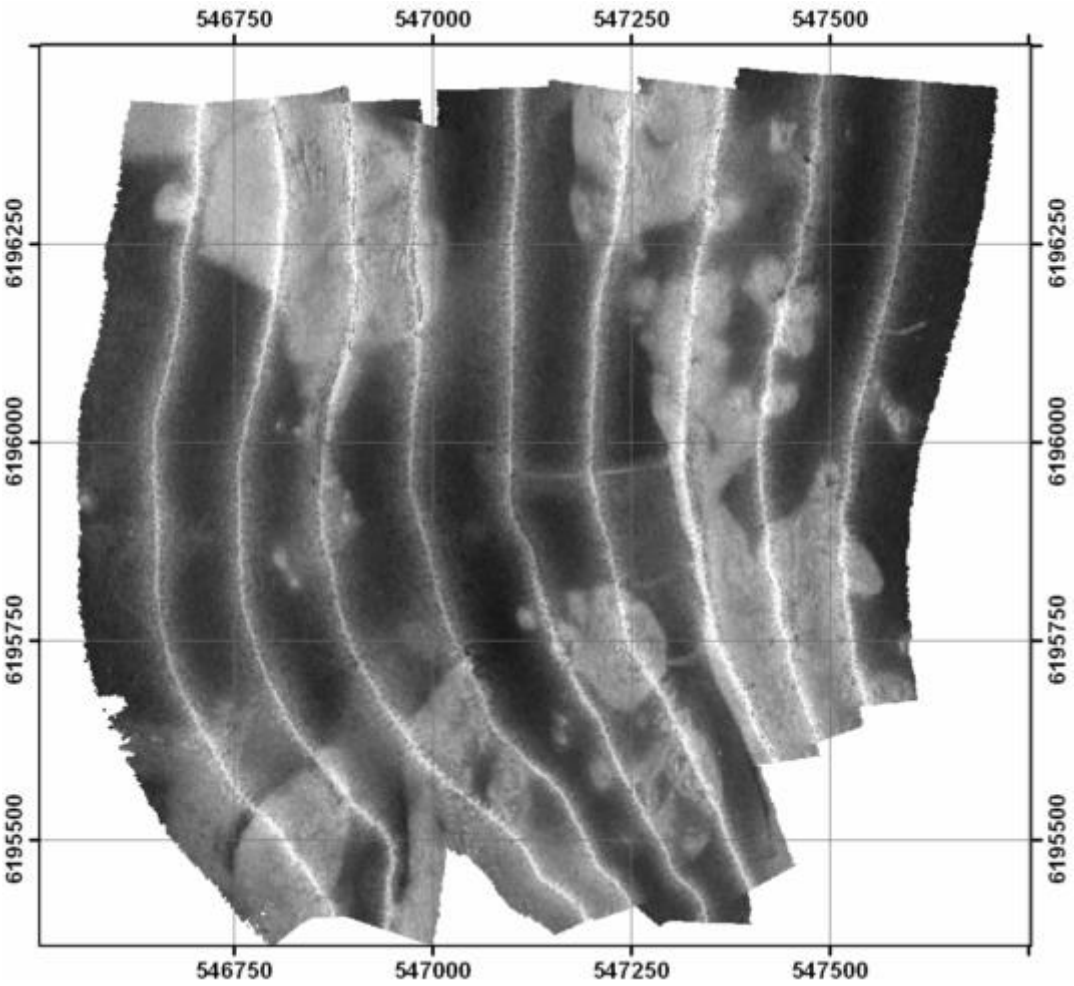

Figure 3. Acoustic backscatter mosaic compiled with no AVG correction (Fonseca & Calder, 2007).

3 Lakes in volcanological environment

Lakes are found all over the surface of the Earth, both freshwater and a mixture of freshwater and seawater. Lakes generally are present where the groundwater table is above the surface, typically where there are depressions in the topography. In many places these depressions occur where tectonics form the landscape, e.g. Botnsvatn in northern Iceland (Sæmundsson & Karson, 2006), where volcanoes play the dominant role, e.g. Öskjuvatn (Sæmundsson & Sigmundsson, 2012) and Crater Lake (C. R. Bacon & Lanphere, 2006; Charles R Bacon et al., 2002), and where the two deformation forces act together, e.g. Thingvallavatn (Sæmundsson, 1992).

3.1 Crater Lake

Mount Mazama is a volcano in the Cascade mountain arc in the western part of North America. It hosts the famous Crater Lake caldera which was formed in a 50 km^3 climactic eruption of mainly rhyodacitic magma ~7700 years ago (C. R. Bacon & Lanphere, 2006; Charles R Bacon et al., 2002; Nelson, 1967). Crater Lake is the deepest lake in the United States with maximum depth recorded to be 593.5 m (1947.2 feet) and volume of 18.7 km^3 of water (Charles R Bacon et al., 2002).

3.1.1 Geological setting and eruptive history

Mount Mazama is located in the Cascade Mountain Range in Oregon, USA. The Cascades are built up as the Juan de Fuca plate submerges under the North America plate. Mazama is located on the eastern side of the Cascades and its eruptive history spans ~420 k.y. It began with mainly dacitic eruptions which then changed into andesitic-dominating period of volcanism. The andesitic volcanism built much of the edifice height and volume, but in between it erupted dacitic lavas, one of which ended this period ~215 ka. Renewed volcanism started again ~170 ka after some 45 k.y. of little or no activity. A large andesitic shield was built northwest of the Mazama summit. The two largest shield volcanoes in the area were also active at that time. Until ca. 70 ka the eruptions were characterized by mainly andesitic and dacitic flank lava effusion with few voluminous dacitic lava flows

and pumice falls. The last 55-60 k.y. Mazama mainly produced flank dacite, central vent andesite lavas and summit dacite domes (C. R. Bacon & Lanphere, 2006).

The 7.7 ka climactic eruption of Mazama changed the shape of the edifice significantly, from being a voluminous stratovolcano to a caldera-topped edifice. The eruption also changed the landscape tens of kilometres away from the volcano, it devastated the vegetation and sent pyroclastic flows from Mazama as far as 70 km away. The ~50 km^3 of magma was mainly of rhyodacitic pumice composition and left a 60 km^2 caldera at the top of Mazama (C. R. Bacon & Lanphere, 2006; Charles R Bacon et al., 2002). The caldera is now occupied by the famous Crater Lake, in which there are some indications for post-caldera volcanism. The most prominent indicator is Wizard Island, a 1.22 km^2 island in the western part of the lake (Charles R Bacon et al., 2002).

3.1.2 Bathymetric studies

Until 1886 there was very little knowledge about the subsurface of Crater Lake. In 1886 a party from U.S. Geological Survey made 186 soundings in the lake with piano wire and a weight and determined that the lake was 1996 feet (~600 meters) deep. These soundings were made by M. B. Kerr under the direction of Major C. E. Dutton. They observed two features rising up from the lake bottom, one at depth of 450 feet (137 m) and the other at 825 feet (251 m) depth. Later, two submerged cones were indicated in the lake, one of them near the northern shore of the lake (Williams, 1961).

The National Park Service, under the direction of John E. Doerr, made additional soundings in Crater Lake in 1938-1940. These measurements were used to reproduce the map made earlier. In July and August 1959 a party from the U.S. Coast and Geodetic Survey, directed by R. E. Williams, performed over 4000 acoustic soundings in Crater Lake. The following summer Carlton Nelson dredged samples of rocks from the flanks of the two known submerged cones for further studying (Williams, 1961). A contour map of the lake was made from these soundings, showing depth in fathoms (Figure 4). The map gave people a better idea about the bathymetry of the lake than previous maps. Probably the most extraordinary feature on the lake floor was a 1320 foot (~400 m) high near perfectly circular cone, Merriam Cone, located near the northern shore of the lake. The base of the cone was measured approximately one mile (~1.6 km) across. The other cone mentioned earlier is partly subaerial, named Wizard Island, and is located just off the western shore of Crater Lake (Figure 4). The dredge samples were used along with the

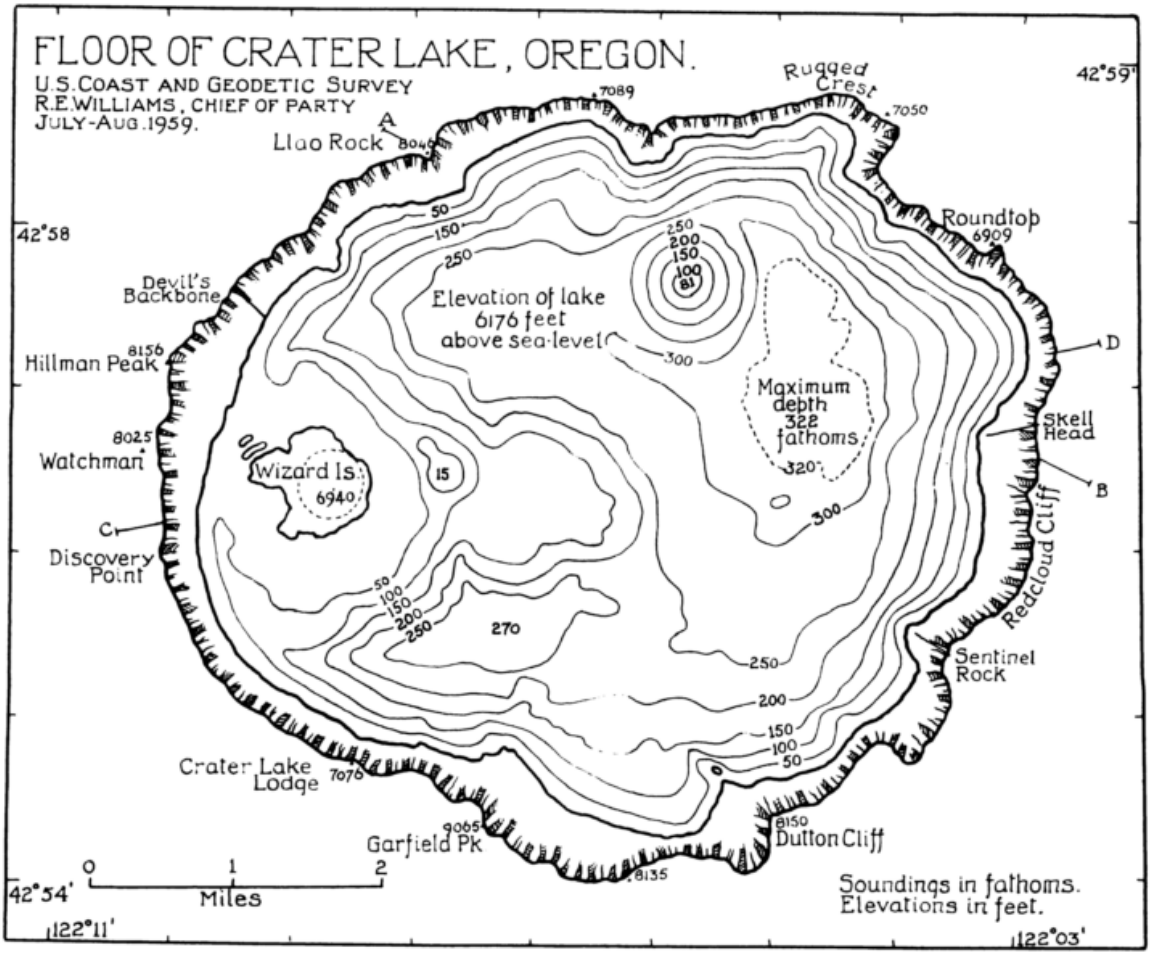

Figure 4. Contour map of Crater Lake made by Williams (1961). Note the cone in the central north part of the lake (Merriam Cone) and Wizard Island just off the western shore.

contour map to understand the nature of these cones, how they formed and the circumstances when they formed (Williams, 1961).

The slopes of Merriam Cone were measured at angles of 31-33° which is approximately the same as for a cone formed subaerially. This suggests that the cone must have formed shortly after the formation of Crater Lake caldera, or some 7.6 k.y., and before the lake level had risen very far. The fact that Merriam Cone has no crater at its top suggests gradually diminishing explosive activity until the cone stopped erupting. Dredge samples from the southeast flank of Merriam Cone closely resembled few of the andesitic lavas found on Wizard Island. Lava flows were present southeast of Merriam Cone, probably originated from fissures near its base (Williams, 1961). A lava field extending about two miles east of Wizard Island and rising about 60-70 meters above the lake floor is probably originated from the island but covering something older. Dredge samples from the lava plain, indicating the presence of dacite, and similarities with the parasitic cone of

Zapicho which was covered by lava flows from Mount Paricutín state that under the lava flow is the top of a Pelean dome (Williams, 1961).

During five days in July and August 2000 Crater Lake was surveyed nearly to its shoreline by a team from the U.S. Geological Survey, the University of New Hampshire, C and C Technologies, Inc., and the National Park Service. The system used included a high-resolution multibeam echo sounder (Kongsberg Simrad EM1002 MBES), a motion sensor within the vessel to account for vessel motion, and a dual-differential GPS navigation system. All this was mounted on the 8 meter long Surf Surveyor which was used for the survey. Over 16 million soundings with vertical accuracy of 0.2% of water depth and horizontal accuracy of just under ±1 m were collected. The instruments also collected information about the intensity of the backscatter (Charles R Bacon et al., 2002). The soundings were used to compile a bathymetric map and a backscatter intensity map of Crater Lake (see Figure 5 and Figure 6) which, along with measured slope maps, were used to produce a generalized geologic map of the floor of Crater Lake. The backscatter intensity map revealed locations of soft sediments, lavas and breccias and together with the bathymetry, provided a good understanding of the lake floor (Charles R Bacon et al., 2002).

The surface level of Crater Lake was 1882.6 m.a.s.l. and the maximum depth was recorded 593.5 m, or a minimum elevation of 1289.1 m.a.s.l. Wizard Island is essentially a volcano inside the Crater Lake caldera, rising 750 m above its lowest point with a footprint of 9.0 km^2 and volume of at least 2.6 km^3. It's composed of numerous superimposed lava flows that were erupted either in subaerial conditions and then run into the lake, or subaqueous conditions. The passage zones of the subaerial lava flows, where they entered the lake and fragmented, record the former lake levels during the growth of Wizard Island. They are often referred to as "drowned beaches". The same theory applies to the central-platform volcano east of the rhyodacite dome (see Figure 5). Lavas from the central-platform volcano were spread out in the central part of the lake. These "drowned beaches" are found at elevations of 1540 m.a.s.l., 1560 m.a.s.l., 1600 m.a.s.l., 1700 m.a.s.l. and 1805 m.a.s.l. and are considered to have coincided with the filling of Crater Lake (Charles R Bacon et al., 2002).

Williams (1961) provided a generally good overview of the morphology and formation of Merriam Cone although he considered that the eruption was subaerial. However, Nelson et al. (1994) provided evidence for subaqueous eruptions at Merriam

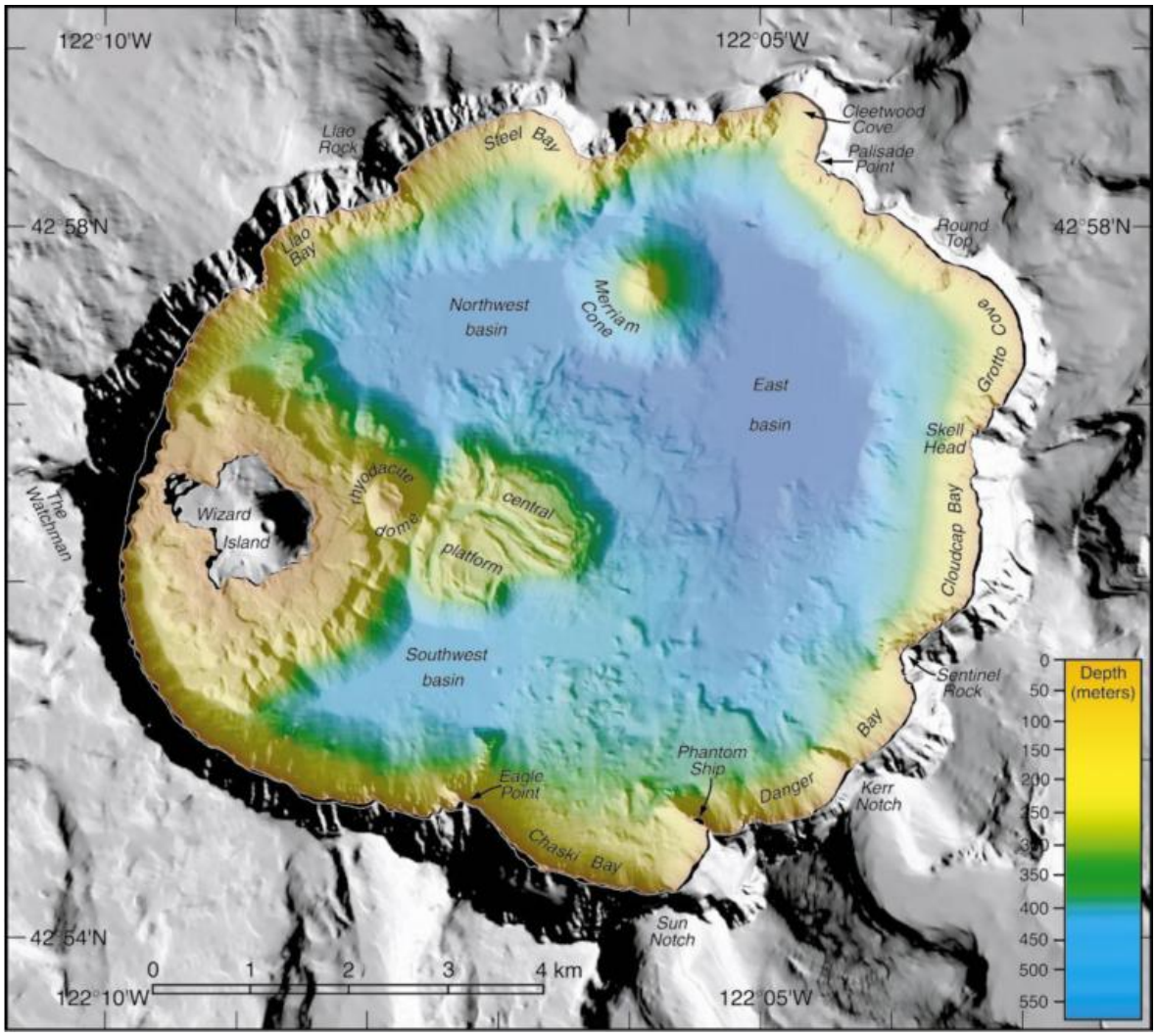

Figure 5. Bathymetric map on top of a shaded relief map of the floor of Crater Lake. The map is from Charles R Bacon et al. (2002).

Cone such as pseudopillows and other features indicative of rapid chilling of magma. The rocks at Merriam Cone were also lacking surface oxidation. Charles R Bacon et al. (2002) concluded that at least the final eruption at Merriam Cone occurred in shallow water, and therefore its formation was similar to Wizard Island, but Merriam Cone failed to produce topset lava.

A small dome is present between Wizard Island and the central-platform volcano, primarily composed of rhyodacite. Its slopes have high backscatter and are composed of talus or breccias that overlie both the Wizard Island and central-platform volcanoes. Because the dome was formed subsequent to Wizard Island, Charles R Bacon et al. (2002) concluded that much, if not all, of the rhyodacite dome erupted under water.

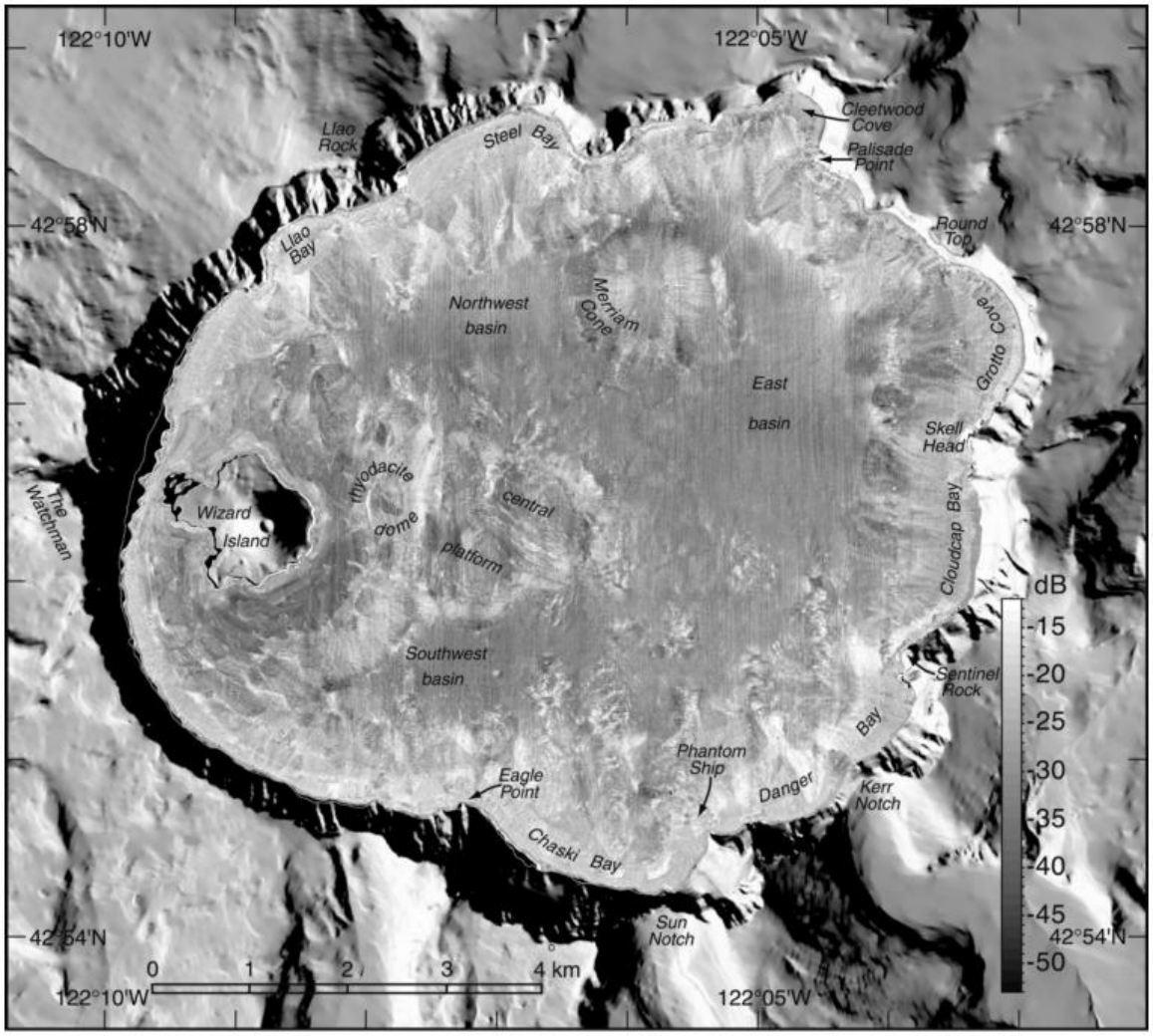

Figure 6. Backscatter intensity map of Crater Lake. The map is from Charles R Bacon et al. (2002)

The caldera walls are composed of both exposed bedrock and talus, rockfalls and debris flows. These debris flows have cut embayments, such as Chaski Bay, Steel Bay and Danger Bay, into the northern, eastern and southern caldera walls and left bedrock promontories between them, e.g. Eagle Point, Phantom Ship and Llao Rock (see Figure 5). These debris flows/rockfalls/taluses are most extensive below the deepest embayments and they occur both as subaerial and subaqueous. The subaqueous taluses tend to have gentler slopes than the subaerial ones (Charles R Bacon et al., 2002). Landslides and debris-avalanches are present in a few locations around the Crater Lake caldera floor, the most prominent one below Chaski Bay. They can be recognized by hummocky topography on the caldera floor and large scattered blocks of rock that once were parts of the caldera walls. The Chaski Bay debris-avalanche covers 4.9 km^2 and has a volume of at least 0.21

km^3 with the largest blocks, up to ~300 m long, having travelled 2-3 km from its source (Charles R Bacon et al., 2002).

3.2 Lake Öskjuvatn

3.2.1 Geological setting

Askja central volcano, also called Dyngjufjöll volcanic centre, is located on the 100 km long Askja fissure swarm in the Northern Volcanic Zone (NVZ) of Iceland. The south end of the Askja fissure swarm lies under the northern part of Vatnajökull glacier, to the north extends a 100 km long and 20 km wide zone with eruption fissures and tectonic fractures (Hjartardóttir, 2008; Sæmundsson & Sigmundsson, 2012; Sæmundsson, 1982; Sigvaldason, 2002). Askja towers ca. 700 m above its surroundings with the highest peak (Thorvaldstindur) at 1,510 m.a.s.l. and has an aerial extent of about 400 km^2 (Þ. Einarsson, 1962; Sigvaldason, 2002). It was built up by basaltic subglacial and subaqueous eruptions from Pleistocene and is thus mostly made of hyaloclastite. Holocene lava flows from fissures transecting Askja dominate its surroundings (Hjartardóttir, 2008; Johnstrup, 1877; Sæmundsson & Sigmundsson, 2012; Sigvaldason, 2002).

An early Holocene Plinian eruption (1-2 km^3 dense rock equivalent) occurred in Askja and changed the landscape of the edifice, Askja caldera had been formed (Figure 7). The eruption was of rhyolitic composition and left deposits of ash and pumice in coastal areas in northern and eastern Iceland (Þ. Einarsson, 1962; Sigvaldason, 2002).

After the early Holocene Plinian eruption lavas have partially filled the Askja caldera. Einarsson (1962) suggests that the lava currently covering the Askja caldera floor erupted from a crater row near Trölladyngjuskarð in the southwest corner of Askja caldera. The caldera is 45-50 km^2 and was deformed by an explosive eruption in its southeast corner on 28th-29th March 1875, resulting in the formation of Öskjuvatn caldera, an 11 km^2 caldera partially filled by Öskjuvatn (Þ. Einarsson, 1962; Ó. Jónsson, 1942; Sæmundsson & Sigmundsson, 2012; Sigvaldason, 2002)

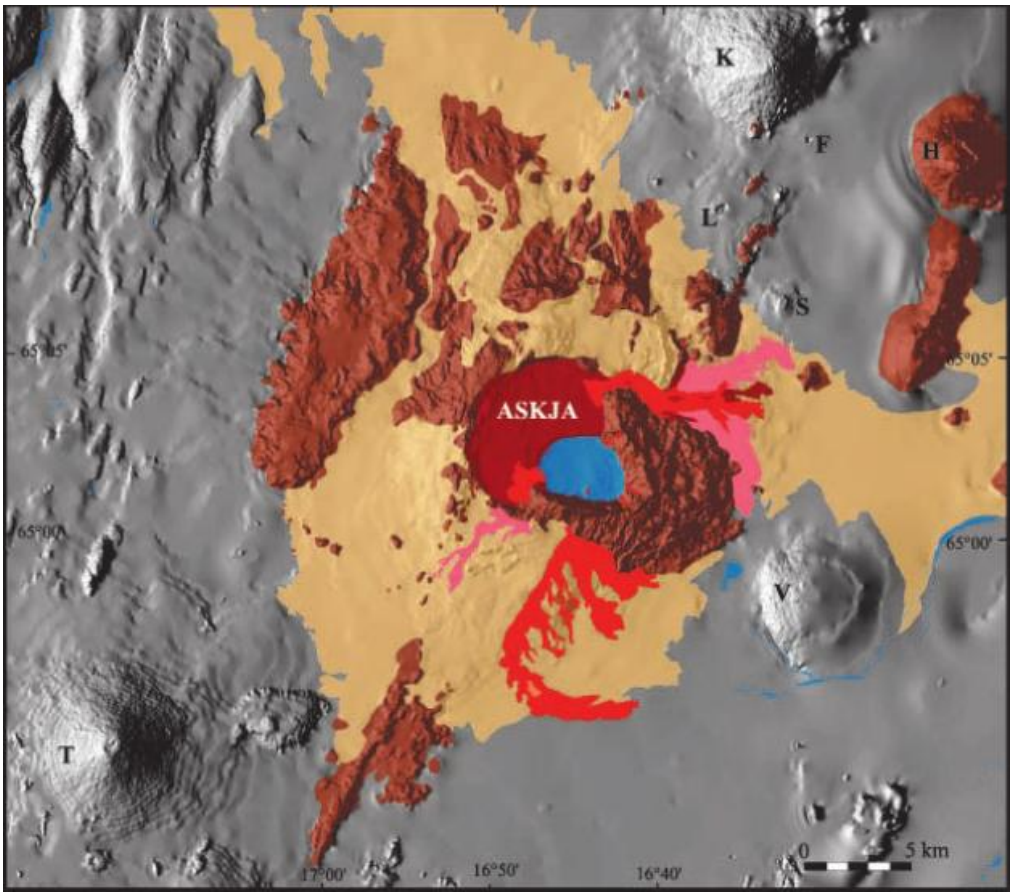

Figure 7. Various lava formations shown on top of a digital elevation map of Askja. Hyaloclastites from Pleistocene are marked brown, *lavas older than 6.6 ka are* tan, *lavas erupted between 6.6 and 2.9 ka are* pink, *lavas on the Askja caldera floor younger than 2.9 ka are* red-brown *and lavas erupted in the 20th century are* red. *Water is* blue. *A few lava shields are also shown in the map: Kollóttadyngja (K), Trölladyngja (T), Flatadyngja (F), Litladyngja (L) and Svartadyngja (S). Other volcanic structures include: Herðubreið (H) and Vaðalda (V). Map originally from Sigvaldason (2002).*

3.2.2 Historical eruptions in Askja and previous research

Historical records of volcanic activity/unrest in Askja date as early as 1874. Seismic unrest was reported in eastern Iceland during the fall of 1874 and again in December same year (Gunnarsson, 1875). The earthquakes were felt from Skagafjörður in the west to Múlasýslur in the east (Ísafold, 1875). Late 1874 and during the first days of 1875 two eruption columns were reported at or near Askja (Gunnarsson, 1875; Ísafold, 1875). After the events in December 1874 and January 1875 a group of four people travelled to Askja on 15th February to visit and investigate the site of the eruptions. They arrived in Askja on

16th February and located the eruption site in the southeast corner of Askja caldera, most likely near the centre of the present day Öskjuvatn. Three source vents were observed. The largest one, also farthest to the southeast, was surrounded by a ring shaped scoria/spatter cone, 65-85 m high, which was positioned on a flat ground with no fresh lava. It emitted ash plumes, mud and steam but no lava at that time. A small collapse depression was observed ~130-170 m west of the main source vent, in a snow-free field of smooth lava. It was bounded by ~10 m high fault scarps, deepest to the northwest, and had aerial extent of 10-12 "dagslátta" or 34000-41000 m^2. In the depression they located two vents, one of them had produced a small lava flow and water was flowing away from it and into a small pond in the northwestern part of the depression, and the other one only produced fumes at that time (Ísafold, 1875; Sigurðsson, 1875). The activity in Askja continued until it reached its climax on 28th-29th March 1875 with an explosive eruption in the southeastern part of Askja caldera. Before noon, pumice fall was observed in eastern Iceland (Gunnarsson, 1875).

The first men to visit the eruption site at Askja following the eruption on 28th-29th March 1875 were a part of an expedition led by Lord William Watts (Watts, 1876). Watts travelled to Askja along with two Icelandic guides, they travelled over Austurfjöll, near Drekagil, and arrived at the eruption site on 16th or 17th July 1875. Watts described "Öskjugjá" or Askja chasm as triangular, ~8 km in circumference, the base facing towards northwest and the chasm being about 1 ¼ English miles (2 km) across. From the base there was a nearly perpendicular wall of rock that began to decrease in slope around midway to the bottom of the crater, some 120-150 m (400-500 feet) below the bottom of Askja. The two other sides of the triangle converged in the southeast corner, bound by high mountains rising ~300 m above the floor of Askja caldera. The crater Víti was fully active, located just NNE of the collapse rim with diameter around ¼ Mile (400 m), emitting black mixture of fumes, mud and other earthy materials. It is worth mentioning that Watts' "measurements" were mostly guesses although he measured the circumference of Öskjugjá by counting paces as he walked towards Trölladyngjuskarð, across the caldera floor (Watts, 1876).

Jón Þorkelsson and Sigurður Kráksson from the farm Víðiker in the Mývatn district were the next explorers to visit Askja on 8th February 1876. They arrived at Askja from the west, at Vonarskarð. They estimated the triangular-shaped collapse to be ~8 km in circumference, bounded by steep cliffs on all sides except for the northern side. They climbed down into the collapse, about 650-800 m according to their estimates, where they

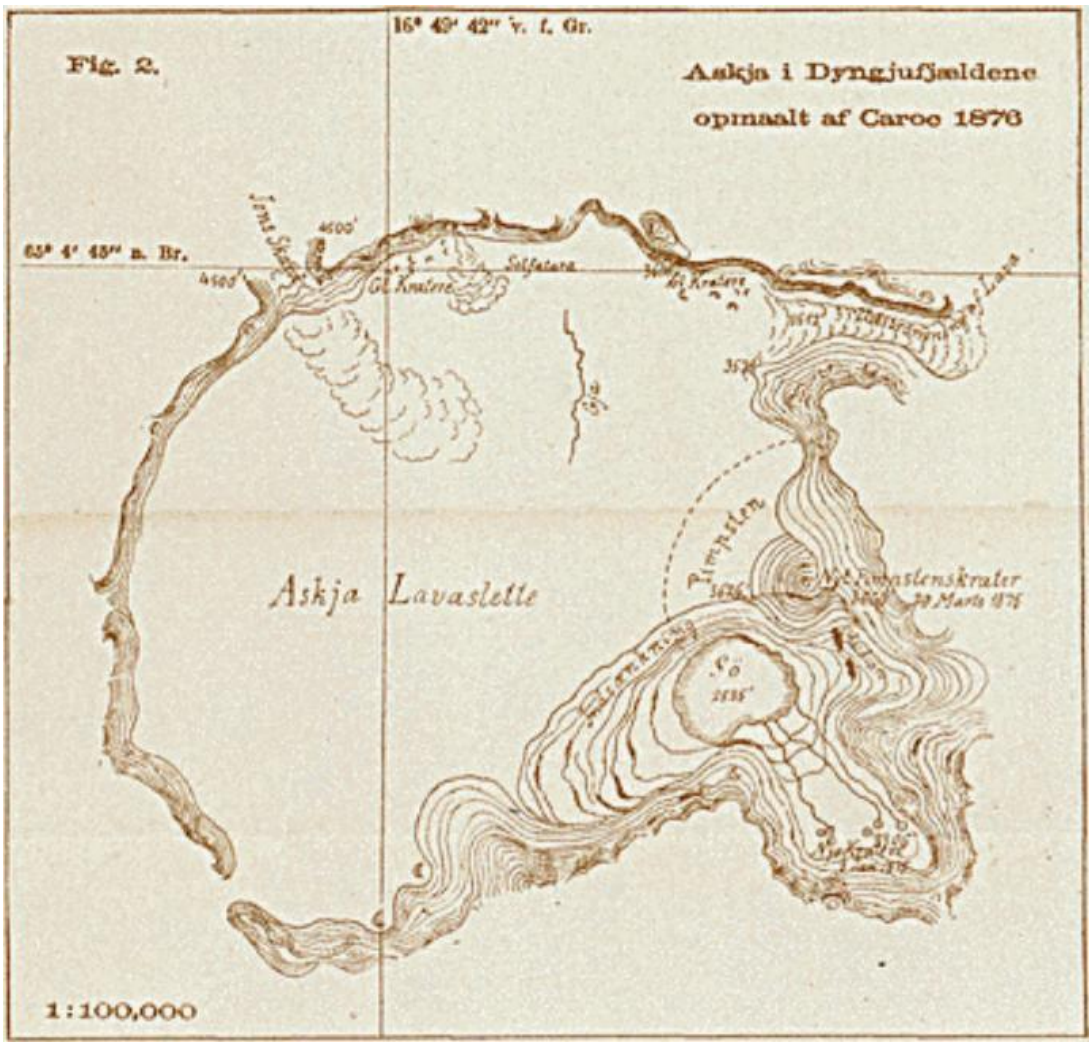

Figure 8. Map of Askja caldera by Lt. Caroc. The surface level of Öskjuvatn was at 2886 feet (880 m) a.s.l., 740 feet (225 m) below the northern rim of Öskjuvatn caldera (Johnstrup, 1877).

found a deep and hot lake, the first evidence of the present day Öskjuvatn. The depth of the collapse was clearly overestimated, according to later observations (Briem, 1877).

In the summer of 1876 between 30th June and 4th July, Professor Johnstrup and Lieutenant Caroc explored the 1875 eruption site at Askja. Caroc drew the first detailed map of Askja caldera and the eruption site (Figure 8) according to his measurements while Johnstrup investigated the geology. According to Caroc's measurements the main collapse

was elongated NE-SW, 4580 m long, and approximately 2500 m in the N-S direction. The northwestern side of the collapse was slightly curved and more than twice the length measured by Watts. A pond, roughly circular in shape, was observed at the bottom of the collapse, 232 m below the floor of Askja caldera. The pond had a diameter of roughly 4000 feet (1220 m) and the water was light-green at the temperature of 22°C. Masses of pumice originated from the eruption on 28th-29th March 1875 were floating on the pond. Southeast of the pond was a chasm, ~2 km long and ~1 km wide, which contained several craters in its southern end from which ran 40°C water into the pond. The chasm sloped down towards the pond from the vents which were 94 m lower than the Askja caldera floor, but 138 m higher than the pond (Johnstrup, 1877). The depth of the pond was not measured but according to Jónsson (1942) it was probably not more than 20-30 m deep.

The next explorer to visit Askja was the Englishman, W. G. Lock, in 1878 and 1880. In 1878 he found the lake at the bottom of the collapse to be ~5 miles (8 km) in circumference and 20.5°C in temperature. According to Lock's estimates the lake was ~600 feet (183 m) below the Askja caldera floor and the lake surface had risen about 40 feet (12 m) between 1878 and 1880. The northwestern side of the collapse was 2 miles (3.2 km) with 400 feet (122 m) high cliffs down to the lake and to the south were steep mountains, ~2000 feet (600 m) high (Lock, 1881). Lock did not mention any changes in the shape of the collapse since Caroc and Johnstrup's measurements. A 1000 yards (~900 m) long chasm going in to the hyaloclastites to the southeast from the lake, bounded by ~180 m high cliffs on either side was observed. In the chasm there were fractures covered in pumice and many vents erupting steam, likely the same vents as Caroc and Johnstrup discovered in 1876 (Lock, 1881).

E. Delmar Morgan was the next explorer to visit Askja in August 1881. He did not make any direct measurements on the dimensions of Öskjuvatn caldera but he measured the temperature of Öskjuvatn to be 12°C (54°F). Morgan also largely agreed with Johnstrup's observations about the craters in the southeast corner of the Askja mountains (Morgan, 1882).

Thorvaldur Thoroddsen and Ögmundur Sigurðsson arrived at Askja on 25th July 1884 to explore Öskjuvatn caldera. Thoroddsen used Caroc's map as a reference point for major features and thus is very difficult to detect any changes in the shape and depth of the Öskjuvatn caldera. Nevertheless, he measured the length of the northwestern side to be 10000 feet (3200 m) and the depth down to the lake to be 150 m. The surface of Öskjuvatn

had risen 82 m from 1876 to 1884 and the craters south of the lake were 56 m above the lake surface. Thoroddsen measured the temperature of Öskjuvatn to be 14°C (Thoroddsen, 1905). It is very likely that the shape of the caldera collapse had changed significantly since Caroc and Johnstrup made their observations, from being triangle in shape to being more like oval triangle or ellipsoid, especially if the southeast chasm is discounted (Ó. Jónsson, 1942).

The next explorers to make any scientific contribution to the evolution of Öskjuvatn caldera were Dr Walter von Knebel, the painter Max Rudloff and a geologist named Hans Spethmann. They arrived in Askja on 1st July 1907 but unfortunately Von Knebel and Rudloff drowned in the lake on 10th July that year. Spethmann continued the research and found the shape of the lake to have changed significantly since 1884. It had an almost rectangular form with round corners and dimensions of ~5 km by ~3 km. Jónsson (1942) considered the length of 5 km to be an overestimation, based on later measurements. Continuous rock-fall at the southern boundary of the lake clearly affected the shape and size of the lake. Lake level was 60 m below the caldera rim on the northwestern side (Ó. Jónsson, 1942).

Hans Reck, a German geologist, arrived at Askja in the summer of 1908 and measured the dimensions of Öskjuvatn to be 4.5 km by 3 km. He found that the lake level had not risen since 1907 but he made depth measurements on the lake. According to his findings, the greatest depth was in the southwest sector of the lake where a 140 m sounding line didn't reach the bottom. The southern boundary of the lake was slightly curved to the north and relatively fresh scars were observed in the cliffs south and east of the lake. Average temperature of Öskjuvatn was 6.5°C, although it could be different from one place to another (Reck, 1910).

W.S.C. Russell went to Askja in 1917 and observed smoking solfataras at the eastern shore of the lake. He also sketched a map of the Öskjuvatn caldera but since no dimensions are given, the map is of little use. The lake surface was recorded at an altitude of 1011 m.a.s.l. with temperature of 7.5°C (Russell, 1917).

In 1932 Hans Reck was sent to Askja by the Military Commission (Herforingjaráð) to measure Öskjuvatn. He found that the lake had changed in shape; the northwestern corner was nearly 90° and it had also extended to the south and northwest. Reck also noted several lava flows from fissure eruptions around the lake in the 1920s (Ó. Jónsson, 1942). These lavas include: Bátshraun (March 1921), which flowed into Öskjuvatn from the

slopes of Austurfjöll east of Víti, Mývetningahraun (November 1922), which flowed from a fissure in Suðurskörð and into Öskjuvatn in the southwest corner, Kvíslahraun (1922/23) and Suðurbotnahraun (1922/23) originated in the slopes of Austurfjöll east of Öskjuvatn, and the island Askur (1926) which was created in a phreatomagmatic eruption near the southern shore of Öskjuvatn (Þ. Einarsson, 1962).

After 20 days of earthquakes, solfatara-activity and steam eruption in a mud volcano, a lava eruption started on a 750 m long E-W striking fissure in Askja at Öskjuop on 26th

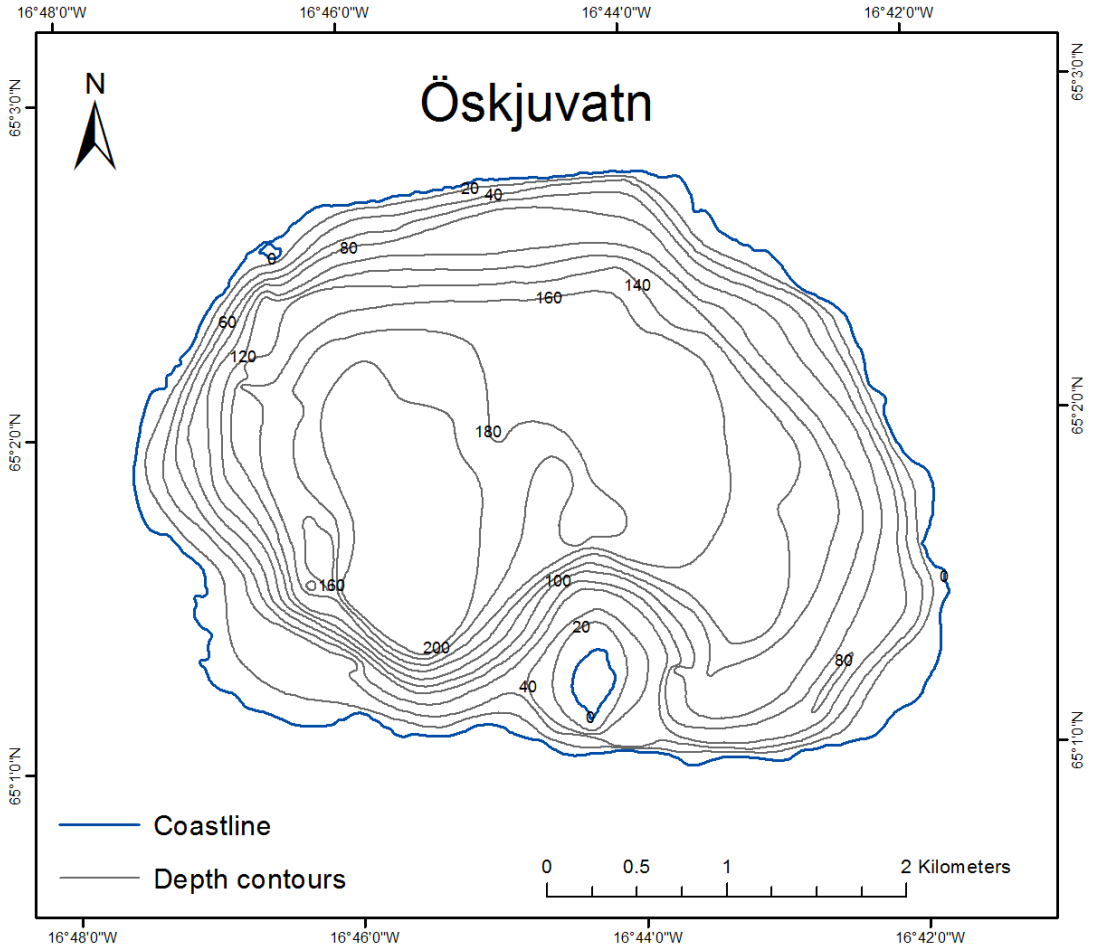

Figure 9. Bathymetric map of Öskjuvatn. The data is originally from Rist (1975) and has been digitized by the Meteorological office in Iceland. Redrawn by Árni Friðriksson.

October 1961. The fissure follows the ring-fault structure of Askja caldera. The eruption column rose to 10000 m elevation in the first day and to 2000 m on the second day, but this eruption showed typical lava fountain activity. New lava, Vikrahraun, was produced in this eruption. It is 9 km long and covers 11 km^2 (Þ. Einarsson, 1962).

Öskjuvatn caldera was highly studied during the first decades of its development and the filling of Öskjuvatn, but it wasn't until 1963 that a bathymetric survey was conducted on the lake. The survey was conducted as a series of profiles along the lake with a singlebeam echo sounder. The profiles were then compiled to make a bathymetric map (Figure 9) (Rist, 1975).

3.3 Lake Thingvallavatn

Lake Thingvallavatn is the second largest lake in Iceland, 83 km^2, and 114 m deep. The lake lies in a basin which was originally formed by glacial erosion and tectonic subsidence some 10000 years ago, but has since then been deformed greatly by volcanic and tectonic activity. The catchment area of Thingvallavatn has been estimated to be about 1000 km^2, stretching from Hengill in the south and up to Langjökull in the north (Sæmundsson, 1992). The river Sog is the only outlet from Thingvallavatn and since the Steingrímsstöð power plant was constructed at the outlet in 1960, the water level has been held at an average 0.2 m higher than before, to prevent drastic effect on the life in Thingvallavatn (Aðalsteinsson, Jónasson, & Rist, 1992).

3.3.1 Geological setting

The Thingvallavatn area is a part of the axial rift zone of SW-Iceland from the Hengill triple junction in the southwest up to Langjökull in the northeast. In principle the rift zone is a graben about 20-25 km across in the north but narrowing to about 10 km in the south. According to Sæmundsson (1965) the width of the graben is about 4 km south of Thingvallavatn. The graben is asymmetric with a few large faults on a narrow zone on the northwestern side, but numerous smaller faults across the graben on the southeast side. These features can be seen north of Thingvallavatn e.g. Almannagjá on the northwestern side and Hrafnagjá on the southeast side (Sæmundsson, 1965, 1992). There are a few intersecting volcanic systems in the Thingvallavatn area, two systems lie to the north with one of them centred in the southwest corner of Langjökull and the other one a little bit further east, responsible for landmarks such as Skjaldbreiður, Hrafnabjörg and Tindaskagi. The volcanic systems stretching south from Thingvallavatn are the Hengill (southwest) and Hrómundartindur (southeast) volcanic systems. The volcanic systems north of Thingvallavatn are characterized by rows of voluminous lava shields and table mountains. The Hengill and Hrómundartindur volcanic systems on the other hand are characterized by

small fissure eruptions. In between these volcanic systems, there hasn't been very much magmatic activity in the lake basin itself in Weichselian and postglacial time. The basin has instead been a locus of ground deformation, mostly without magmatic activity (Sæmundsson, 1992).

The oldest rocks exposed in the Thingvallavatn area are from Plio-Pleistocene (3.1-0.7 M.yr). This sequence is built up of alternating basaltic lava flows and hyaloclastite glacial deposits. Rocks from Plio-Pleistocene are found on a 6 km broad belt from the northwestern side of Thingvallavatn and ca 30 km to the north. Immediately to the east of this sequence are interglacial lavas and hyaloclastite from glacial times. Basalt flows and hyaloclastite ridges from upper Pleistocene are found at Grafningur south of Thingvallavatn probably from the third last interglacial/glacial cycle (Sæmundsson, 1992). Most of the rocks in the Thingvallavatn area are from Upper Pleistocene and Holocene. Rocks deposited in glacial times are primarily hyaloclastite ridges and table mountains e.g. Hrafnabjörg, Kálfstindar, Ármannsfell, Hengill mountain complex, Miðfell and Arnarfell. Two postglacial lavas are known to have flown into Thingvallavatn after the last glaciation, Thingvallahraun lava from the north and Nesjahraun lava from the southwest (Sæmundsson, 1965, 1992). The age of Thingvallahraun lava was determined by Kjartansson (1964). His results gave 9130 ± 260 years. Sæmundsson (1992, 1995) dated the Nesjahraun lava at 1880 ± 65 years. Therefore, Nesjahraun lava is the youngest lava in the Thingvellir area. Not only did it flow into Thingvallavatn but during the eruption an island, Sandey, was formed at the northern end of the eruptive fissure. Sandey is a double-cratered tuff cone rising from ~100 m depth to 74 m above the lake level. The island is highest on the east side and the ash from the eruption was blown mainly to the east. Sandey was built in a similar manner as Surtsey and Askur in Öskjuvatn, in a phreatomagmagic eruption that occurred in water (Sæmundsson, 1992).

In July 1958 a bathymetric survey on Thingvallavatn was conducted with a singlebeam echo sounder. The survey was run as individual depth profiles across the lake which were then compiled to make a bathymetric map (see Figure 10) (Rist, 1975).

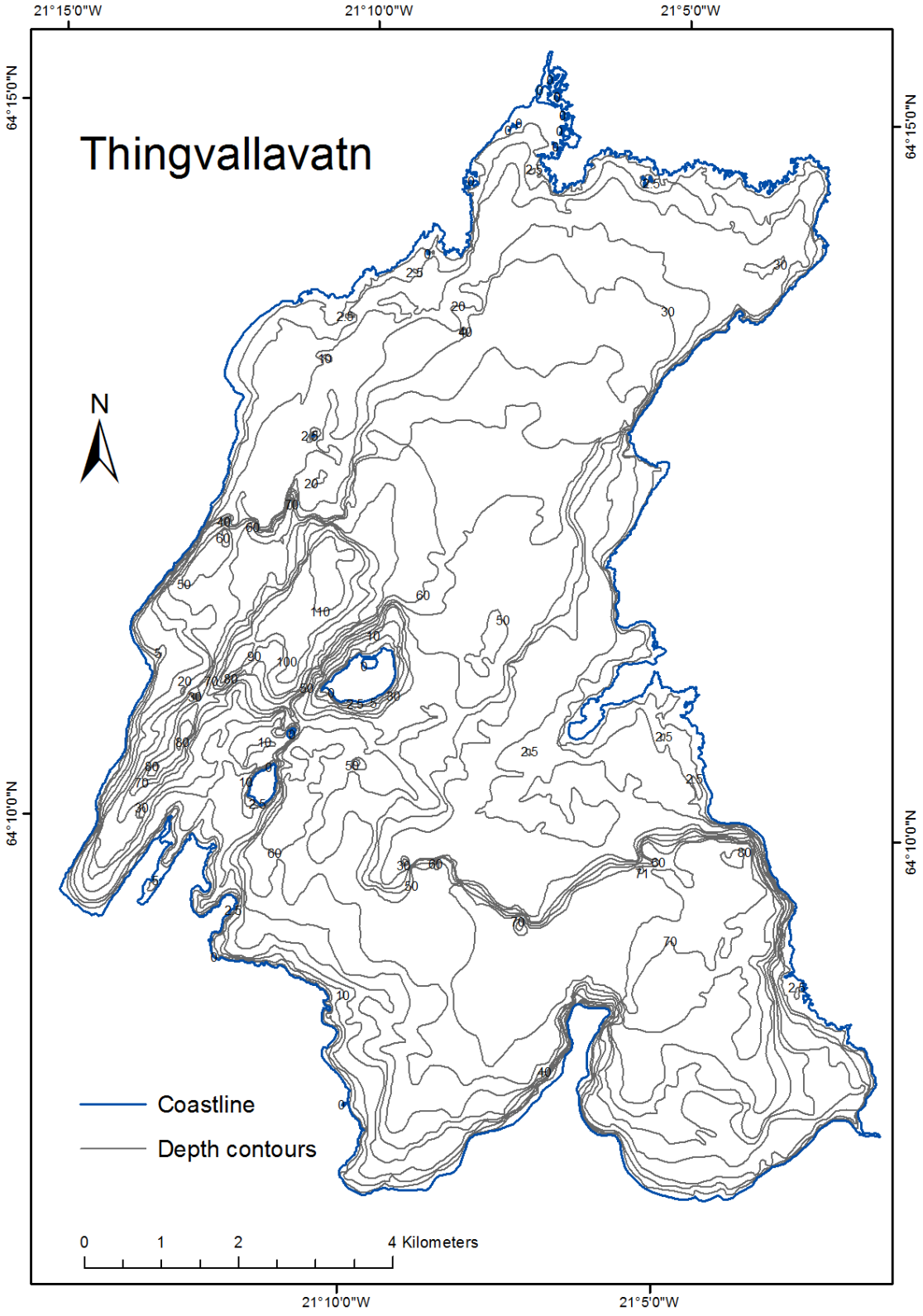

Figure 10. Batrymetric map of Thingvallavatn compiled from individual depth profiles. Measurements are originally from Rist (1975) and the data were digitized by the Meteorological office in Iceland. Redrawn by Árni Friðriksson.

Thors (1992) surveyed the Thingvallavatn basin using side-scan sonar and a seismic reflection profiler. A map compiled from the survey is shown in Figure 11. The map shows all major faults, where the apparent throw is more than 10 m, basement rocks, 20m contour lines and steep lava fronts, where they are apparent.

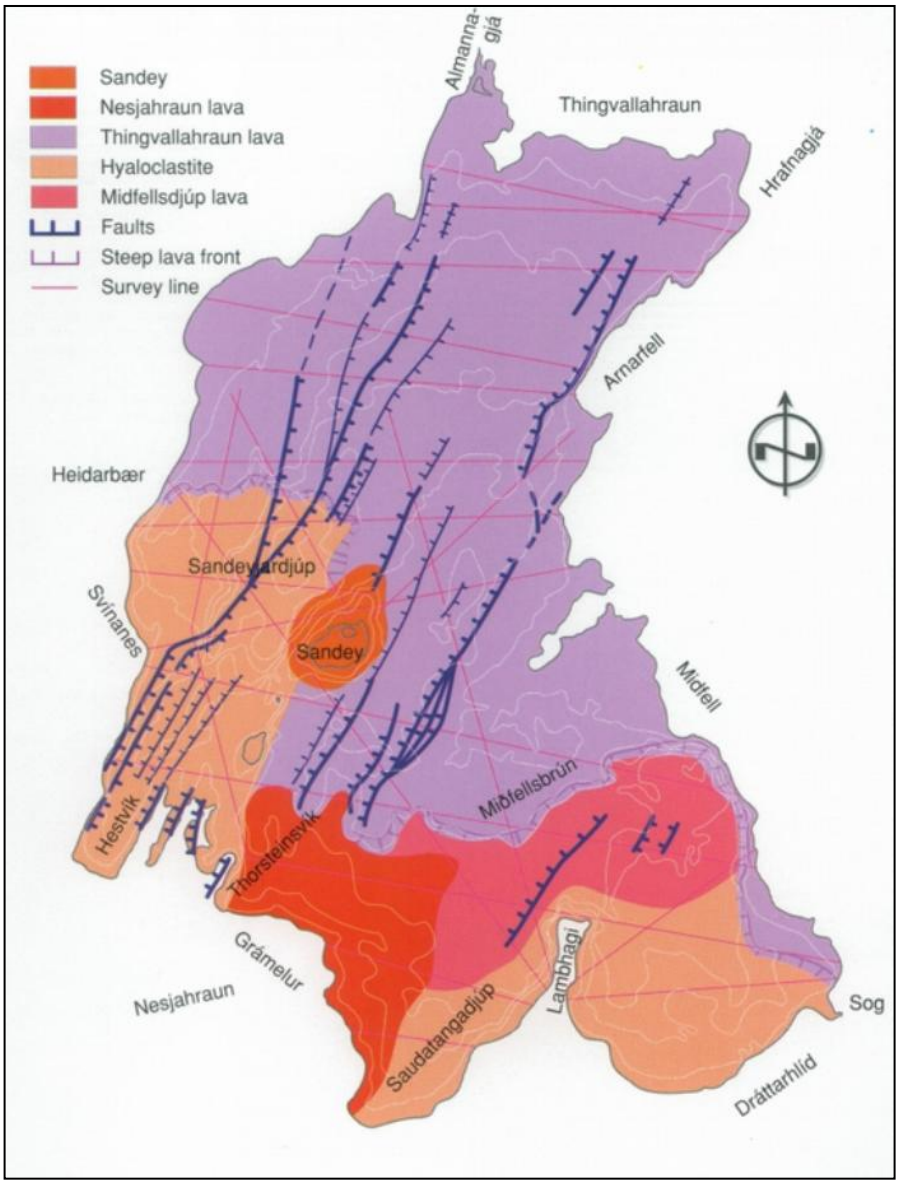

Figure 11. Map of basement rocks and faults in Thingvallavatn. Faults with throw greater than 10 m are marked with heavy lines. Note the coverage of Thingvallahraun lava and Nesjahraun lava. Map originally from Thors (1992).

3.4 Lake Kleifarvatn

Lake Kleifarvatn is located on the Reykjanes Peninsula in SW-Iceland, on the northern edge of the Krýsuvík area (Clifton, Pagli, Jónsdóttir, Eythorsdóttir, & Vogfjörð, 2003). The lake surface is at 140 m.a.s.l. and the lake is 7.5-10 km^2, depending on the water level (Aðalsteinsson, Rist, Hermannsson, & Pálsson, 1989). Kleifarvatn has very small catchment area, very little inflow and no outflow. Therefore the lake level is much dependent on groundwater table and fractures in the ground (Clifton et al., 2003).

3.4.1 Geological setting

Reykjanes Ridge goes onshore at the southwestern tip of the Reykjanes Peninsula and the rift zone extends there about 70°N along the whole peninsula to the Hengill triple junction. The structure of the Reykjanes Peninsula is characterized by volcanic systems arranged en echelon along the plate boundary. The fissure swarms are arranged about 35°N, oblique to the plate boundary and extend several tens of kilometres north and south (P. Einarsson, 2008). Both volcanic and tectonic features are arranged along these volcanic systems and thus Kleifarvatn is elongated roughly in the same direction. The lake is surrounded by volcanic features of Holocene and upper Pleistocene age, mostly hyaloclastites and also pillow lavas and other lavas of postglacial age. J. Jónsson (1978) constructed a geologic map of Reykjanes Peninsula. According to his map Kleifarvatn is bounded by the hyaloclastite ridge of Sveifluháls to the west and mostly by hyaloclastites and shield lavas to the east. West of Sveifluháls there are several crater rows of the Trölladyngja volcanic system from which a few postglacial lavas have run. Crater rows of the Brennisteinsfjöll volcanic system are found ca. 10 km east of Kleifarvatn. Lavas have run from these craters to Kleifarvatn and into the lake in at least two places. Upper Pleistocene rocks, younger than 700 ka, are exposed near the eastern boundary of Kleifarvatn.

Several geothermal systems are found on the Reykjanes Peninsula, these include the Krýsuvík and Svartsengi geothermal systems. These geothermal systems have been highly explored by geothermal mapping (Arnórsson, Björnsson, Gíslason, & Guðmundsson, 1975; Khubaeva, 2007; Mawejje, 2007). It is not unlikely that the Krýsuvík geothermal system extends into Kleifarvatn, although it could depend on the surface level of the lake. After the >4.5 M_w earthquake on 17th June near the eastern shore of Kleifarvatn, the lake level dropped by more than 4 meters during the following months. A study by Clifton et al.

(2003) revealed fractures on the northern lakeshore, extending into the lake, which were the most probable cause of the water drainage.

Kleifarvatn has not been a great focus of study but some research has been done on the lake level fluctuations and the bathymetry of the lake bottom (Clifton et al., 2003; Morales, 1992; Rist, 1975). Not much was known about the bathymetry and morphology of the lake bottom in Kleifarvatn until Sigurjón Rist measured the lake in April 1964 using

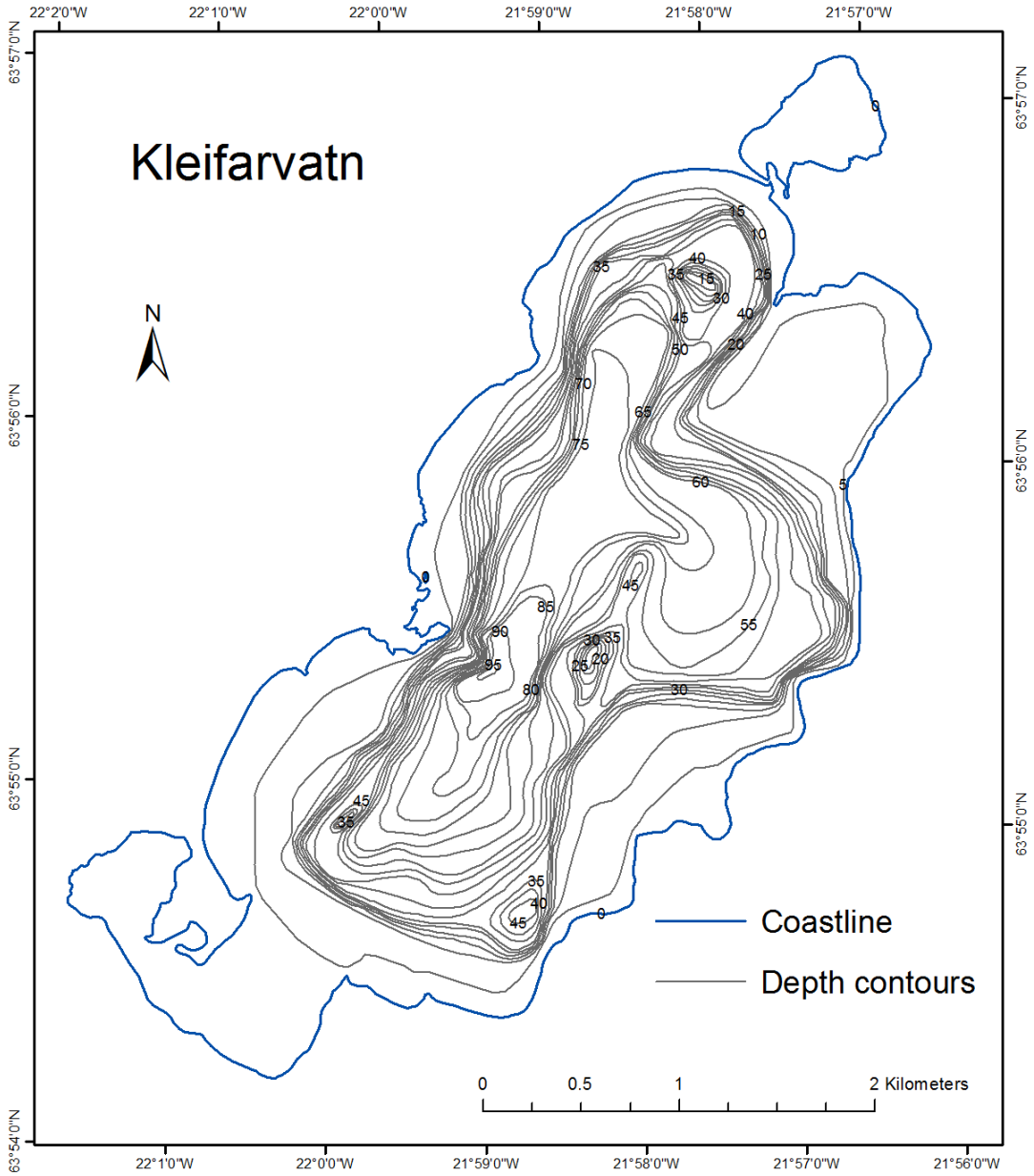

Figure 12. Bathymetric map of Kleifarvatn made from data gathered by Rist (1975). Map was later digitized by the Meteorological office in Iceland. Redrawn by Árni Friðriksson.

a singlebeam echo sounder (Rist, 1975). He measured profiles across the lake and compiled them to make a bathymetric map of the lake bottom (Figure 12). Morales (1992) interpreted the bathymetry of the lake bottom in Kleifarvatn and the area around the lake (Figure 13). Numerous faults are present in the surroundings of the lake and therefore most likely on the lake bottom as well. Syðri-Stapi is an outlet of hyaloclastite to the southeast from Sveifluháls hyaloclastite ridge. Just southeast of Syðri-Stapi is the deepest part of Kleifarvatn. A few prominent features are present on the lake bottom, including elongated hills/ridges and depressions. One crater-like depression is present in the southeast corner of the lake. The hills are all elongated NE-SW as the lake itself. The hyaloclastite/pillow lava ridge of Lambhagi (in the northeast) is considered to extend into the lake, even as far south as Syðri-Stapi. Flat shoals extending out to depths of 10-15 m are present along most of the western and southern shores, part of the eastern shore (southwest of Vatnshlíð) and in the NE-corner of the lake, south of Lambhagi. These shoals are considered to have formed by streams which have run into the lake, except for the western side of Kleifarvatn which is most likely formed by sediments from Sveifluháls.

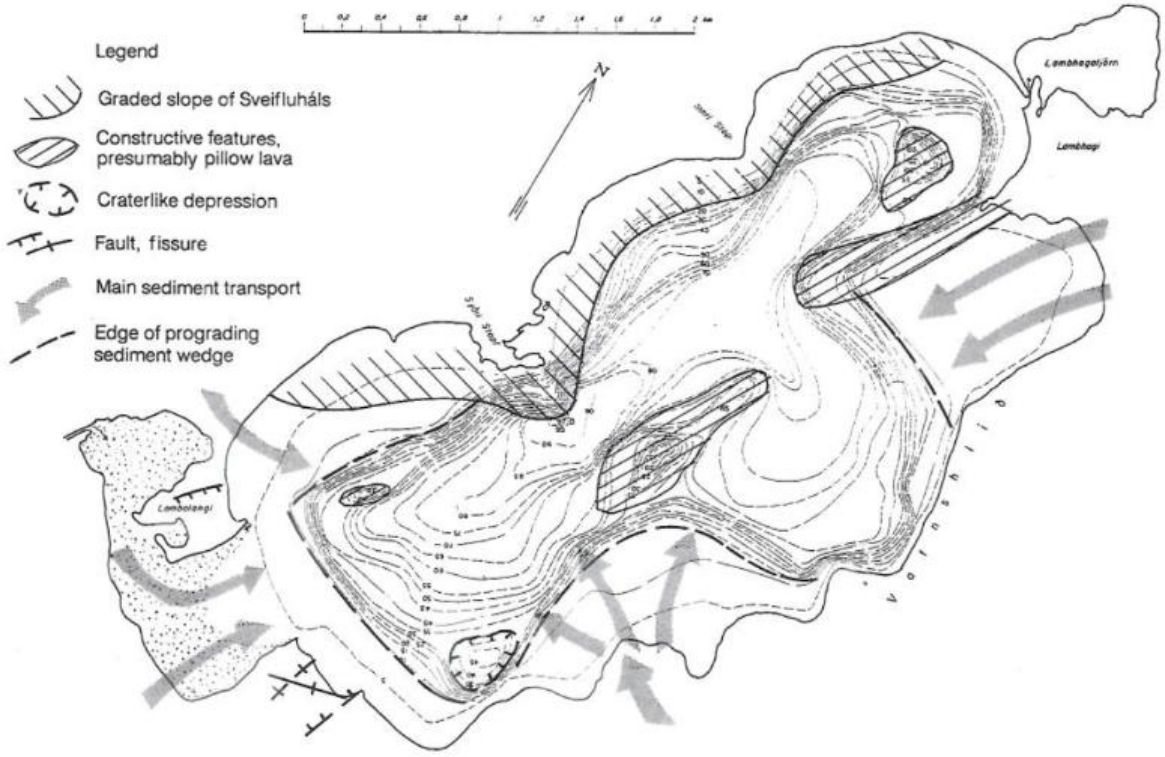

Figure 13. Interpretation of the bathymetry of Kleifarvatn by Morales (1992). Note the shallow shoals in the northeast and south parts of the lake and NE-SW direction of the entire depression.

4 Materials and methods

4.1 Study area

The study area consists of three lakes in Iceland, Öskjuvatn in central Iceland, Thingvallavatn in southwest Iceland and Kleifarvatn on the Reykjanes Peninsula in southwest Iceland. Refer to chapters 3.2 through 3.4 for more information about the study areas. During the surveys of Öskjuvatn, Kleifarvatn and Thingvallavatn, contour maps of the lakes from Rist (1975) were used as guidelines. Areas shallower than 4-6 meters deep were generally not surveyed. Öskjuvatn was surveyed nearly to its shore and almost completely covered. Unfortunately, weather conditions did not allow for further measurements and therefore a portion of the lake in the southeast part was not surveyed. Wind speed gradually increased during the survey of Öskjuvatn which added uncertainty to the data. Problems with the maximum depth in the instruments resulted in loss of data in the northeast part of the lake. More uncertainty was added to the data where geothermal areas occur at the lake floor due to air bubbles rising through the water column. They affect the acoustic waves and may result in inaccurate depth measurements. Kleifarvatn was also surveyed nearly to its shore apart from areas shallower than 4-6 meters. Those are areas with extensive beaches into the lake. A relatively small part of Thingvallavatn was surveyed, area comparative to Kleifarvatn in size. This area covers the bay of Hestvík and north to Sandeyjardjúp, west of the island Sandey. A few separate profiles were surveyed additionally.

4.2 Research equipment

A 5 meter long survey vessel was used to survey the three previously mentioned lakes in the summer and fall of 2012 and in the fall of 2013. The multibeam echo sounder mounted in the survey vessel is Simrad EM3002 from Kongsberg Maritime. The echo sounder consists of a *sonar head (transducer), processing unit, hydrographic working station, MRU (motion detector), GPS system, sound velocity probe and a display screen*. A few operational specifications are listed in Table 2. Most of these specifications can be altered during operating time, e.g. the depth range can be set to a specific value and the angular

coverage can be increased/decreased on one side or both sides simultaneously (Kongsberg, 2006). The operating program for the Simrad EM3002 is called SIS (Seafloor Information Systems).

CARIS Hips & Sips 8.1 software was used to process the bathymetric, backscatter imagery and water column data from the surveys of Öskjuvatn, Thingvallavatn and Kleifarvatn. Water column data was only collected in Thingvallavatn and a small portion of Kleifarvatn. No water column data was collected in Öskjuvatn. ArcGIS 10.1 is software from ESRI which is used to analyse, edit and create geographical features. It was used to create geologic, bathymetric and backscatter intensity maps of the survey area.

*Table 2. Operational specifications of the Simrad EM3002 multibeam echo sounder. *Equidistant means that the beams are spread evenly by distance (meters) over the swath. Equiangular means that the beams are spread evenly over the swath by the angle of transmission e.g. 1 beam for 1 degree.*

Specification	*Value*
Name	Simrad EM3002
Frequency	300 kHz
Depth range	From < 1 meter to > 200 meters
Number of soundings per ping	Max 254
Beam spacing	Equidistant or equiangular*
Maximum ping rate	40 Hz
Maximum angular coverage	130 degrees
Depth resolution	1 centimeter
Transducer geometry	Mills Cross

4.3 Methods and measurements

Properties of the surveys of each lake are shown in Table 3. Kleifarvatn was the first lake to be surveyed and Thingvallavatn the last (Table 3). Straight survey lines provide the most consistent coverage of the lake floor whereas sharp turns of the research vessel result in partially less coverage of the lake floor. As more surveys are conducted, more experience is gained, therefore Thingvallavatn was surveyed with the best technique and provided the best results. The first thing that was done during each survey was to make a *sound velocity profile* through the water column. The processing unit uses it to calculate precise paths for

each beam and its echo. Next the system was calibrated for heading, roll, pitch and sound velocity. The technique used for calibration not explained here but it is very important for obtaining correct depth measurements. All three lakes were surveyed with the same technique except Thingvallavatn which was surveyed at less speed than Öskjuvatn and Kleifarvatn for better resolution.

Table 3. Survey properties for Öskjuvatn, Thingvallavatn and Kleifarvatn.

Operation	*Öskjuvatn*	*Thingvallavatn*	*Kleifarvatn*
Survey date	9th Sept. 2012	8th, 18th, 20th, 22nd and 23rd Nov. 2013	19th-20th June and 14th Nov. 2012
Data collected	Bathymetry and backscatter	Bathymetry, backscatter and water column	Bathymetry, backscatter and partly water column
Wind speed	Gradually increasing during the day	Low	Low
Survey speed	~5 knots	2-4 knots	~5 knots
Angular coverage	120 degrees	70-120 degrees	120 degrees
Ping rate	40 Hz	40 Hz	40 Hz
Beam spacing	Equidistant	Equidistant	Equidistant

Raw data files from the *hydrographic working station* were processed with CARIS Hips & Sips 8.1. In Hips & Sips 8.1 the raw data files were compiled to make bathymetric maps with various resolutions, depending on the resolution of the data and the recorded depth. Each measured profile consists of various numbers of pings, each and every one of which were checked for errors, which were then filtered out. Corrections for tidal effects, which only apply to oceans, and sound velocity were made before the profiles were merged to work together. Then Hips & Sips was used to calculate TPU (Total Propagated Uncertainty) to assign horizontal (HzTPU) and depth error (DpTPU) estimates to each sounding. A BASE (Bathymetry Associated with Statistical Error) surface is a georeferenced image with multi-attributed surface which can also contain visual representation of horizontal and vertical uncertainty (Caris, 2013). BASE surfaces using the CUBE (Combined Uncertainty and Bathymetry Estimator) method were compiled from

the merged profiles. Maps showing backscatter intensity were also compiled from the same data files and used with the bathymetry for bottom material interpretation. Hips & Sips has two processing engines, Geocoder and SIPS, which can be used to process backscatter imagery data. Most backscatter data processed in Hips & Sips is stored as GeoBaRs (Georeferenced Backscatter Rasters). The Geocoder engine with beam average (one measurement of average backscatter intensity for each beam) as source data type was used on all data sets. First, one GeoBaR was produced with automatic AVG and TVG corrections and strong despeckle. From this GeoBaR a beam pattern correction file was produced. Beam pattern correction removes acoustic artifacts caused by imperfections in the echo sounder (Caris, 2013). GeoBaRs were produced for all survey lines using the appropriate beam pattern correction files. Complete mosaics were then produced from the GeoBaRs. The 3D module of Hips & Sips 8.1 was used to view the data from different angles with various levels of shading and vertical exaggeration. The mosaics were draped on top of BASE maps in 3D view, that way both bathymetric and backscatter intensity data could be viewed at the same time in 3D which allowed for visual interpretation of the data.

ArcGIS 10.1 was used for generation of maps which are presented in chapter 5. Bathymetric maps and backscatter intensity maps were exported from Hips & Sips as ASCII files and regenerated in ArcMap with the *Topo to Raster* tool. Geologic maps were generated from the bathymetric and backscatter intensity maps using ArcMap. Polygons were generated for each geologic feature found on the floor of each lake. Faults and thermal features (solfataras) were mapped with lines and dots respectively.

5 Results

In this chapter maps will be presented showing bathymetry, backscatter intensity and geology of Öskjuvatn, Thingvallavatn and Kleifarvatn. To simplify, landslides and debris avalanches were mapped as one category in all of the following geologic maps. Table 4 shows values for total areas, lake levels and maximum depths of Öskjuvatn, Thingvallavatn and Kleifarvatn. It also presents values from volume calculations of the lakes. Thingvallavatn is the largest lake by area but less than 10% of it was surveyed. According to the bathymetric measurements of 2012 the greatest depth of Öskjuvatn is 244.5 m, measured in a solfatara, compared to 217 m measured by Rist (1975). He also measured Thingvallavatn to be 114 m deep and Kleifarvatn to be 97 m deep. Based on the values in Table 4 Thingvallavatn is 112 m deep, with the lake level at 103 m.a.s.l., and Kleifarvatn is 89.5 m deep, with the lake level at 135 m.a.s.l.

All maps in this chapter were produced using ArcMap 10.1 but other images showing more detailed features are directly from Hips & Sips. Detailed bathymetric maps in A3 size exported from Hips & Sips are displayed as an appendix of this thesis.

*Table 4. Values for area (total and surveyed), volume, depth and lake level. Values for surveyed areas, volume and maximum depths are from bathymetric surveys by the author of this thesis. Values for lake levels and areas are from the National Land Survey of Iceland (Iceland, 2011). *Areas with no data may result in inaccuracy of volume estimations. **Maximum depth of 244.5 m in Öskjuvatn might be the result of inaccurate measurements due to geothermal activity. *** Lake level is based on data from the National Land Survey of Iceland.*

Lake	*Öskjuvatn*	*Thingvallavatn*	*Kleifarvatn*
Lake level (m.a.s.l.)	1053	103	135
Area (km^2)	11.5403	82.065	7.3615
Area surveyed (km^2)	9.3917	7.5884	5.6442
Volume (km^3)	1.3394*	0.511*	0.256
Max depth recorded (m)	244.5**	112	89.5
Max. depth (m) (Rist, 1975)	217	114	97
Lake level (m.a.s.l.) (Rist, 1975)	1050	100.5***	140

5.1 Öskjuvatn

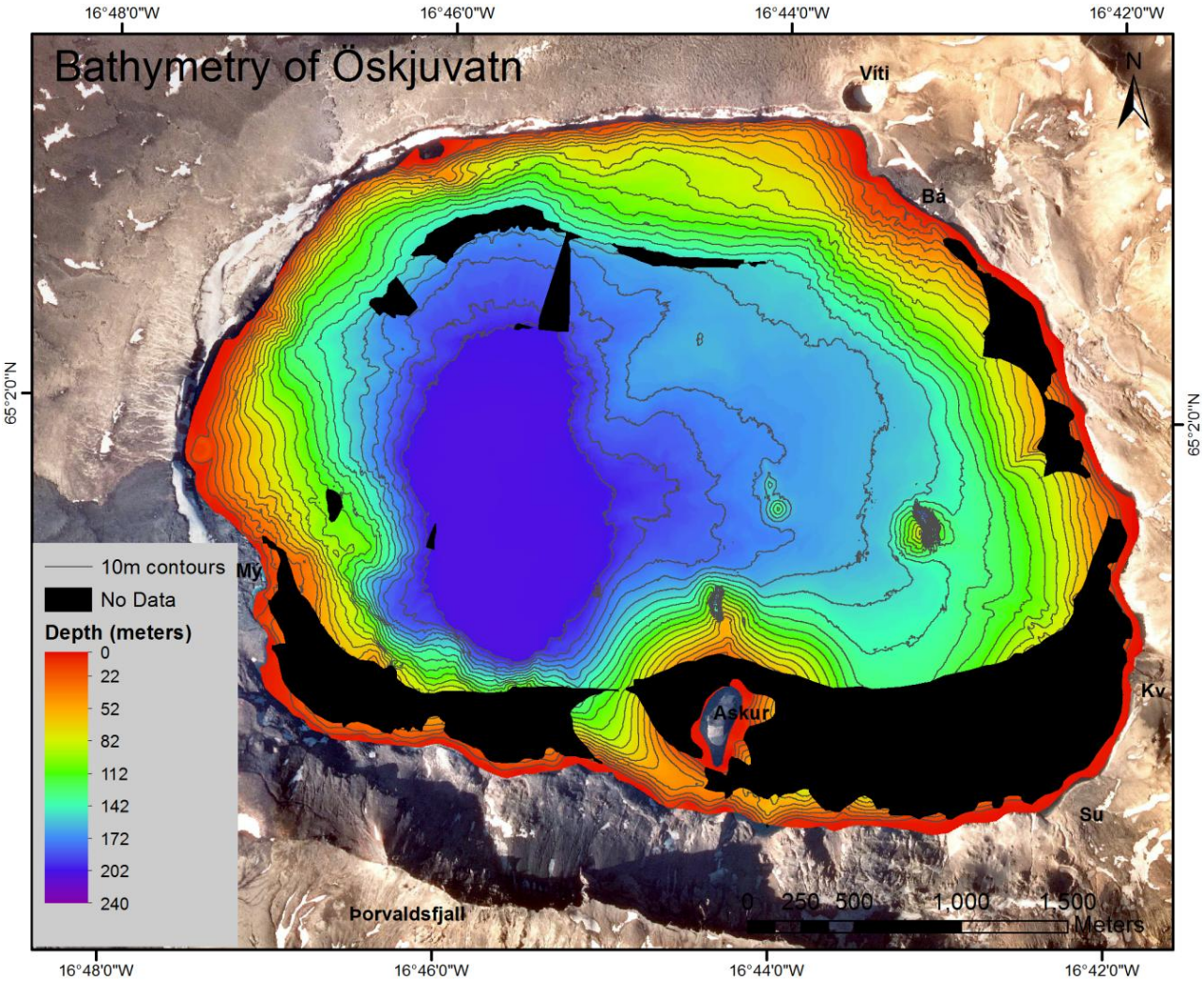

Figure 14. Bathymetric map of Öskjuvatn with 10 meter contours. Black represents areas with no data acquired. Bá (Bátshraun), Kv (Kvíslahraun), Su (Suðurbotnahraun), Mý (Mývetningahraun). Horizontal resolution of bathymetry is 2 meters. Surrounding is an aerial photograph from Loftmyndir ehf.

Not much was known about the subsurface of Öskjuvatn prior to the bathymetric survey of 2012, except for the approximate depth and structure of the bottom (Rist, 1975). Figure 14 presents the features of the lake bottom, colour coded and with 10 meter depth contours. Many unknown features are revealed on this map and in Figure 15, where the backscatter intensity of the lake bottom is presented. Figure 16 presents a geologic map of Öskjuvatn where the bathymetry and backscatter intensity data were used as guidelines. The survey of 2012 clarifies many things such as lava extendings into the lake, structure of subsurface features, accurate depth and morphology of the subaqueous parts of the Öskjuvatn caldera.

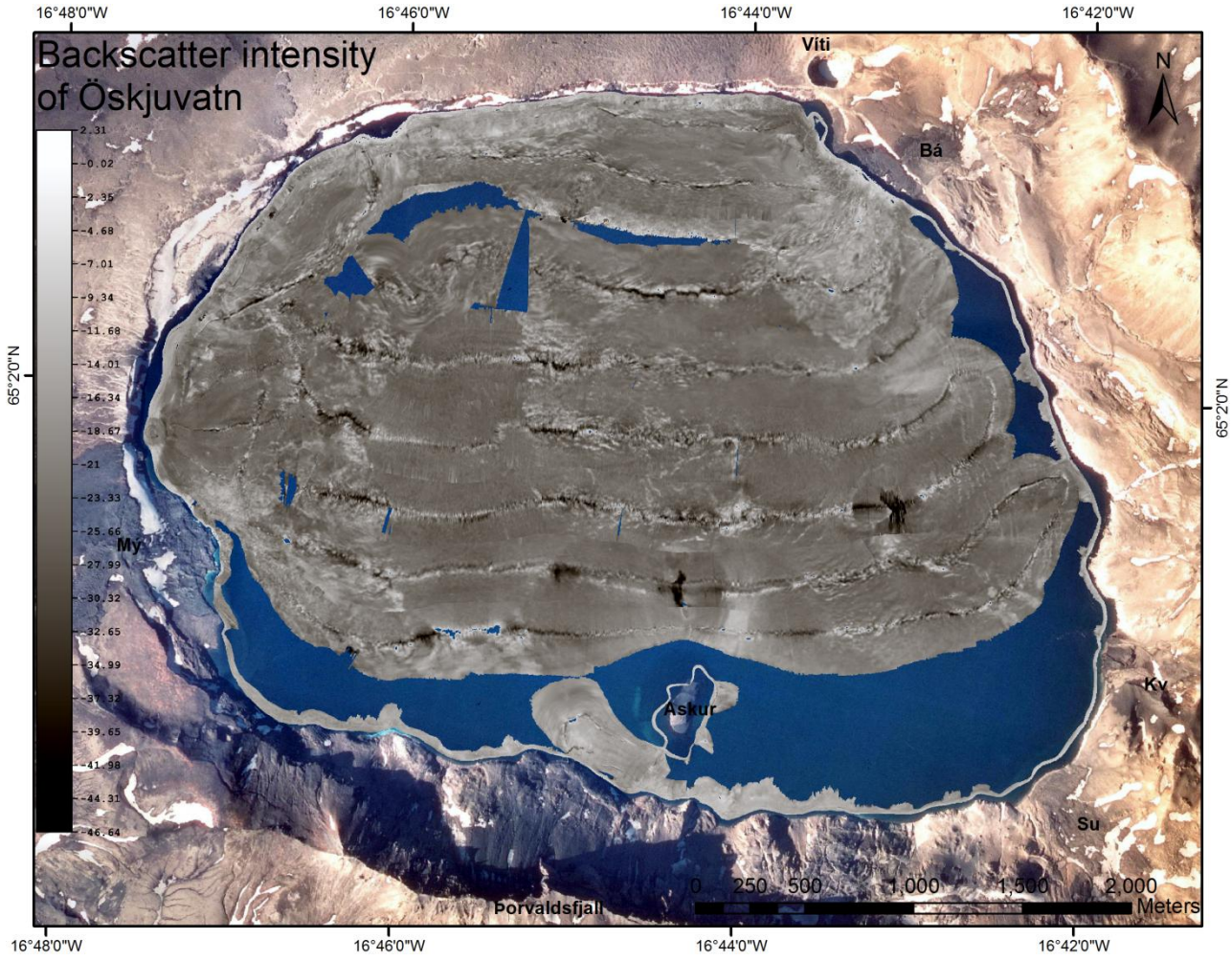

Figure 15. Backscatter intensity map of Öskjuvatn. Units of backscatter intensity are described in decibels. Labels surrounding the lake are the same as in Figure 14. Horizontal resolution of backscatter data is 2 meters. Surrounding is an aerial photograph from Loftmyndir ehf.

5.1.1 Volcanic features

The floor of Öskjuvatn is largely occupied by volcanic features such as craters, tephra and lavas.

Askur volcano

The island Askur was formed in a phreatomagmatic eruption in 1926 (Þ. Einarsson, 1962). It's mainly made up of one cinder cone but bathymetric data reveal a much larger footprint of the entire volcano. Its footprint is approximately 1-1.5 km^2 but cannot be accurately measured due to lack of data. The Askur tephra appears to be much smoother than the

surrounding terrain and is thus distinguishable from other features. A crater is apparent on the northern flank of Askur volcano.

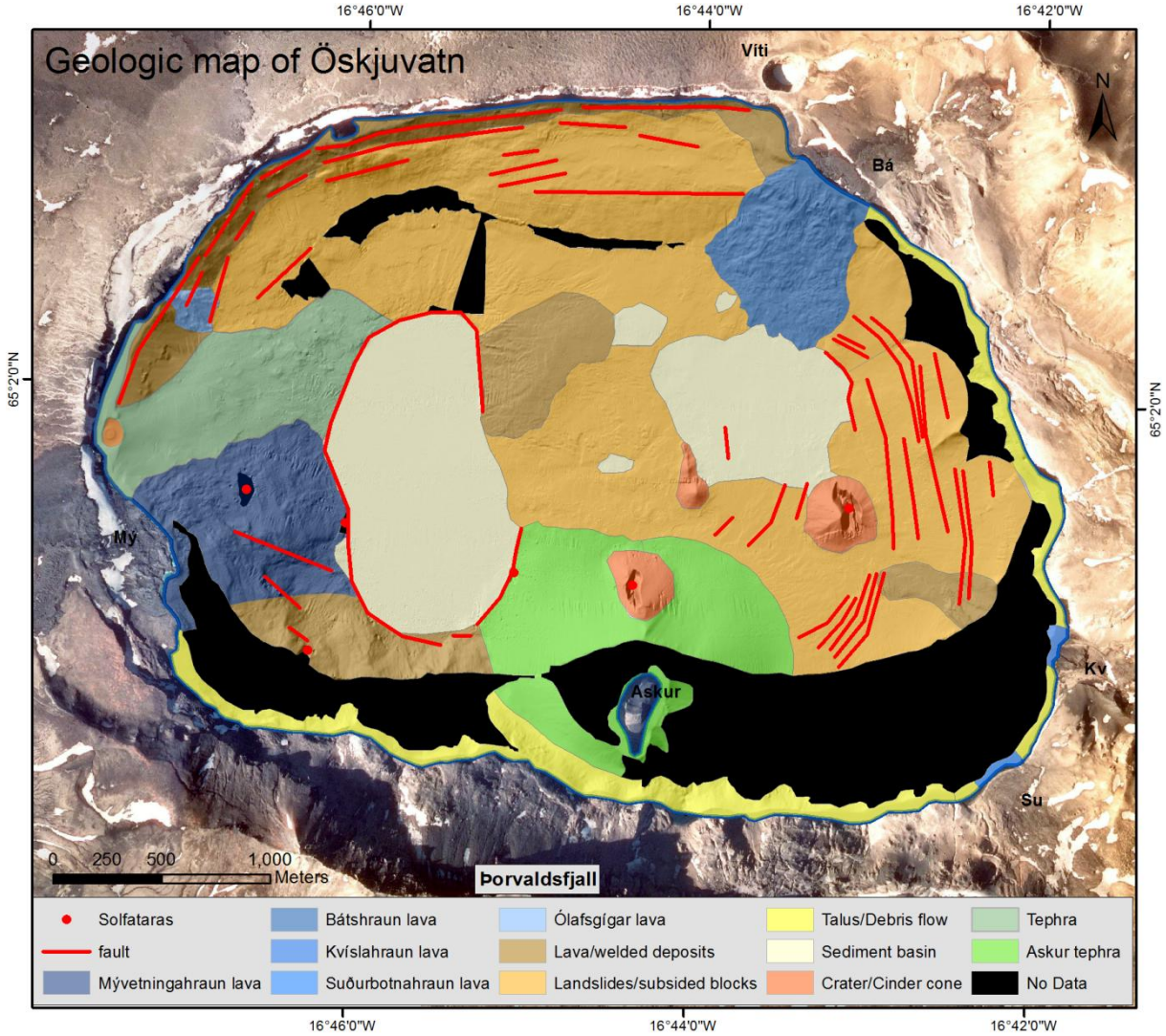

Figure 16. Geologic map of Öskjuvatn draped on a shaded relief map illuminated at 315° azimuth and 45° elevation. Labels surrounding Öskjuvatn are the same as in Figure 14. Horizontal resolution is 2 meters. Surrounding is an aerial photograph from Loftmyndir ehf.

Bátshraun lava

Bátshraun lava was formed in a fissure eruption in 1921 (Figure 14 and Figure 17). The lava entered Öskjuvatn in a narrow stream and was spread all the way to a depth of ~160 meters. The lava front can be traced underwater from where it reaches the lake and all the way to its farthest extent. It appears very rough in the bathymetric data and backscatter intensity data. Its subaerial part has surface area of 0.163 km^2 (Hartley & Thordarson,

2012) but the subaqueous part has surface area of 0.4 km^2. The total extent of the lava flow is thus 0.563 km^2.

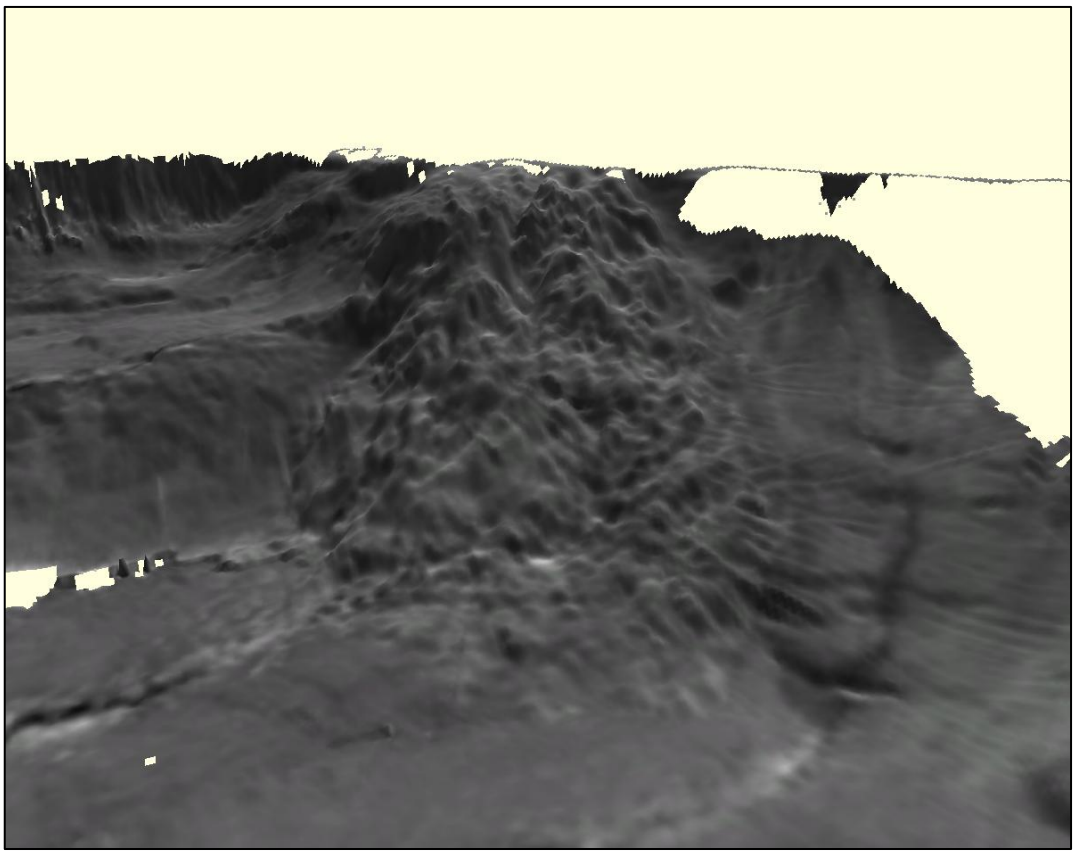

Figure 17. Bátshraun lava seen from south. Backscatter image draped on top of bathymetry with 3x vertical exaggeration. Horizontal resolution is 2 meters. Light source is at 0°N and 60° elevation.

Mývetningahraun lava

Mývetningahraun lava was formed in a fissure eruption in Suðurskörð in the central southern margin of Askja caldera. It spread to the north over an area of 2.062 km^2 and entered Öskjuvatn on its southwestern side (Hartley & Thordarson, 2012). The appearance of the subaqueous part of Mývetningahraun lava is very similar to that of Bátshraun lava, very rough. The tip of the Mývetningahraun lava flow reached 200 meters depth but its margins are harder to follow than those of Bátshraun lava. The surface area of the subaqueous part of Mývetningahraun lava is at least 0.536 km^2 which makes the total surface area approximately 2.6 km^2. Lack of data could result in an underestimation of its extent.

Ólafsgígahraun lava

Lava which originated in Ólafsgígar in the western caldera wall of Öskjuvatn was not known to have flowed into the lake but it is quite easily observed. Its margins are quite clear and it covers 0.037 km^2 underwater. It flowed down to a depth of 135 meters and has a maximum thickness of approximately 20 meters. The lava flow has the same subaqueous appearance as Bátshraun lava and Mývetningahraun lava.

Kvíslahraun and Suðurbotnahraun lavas

Kvíslahraun and Suðurbotnahraun lavas were erupted in the southeast corner of Öskjuvatn caldera in 1922/23. Both lavas reached the lake surface but their extent cannot be estimated due to lack of bathymetric data in the southeast corner of the lake.

Craters and cones

Two unknown craters or cinder cones are apparent in the central and western part of Öskjuvatn. From this point they will be known as Eastern cone and Western cone. The Western cone reaches 40 m above the caldera floor and the Eastern cone reaches 85 m above its base. The Western cone seems to be a part of a small volcanic ridge that is 10-20 m high and 150 m long. The cones appear quite smooth in the backscatter intensity data but the volcanic ridge has lava-like appearance.

A crater is present on the northern flanks of Askur volcano, associated with a solfatara. The crater does not have different backscatter properties than the rest of the Askur volcano indicating that the Askur tephra is also covering the crater. Thus the crater must be older than 1926. This crater was most likely formed when Caroc made his measurements in 1876 (Figure 8). According to his findings there was a crater and a solfatara in the foothills of Thorvaldsfjall mountain just south of the small lake occupying the caldera collapse.

A small triple crater is visible at 6 m depth just north of Mývetningahraun lava near the western margin of Öskjuvatn (Figure 18). The crater is around 10 m deep and 130 m across. The rims of the crater are made up of coarser material than the flanks according to the backscatter intensity data. This crater was not known before. Tephra from this crater is found underwater mainly to the east of it. The tephra flowed down the western caldera wall and all the way down to the large sediment basin. It flowed over parts of the Mývetningahraun lava which makes it younger than 1922. It also flowed over some

collapsed parts of the Ólafsgígar craters, just north of the easternmost part of Mývetningahraun lava.

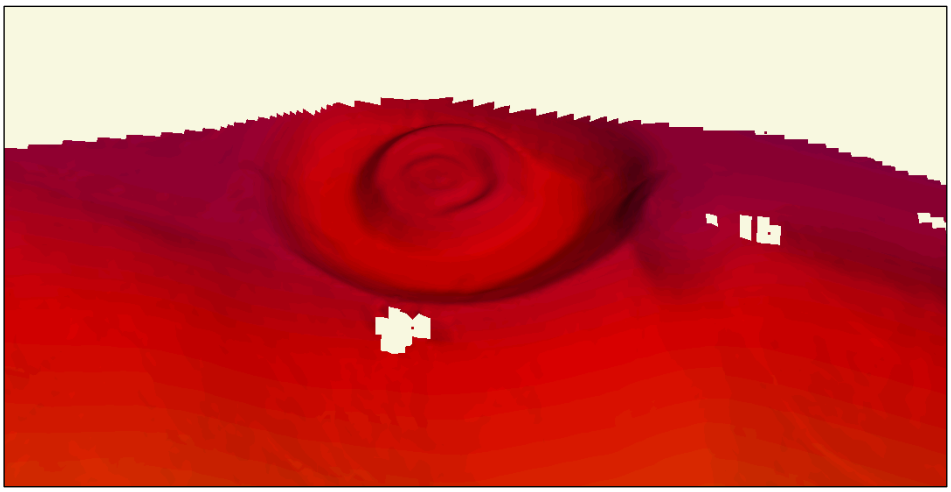

Figure 18. A triple explosion crater in the western part of Öskjuvatn. Purple represents shallow. 4 meters is shallowest. 2x vertical exaggeration and horizontal resolution is 2 meters.

5.1.2 Sediment ponds and basins

Two large basins of the lake floor and several other smaller ponds have smooth, nearly flat surfaces and very uniform backscatter (Sediment basin in Figure 16). These basins are made up of fine grained sediment deposited below slopes of landslides, debris avalanches/flows and taluses. The large sediment basin in the western part of the lake floor will be referred to as Great basin. Similarly, the basin in the Eastern part, just South of Bátshraun lava, will be referred to as East basin. Three smaller sediment ponds were observed on the central and northern part of the lake floor. They were most likely all formed in depressions where flow of fine sediment continued after large landslides or debris flows occurred.

5.1.3 Thermal features

Solfataras are present in six locations on the Öskjuvatn caldera floor, mainly in its southern part. Thermal activity was observed by the multibeam echo sounder as columns of reflections in the water column while surveying the lake. Solfataras are marked by red dots in Figure 16 and in some places coincide with areas where patches of data either are

missing or shown as deep holes. One solfatara is present on the eastern flank of the Eastern crater, at about 100 m depth. Another one is present on the northern flank of Askur volcano. It occupies a crater which cuts out of the flank of the volcano. Another solfatara is present just northwest of Askur volcano, on the southeast margin of the Great basin. One solfatara is present on the western margin of the Great basin, at ~200 m depth, and one is present near the southwest corner of Öskjuvatn at 70 m depth. The last solfatara is located at 105 m depth in Mývetningahraun lava, midway between the Great basin and the shore of Öskjuvatn. In the winter a big hole in the ice has often been observed in the same place as this solfatara, it is thus likely the most powerful one on the lake floor.

As mentioned before, depth measurements in the solfataras are not very accurate due to rising air bubbles. Depth of 244.5 m measured in a solfatara on the eastern margin of the Great basin may be due to inaccuracy in the measurements and should be viewed with caution.

5.1.4 Faults

Large quantities of faults were observed in the Öskjuvatn caldera. Most of them represent steeply inward-dipping ring fractures which are typical for caldera collapse (Gudmundsson, 1998). All the faults face to the centre of greatest collapse, i.e. the western central part of the lake. The majority of the faults are located in the northern and eastern caldera walls, to the west and southeast of Bátshraun lava. The faults in the foothills of Austurfjöll represent step-wise faulting whereas the faults in the northern caldera wall are larger and less organized. The Great basin is bound on almost all sides by faults facing towards the centre of it, indicating the focus of subsidence. The largest fault observed is an E-W striking fault just west of Bátshraun lava, with a throw of 65-70 m. Very few faults are visible in the southern caldera walls, likely due to lack of data and presence of eruptive features.

5.1.5 Caldera walls

The morphology of the shore of Öskjuvatn varies depending on the location around the lake. The lake is bounded by 40-50 m high cliffs on the northern side, west of Víti, and on the western side to the area where Mývetningahraun lava enters it. The southern shore is mostly made up of cliffs and taluses whereas the northeastern and eastern shores are made up of landslides, subsided blocks of Austurfjöll and debris avalanches.

Lavas and welded deposits

Outcrops of pre-caldera lavas and welded post-1875 deposits do not appear as bright as expected in the backscatter intensity data, probably because they are mostly covered with thin layers of sediment. Most of the Öskjuvatn caldera wall from Víti in the east to Ólafsgígar in the west displays exposed lavas or bedrock down to 40-80 m depth. It's also present between Ólafsgígar and Mývetningahraun lava. A 150-200 m wide and 1 km long zone of exposed bedrock of Thorvaldsfjall is present at 80-200 m depth between Askur volcano and Mývetningahraun lava. A 0.21 km^2 area of exposed bedrock is present in the central part of the Öskjuvatn caldera floor. This area is rougher than the surroundings and rises a few meters above its surroundings. This area might be a part of the subsided caldera floor of Askja caldera. It might also be a body of rhyolitic lava intruded into the Askja volcano.

Talus/Debris flows

Talus and debris flows occupy the southern and eastern caldera wall from Mývetningahraun lava north to Víti, except for three locations where Bátshraun, Kvíslahraun and Suðurbotnahraun enter Öskjuvatn. Taluses and debris flows represent relatively smooth, uniform and steep landscape. They are mostly made up of breccia, gravel and sand which have fallen from the flanks of Thorvaldsfjall and Austurfjöll.

5.1.6 Landslides and subsided blocks

Landslides and subsided blocks of pre-1875 lavas occupy areas of approximately 3.6 km^2 of the 11.5 km^2 area occupied by Öskjuvatn. Landslides, subsided blocks and debris avalanches were mapped as one unit in Figure 16. Landslides are characterized by hummocky landscape (Charles R Bacon et al., 2002) as is seen in the northern caldera wall of Öskjuvatn caldera. Enlargement of the caldera to the northwest (Hartley & Thordarson, 2012; Ó. Jónsson, 1942) must be a consequence of landslides, subsiding blocks, rockfalls and debris avalanches observed below the northwestern rim of the Öskjuvatn caldera. The eastern part of the lake floor of Öskjuvatn is largely occupied by debris avalanches, similar to the flanks of Austurfjöll. The topography is relatively smooth and the backscatter relatively uniform in large areas. Based on the reconstruction of Austurfjöll prior to the 1875 eruption made by Hartley & Thordarson (2012), large blocks of rocks from Austurfjöll mountains have subsided into the present day Öskjuvatn caldera.

5.1.7 Eruption volumes

Eruption volumes for Bátshraun, Mývetningahraun and Ólafsgígahraun lavas are shown in Table 5.

*Table 5. Calculated eruption volumes for the lavas erupted post-1875 that extend into Öskjuvatn. No coverage or volume calculations were done for Suðurbotnahraun and Kvíslahraun through lack of bathymetric data. Subaerial coverage and thickness of lavas are from Hartley and Thordarson (2012). Same thickness was used for subaqueous areas as for subaerial. *Thickness of Ólafsgígahraun was estimated from bathymetric data and Hartley and Thordarson (2012).*

Eruption	*Area (subaerial + subaqueous) (km^2)*	*Thickness (m)*	*Total erupted volume (km^3)*
Bátshraun	0.163 + 0.4 = 0.563	5	0.0028
Mývetningahraun	2.062 + 0.536 = ~2.6	5	0.0130
Ólafsgígahraun	~0.01 + 0.037 = 0.047	5*	0.0002

Five lavas are known to have run into Öskjuvatn including Bátshraun, Mývetningahraun, Kvíslahraun, Suðurbotnahraun and Ólafsgígahraun lavas (Figure 16). Hartley and Thordarson (2012) calculated the eruption volumes for these lavas, except Ólafsgígahraun, but lack of evidence about their subaqueous coverage resulted in underestimate of the eruption volumes. More than 70% of Bátshraun and almost 80% of Ólafsgígahraun are subaqueous whereas the majority of Mývetningahraun is located subaerially.

5.2 Thingvallavatn

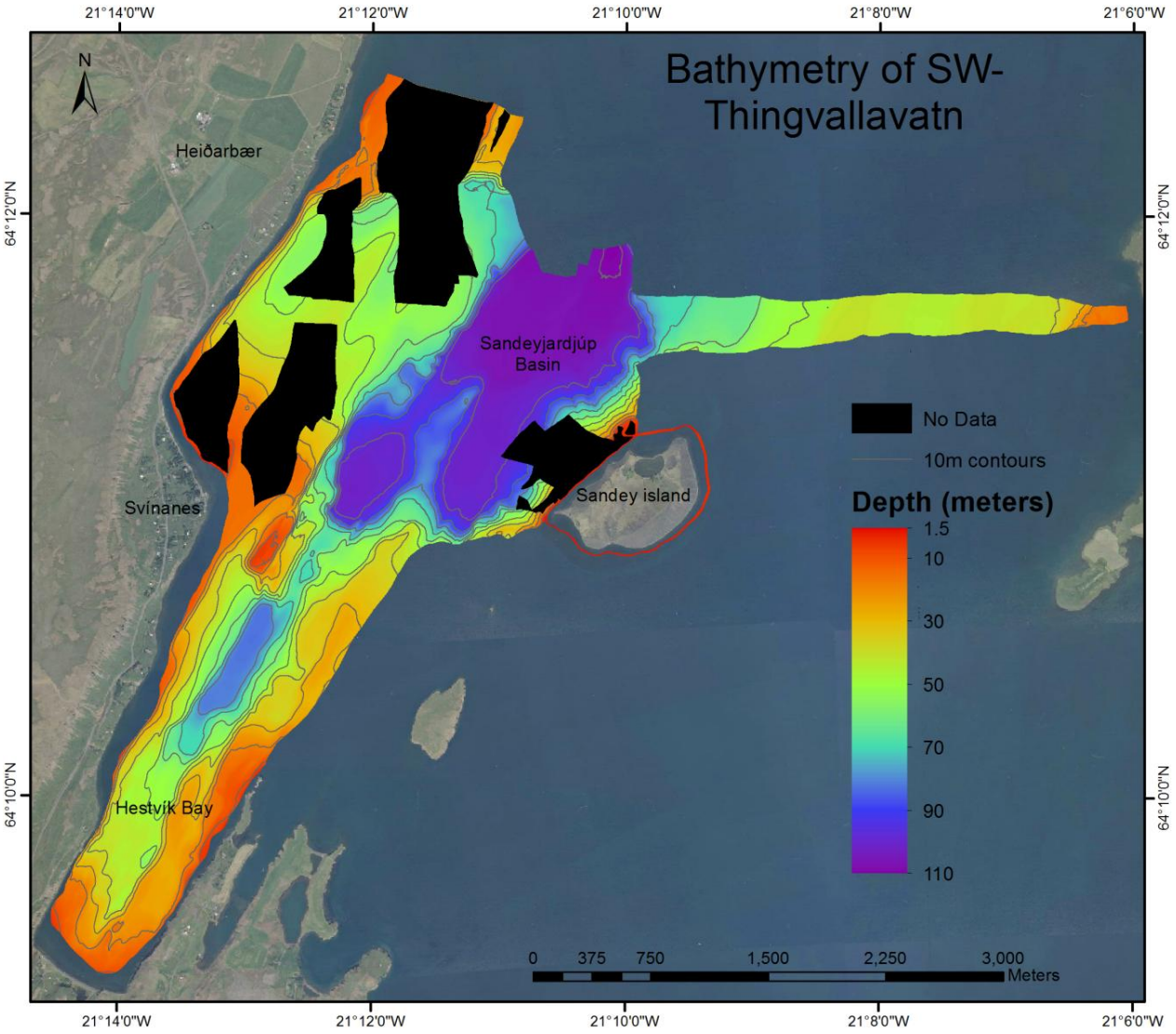

Figure 19. Bathymetric map of SW-Thingvallavatn with 10 meter depth contours. Black represents areas with no data acquired. Horizontal resolution of bathymetry is 2 meters. Surrounding is an aerial photograph from Loftmyndir ehf.

The properties of the lake floor of SW-Thingvallavatn were not known with much detail before the 2013 bathymetric survey (Figure 19). Though, a bathymetric survey done by Rist (1975) (Figure 10) and a sidescan survey by Thors (1992) (Figure 11) revealed some information about the major features of the lake floor. Figure 20 is a map which shows the backscatter intensity of the lake floor in the survey area. The data does not appear well in 2D view but in the 3D view it appears well. The bathymetric and backscatter intensity data were used to make a geologic map of the survey area in SW-Thingvallavatn (Figure 21).

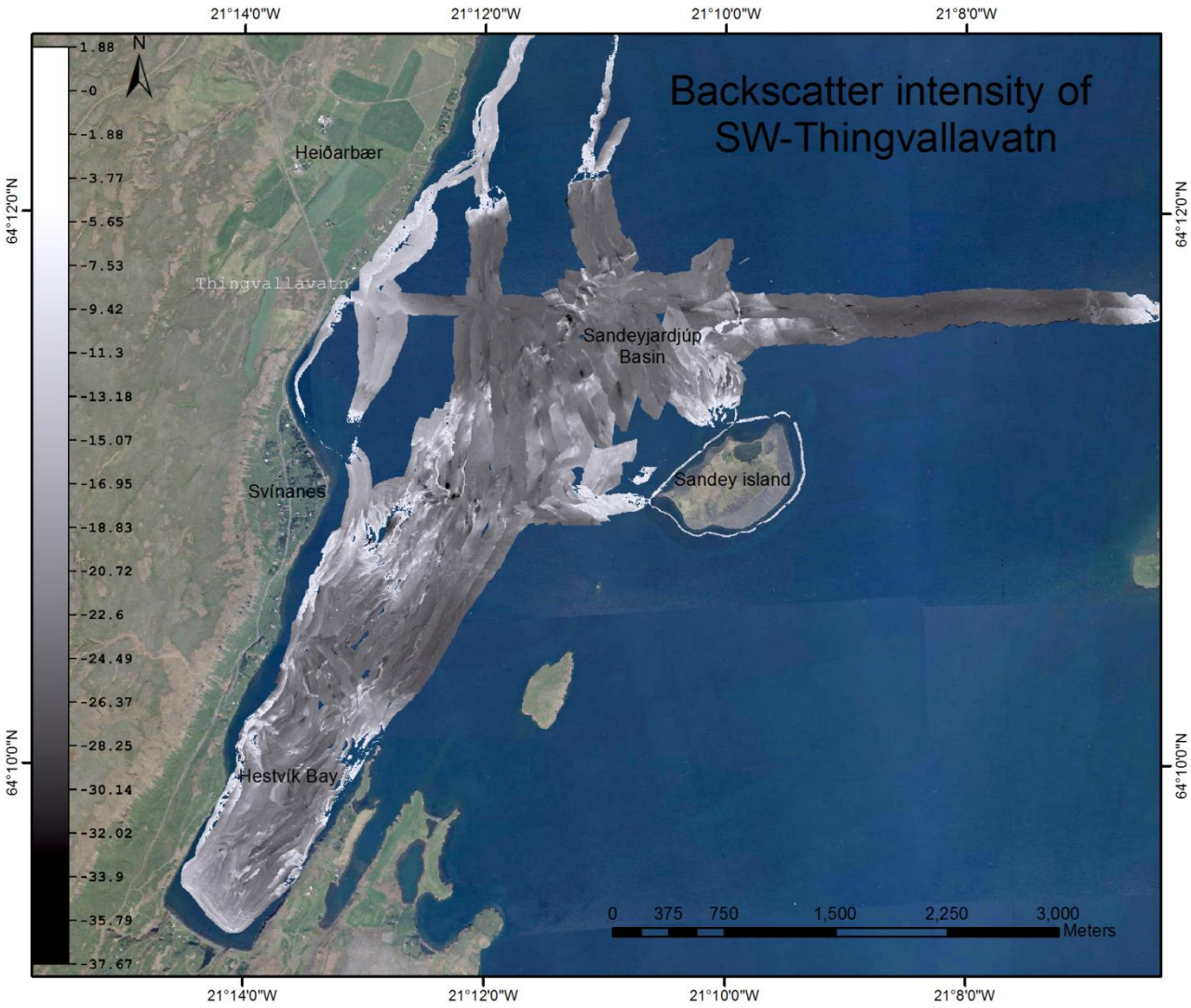

Figure 20. Backscatter intensity map of SW-Thingvallavatn. Horizontal resolution of backscatter data is 2 meters. Surrounding is an aerial photograph from Loftmyndir ehf.

5.2.1 Volcanic features

Sandey tephra

Great amount of tephra was erupted in the Sandey eruption, much of it only went as far as a few tens of meters and ended up on the flanks of the island. The tephra is characterized by low to medium high backscatter intensity and relatively smooth appearance. Coarse material reflects greater amounts of acoustic energy than fine material and therefore the tephra is classified into two categories, fine tephra and coarse tephra, depending on the backscatter intensity.

Flow channels were observed on the northern flanks of Sandey, where fine tephra has been washed down to Sandeyjardjúp basin and coarse tephra is exposed. In general, coarse tephra is found on the flanks near the lake surface and fine tephra on greater depths.

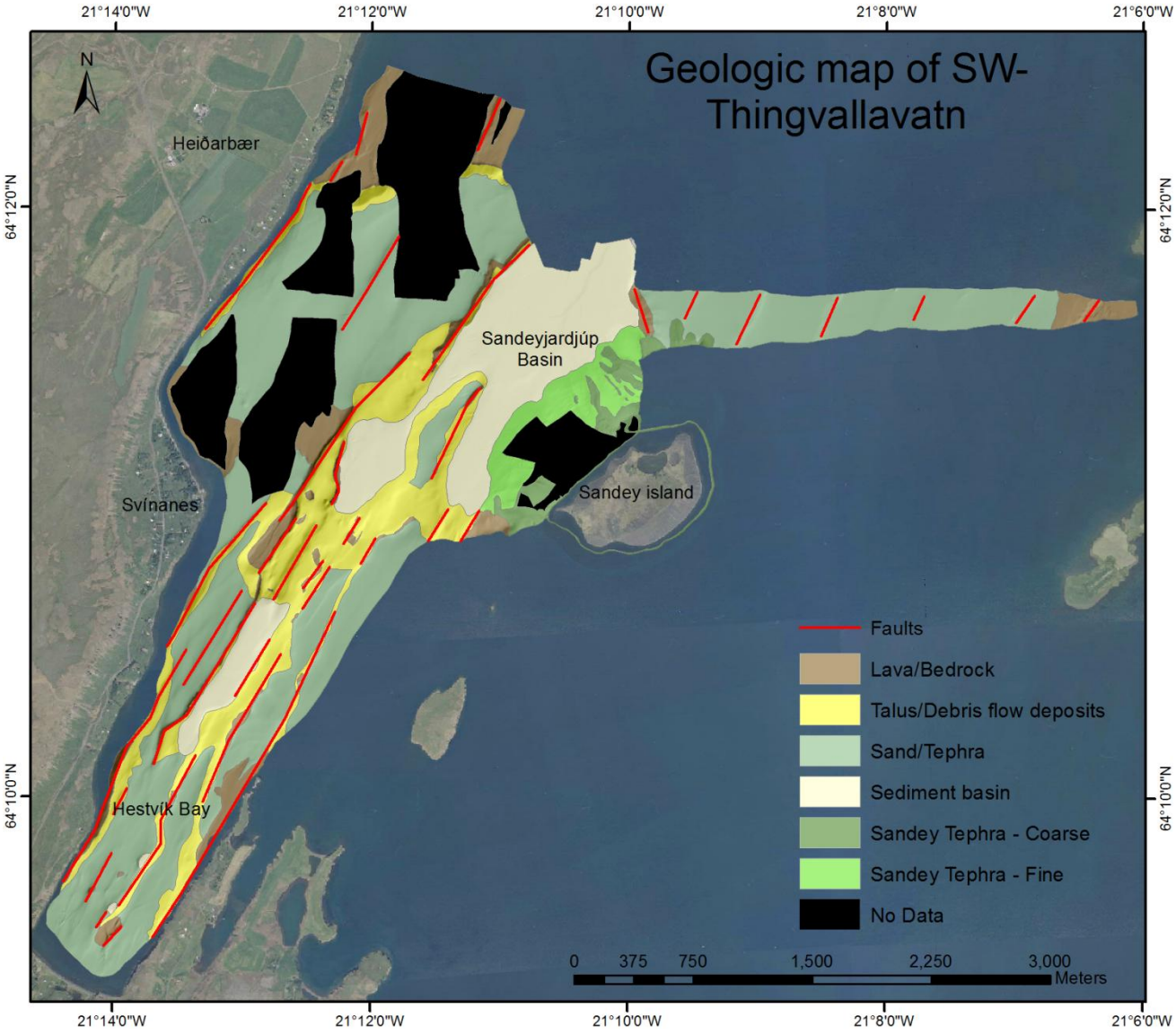

Figure 21. Geologic map of SW-Thingvallavatn draped on a shaded relief map illuminated at 315° azimuth and 45° elevation. Horizontal resolution is 2 meters. Surrounding is an aerial photograph from Loftmyndir ehf.

5.2.2 Faults

Thingvallavatn is located in a tectonically active area where extension of the Earth‘s crust takes place. Evidence of this extension can be found on all sides of Thingvallavatn and also on the lake floor (Sæmundsson, 1992; Thors, 1992). Figure 21 shows locations of faults on the lake floor, most of them had already been mapped by Thors (1992) and Bull et al. (2003) but the detailed bathymetric survey revealed more faults, some of them quite small and many of them are covered with sediment. These faults are all normal faults and make up the Thingvallavatn graben in a step-wise manner. The most prominent fault is the one on the northwestern side of Sandeyjardjúp basin, its segments continue over 3 km to the southwest (Figure 21 and Figure 23). This fault has maximum vertical throw of 45 m just north of Hestvík bay. Faults in Hestvík bay face east on the western side and west on the eastern side (Figure 22). The general rule for the faults in the research area is that faults east of Sandeyjardjúp basin face west and faults west of it face east. This applies if a imaginary line is drawn from Sandeyjardjúp and towards SSW through the middle of Hestvík.

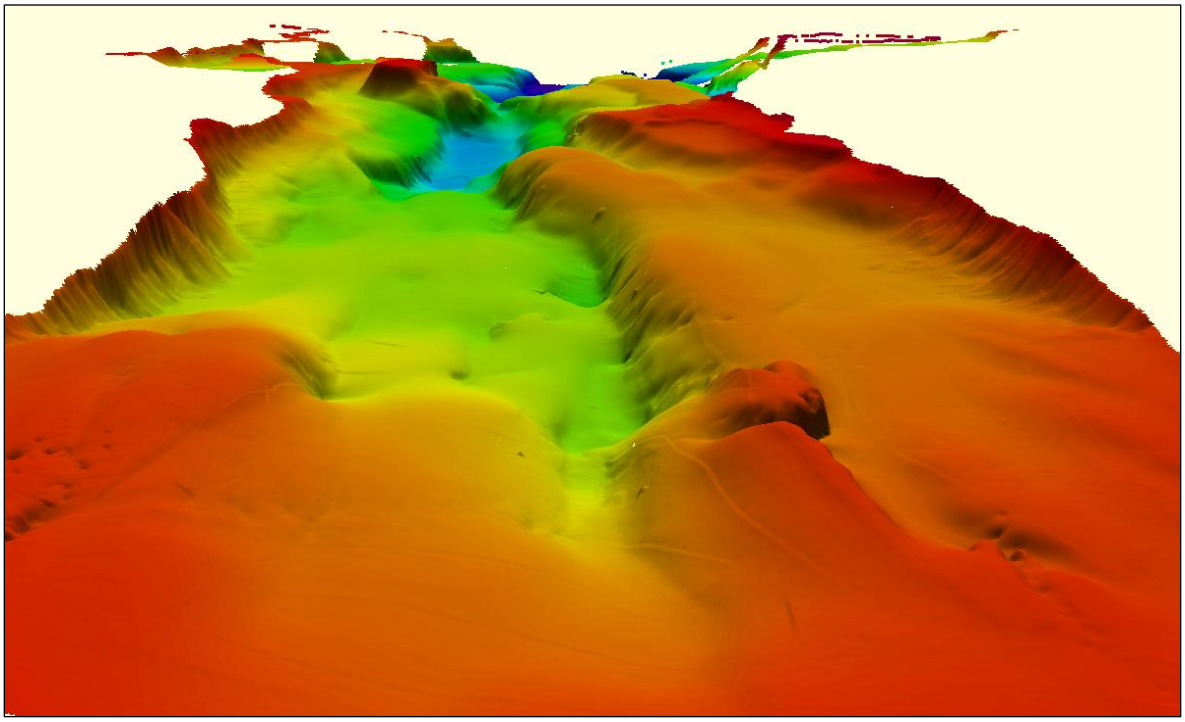

Figure 22. Normal faults facing east (left) and west (right) in Hestvík bay. Looking towards NNE with 2.5x vertical exaggeration. White represents areas with no data. Image is illuminated at 45° azimuth and 60° elevation.

5.2.3 Bedrock outcrops

Bedrock and lavas were discovered in several areas during the survey. The map in Figure 21 does not distinguish between lava flows and exposed bedrock. Bedrock outcrops are characterized by rough topography and various levels of backscatter intensity. These various levels of backscatter intensity are a result of the roughness of the bedrock/lavas.

The two survey lines measured to the north of Sandey across Thingvallavatn display exposed bedrock at the eastern side of the lake floor (Figure 20 and Figure 21). At greater depths than 40 meters it becomes buried with sediment. Exposed bedrock is also present furthest north in the research area. Just north and northeast of Svínanes exposed bedrock is present, some of it partly covered with a thin layer of sediment.

Outcrops of exposed bedrock are visible in various places in the bay of Hestvík and to the northeast of it (Figure 21). Most, if not all, of these outcrops are related to normal faults caused by extension of the crust in the area. The most prominent bedrock outcrop in the research area must be the large block east of Svínanes which towers up to 50 m over its surroundings with faults on both sides (Figure 19 and Figure 23). It is not visible on the map made by Rist (1975) but is mentioned by Thors (1992).

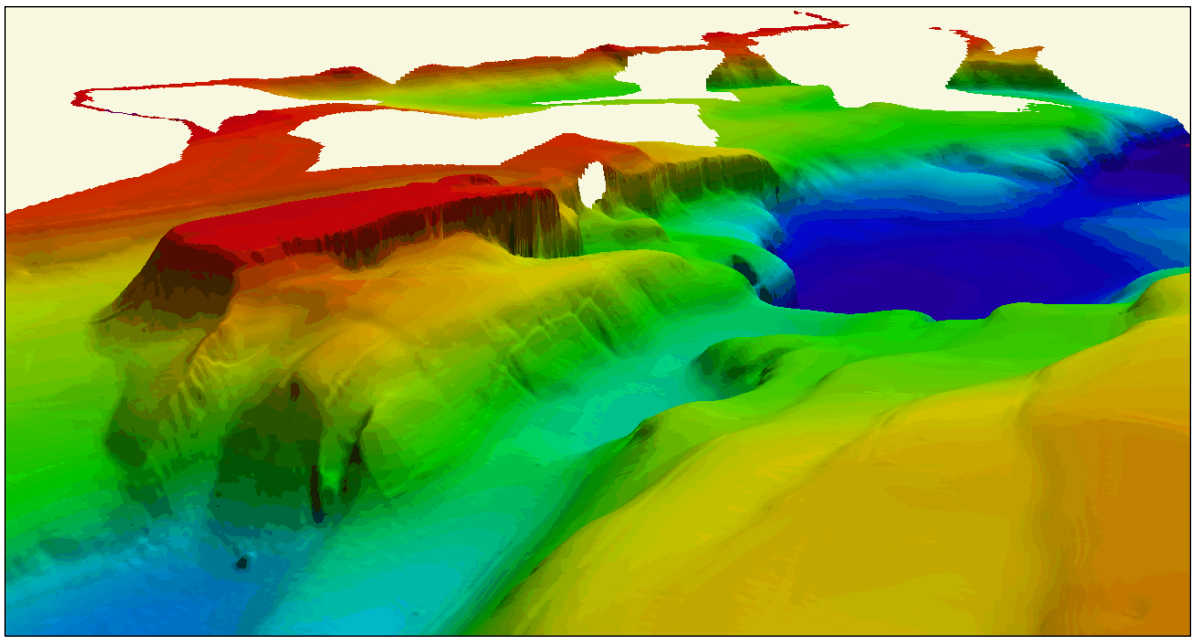

Figure 23. The large block east of Svínanes to the left. Looking towards north, 2x vertical exaggeration with horizontal resolution of 2 meters. White represents areas with no data. Image is illuminated at 45° azimuth and 60° elevation.

5.2.4 Talus and debris flow deposits

Talus and debris flow deposits are classified together on the geologic map (Figure 21) but the debris flow deposits show gentler slopes than the taluses. Overall the deposits display medium backscatter intensity. Most of the talus deposits are located at or below faults in the Hestvík bay region and at the margin of Thingvallahraun east and south of Heiðarbær.

5.2.5 Fine sediment

On the geologic map in Figure 21 fine sediment is categorized into sand/tephra and sediment basin. The main difference is the grain size, where the basins are filled with mostly silt, clay and small amounts of sand, but other areas are covered with sand, tephra and possibly small amounts of fine gravel. The sediment basins are flat areas with relatively low and uniform backscatter intensity (Figure 24). The areas covered with sand and tephra display a wider range of backscatter intensity and the topography is also less homogenous. The beach in southwestern part of Hestvík bay is mostly covered with sand and the lake bottom gently slopes away from the beach. Most of the relatively flat bottom in Hestvík bay is therefore considered as sand or tephra.

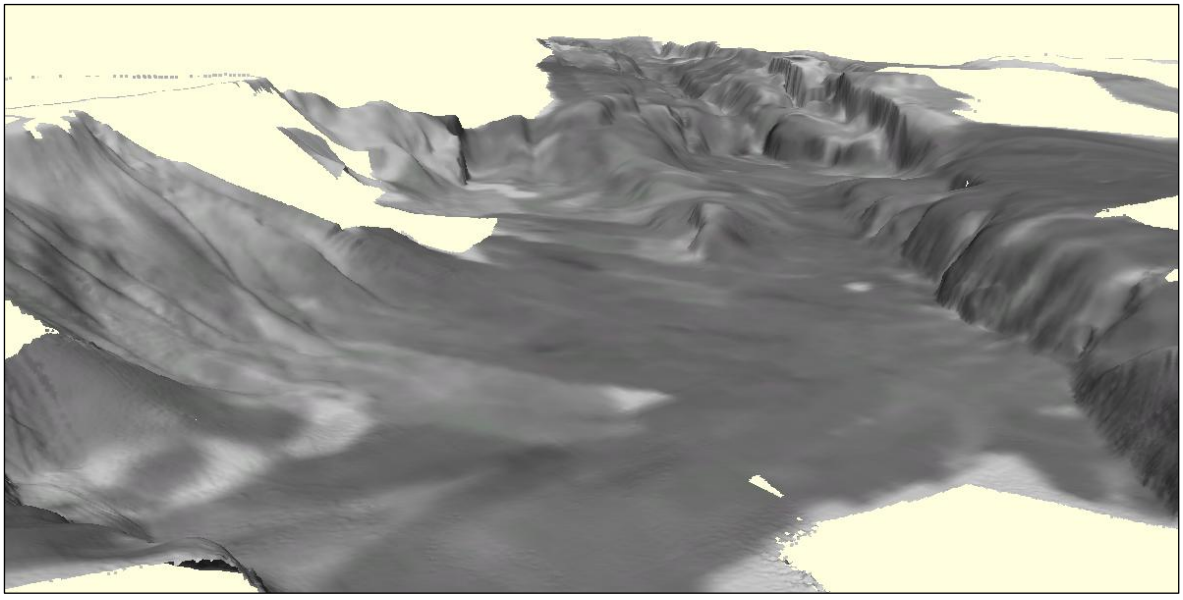

Figure 24. Sandeyjardúp basin in the lower central part of the image, Sandey island to the left and Hestvík bay in the upper central part of the image. Note more uniform backscatter in Sandeyjardjúp basin than in the flanks of Sandey island. Backscatter intensity draped on top of bathymetry with 2.5x vertical exaggeration. Looking towards SSW.

5.3 Kleifarvatn

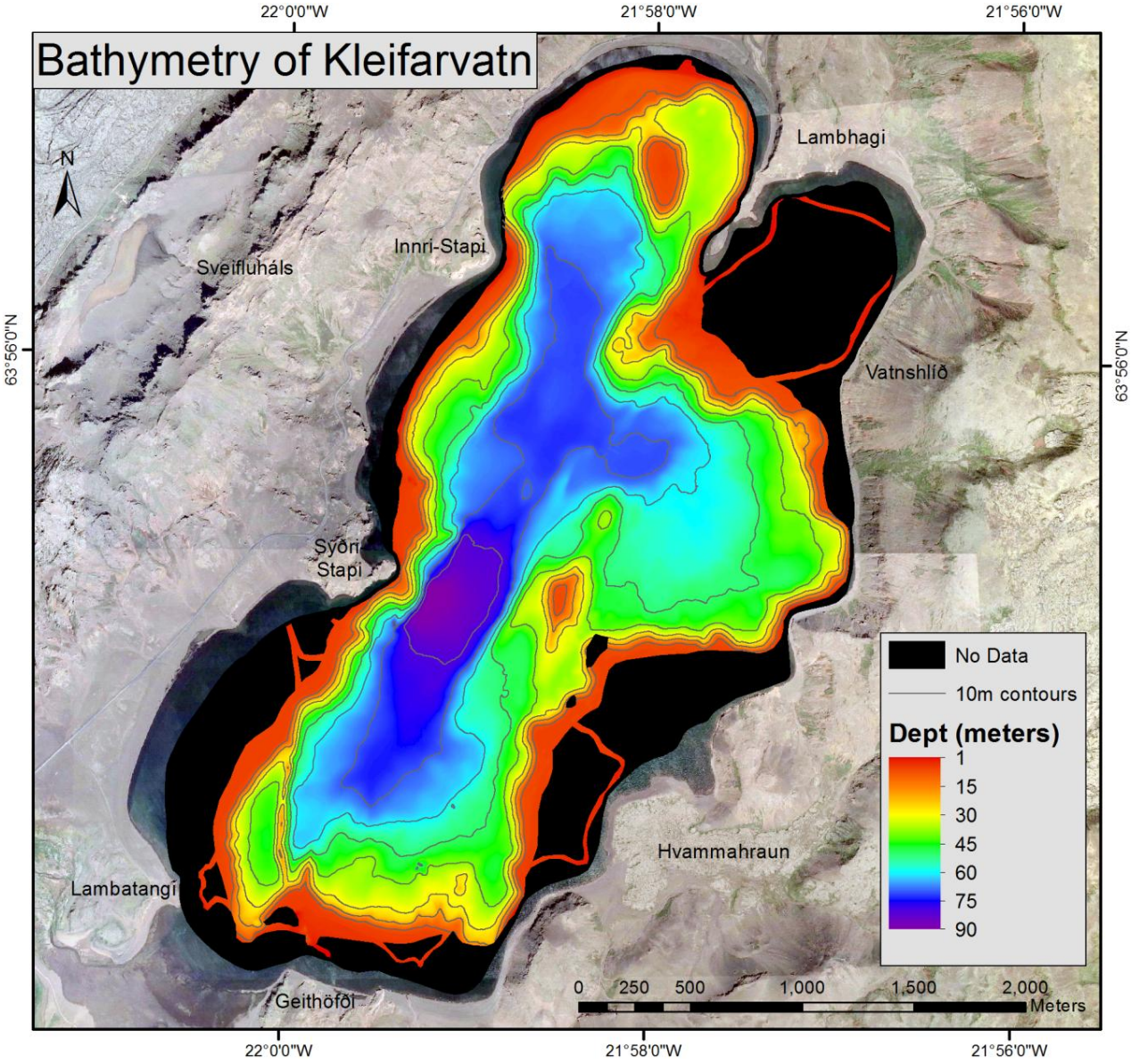

Figure 25. Bathymetric map of Kleifarvatn with 10 meter contours. Black represents areas with no data acquired. Horizontal resolution of bathymetry is 2 meters. Surrounding is an aerial photograph from Loftmyndir ehf.

Kleifarvatn has not been a great focus of research in the past decades, although a bathymetric survey done by Rist (1975) revealed the major features of the lake bottom (Figure 12). The bathymetric survey conducted in June 2012 revealed in great detail the morphology of the lake floor of Kleifarvatn. Figure 25 displays a bathymetric map of the lake floor with 10 m depth contours and Figure 26 displays a map of the backscatter

intensity from the lake floor. These two maps were used as guidelines for a geologic map of the lake floor (Figure 27).

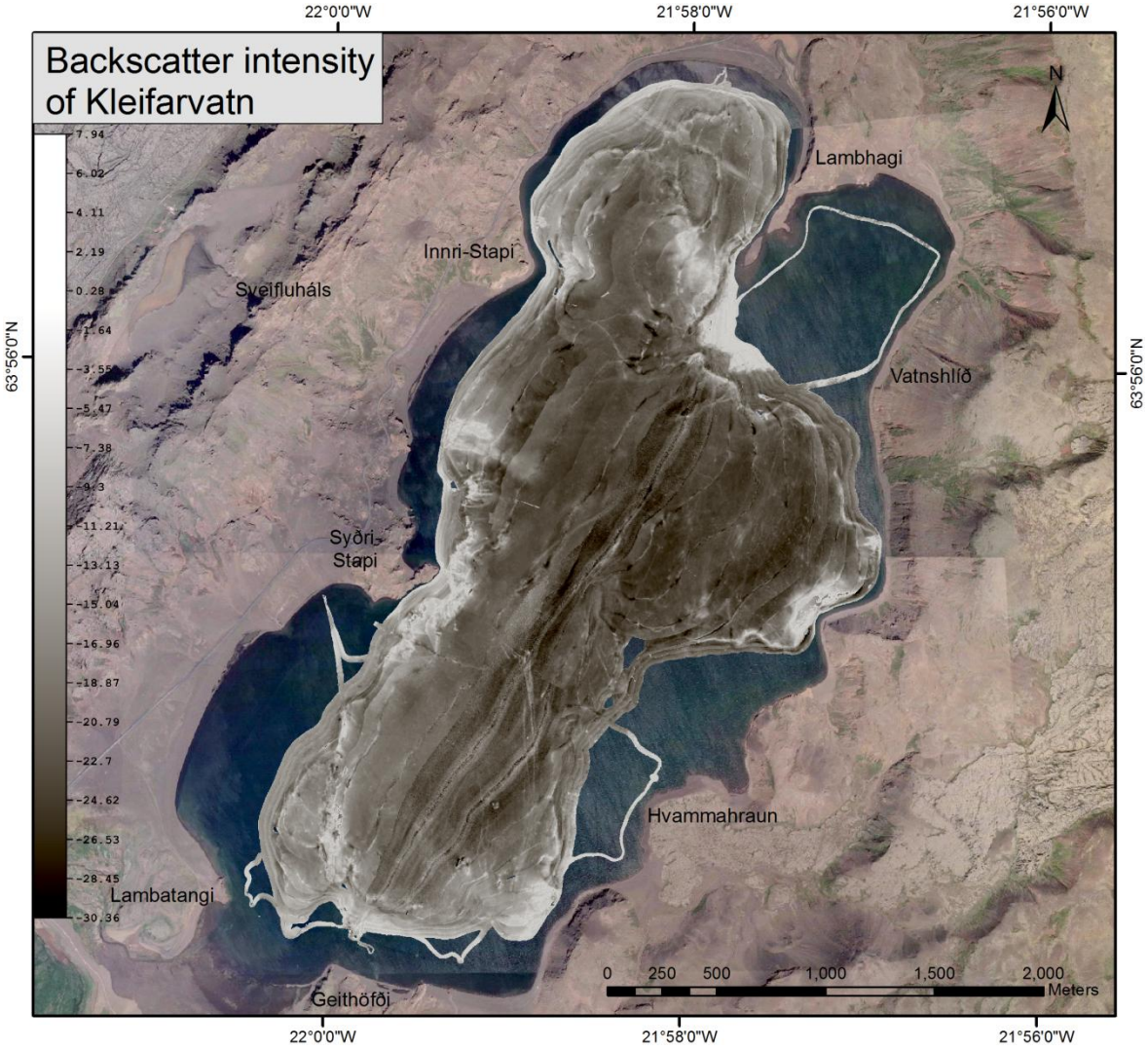

Figure 26. Backscatter intensity map of Kleifarvatn. Units of backscatter intensity are described in decibels. Horizontal resolution of backscatter data is 2 meters. Surrounding is an aerial photograph from Loftmyndir ehf.

5.3.1 Volcanic features

A few volcanic features are found on the lake floor of Kleifarvatn, including two lavas that have run into the lake and four volcanic ridges/hills.

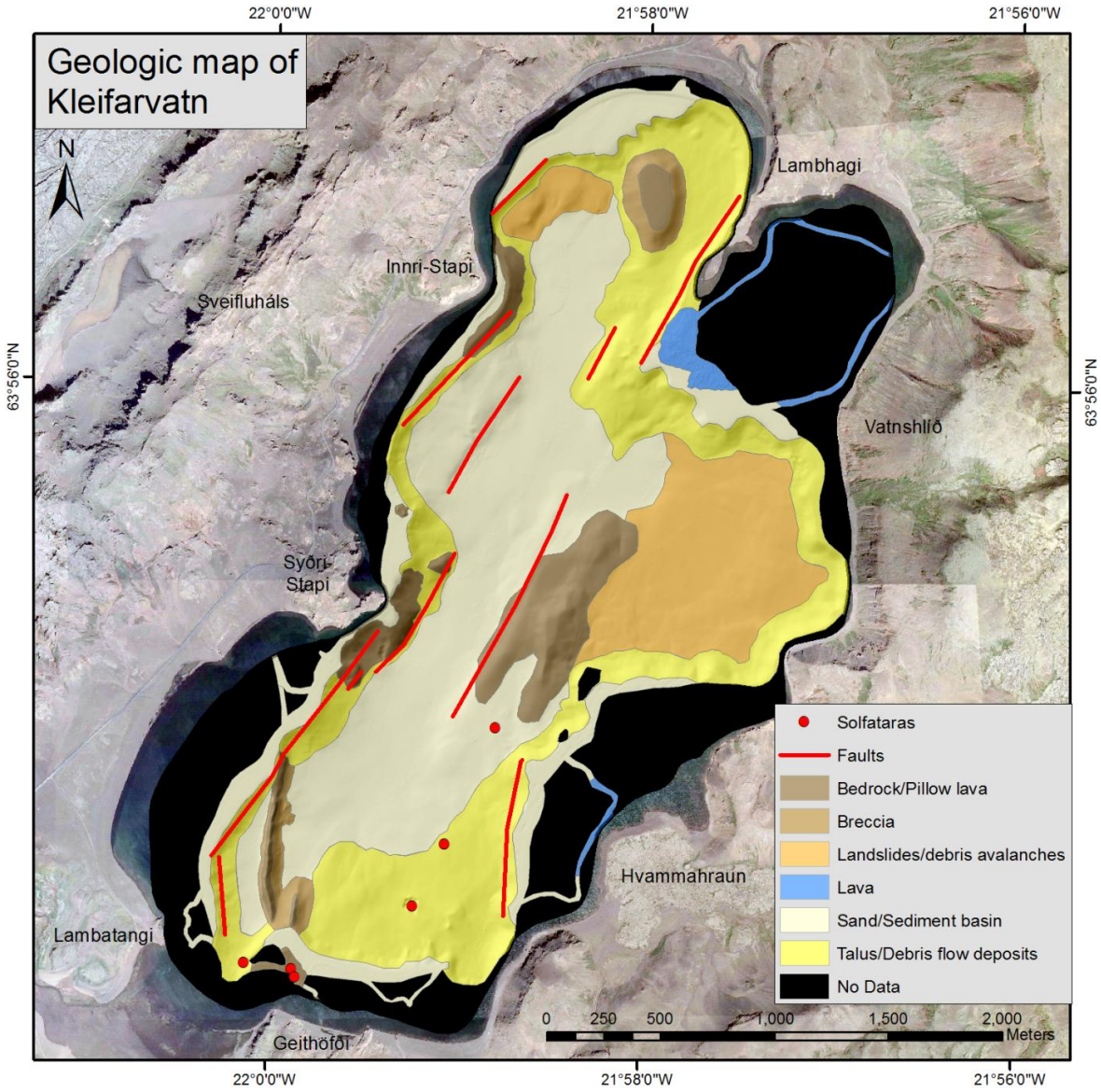

Figure 27. Geologic map of Kleifarvatn draped on a shaded relief map illuminated at 315° azimuth and 45° elevation. Horizontal resolution is 2 meters. Surrounding is an aerial photograph from Loftmyndir ehf.

Lavas

Two lavas have run into Kleifarvatn, both on the eastern side (J. Jónsson, 1978). One is Hvammahraun near the southeast corner of the lake and the other one is in the northern part of Vatnshlíð and ran into an embayment South of Lambhagi (Figure 27). Both lavas show rough topography, medium to high backscatter (-7 to -5 dB) and are found in shallow water.

Bedrock, pillow lavas and breccias

Volcanic features in Kleifarvatn, other than lavas that have run into the lake, are labelled as bedrock/pillow lavas and breccias on the geologic map. Bedrock outcrops are found on the flanks of Syðri-Stapi, facing east. These outcrops display very steep, almost vertical topography, and medium to high backscatter (-11 to -5 dB). Similar outcrops are present on the subaqueous flanks of Innri-Stapi facing east and northeast. Four other bedrock/pillow lavas are labelled on the map, one narrow 700 m long and 20-25 m high ridge elongated N-S located northeast of Lambatangi (Figure 28), one small ridge/dyke north of Geithöfði, one 350 m wide, 950 m long and up to 70 m high ridge elongated NE-SW near the centre of the lake, east of Syðri-Stapi, and one flat-top 50 m high hill in the embayment west of Lambhagi. These bedrock outcrops are all connected to breccias of the same origin except for the largest one near the centre of the lake. The breccias represent rougher topography than the bedrock/pillow lavas and in some cases higher backscatter (~-10 dB).

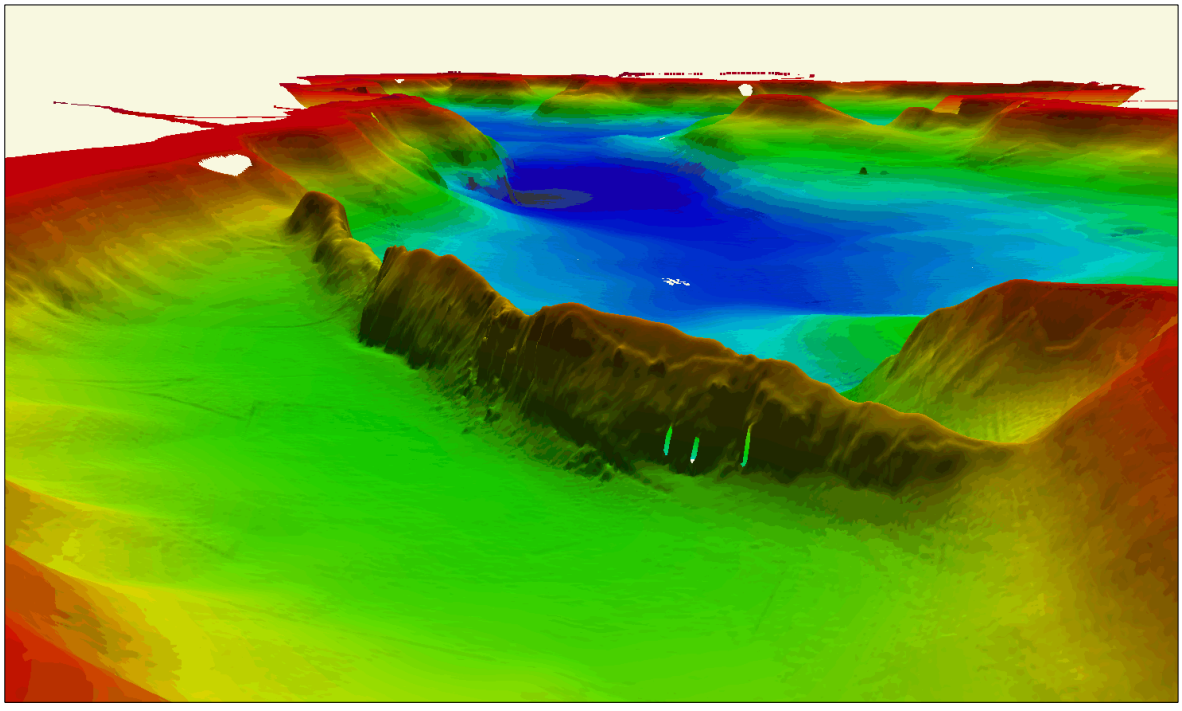

Figure 28. Volcanic ridge elongated N-S located northeast of Lambatangi. 1 m Horizontal resolution and 2x vertical exaggeration. Looking towards northeast. Topography is shaded with illumination at 45° azimuth and 45° elevation.

5.3.2 Thermal features

Solfataras are present at several locations in the southern part of Kleifarvatn. Three solfataras were observed just north of Geithöfði, one of which is the most powerful. When

surveying over the most powerful solfatara, air bubbles rising to the lake surface were noticed. It is worth noticing that the recorded depth down to the base of the solfatara was 10.5 m. Three other solfataras were noticed on a straight line extending NNE-SSW in the southeaster part of the lake (Figure 27). All solfataras in the lake are associated with holes on the lake floor, some of them up to 7 m deep, but only one of them showed evidence of geothermal activity on the surface.

5.3.3 Faults

Several faults were discovered on the lake floor of Kleifarvatn, most of them striking NNE-SSW (Figure 27), the same direction as most of the surrounding topography and the regional faulting. Faults in the central and northern part of Kleifarvatn are aligned NNE-SSW but two faults in the southern part of the lake are aligned almost N-S. If an imaginary line is drawn striking NNE-SSW through the deepest part of the lake, all faults on the eastern side are facing west and vice versa. Some faults have a throw of up to 35 meters (Figure 29).

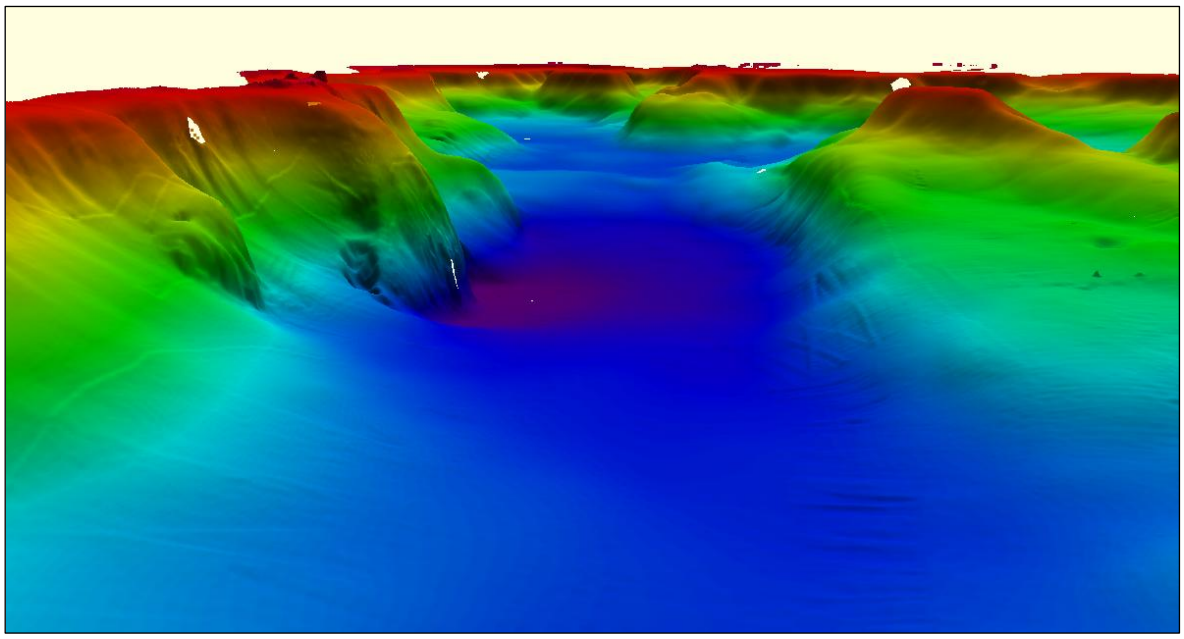

Figure 29. Faults on both sides of the sediment basin. Syðri-Stapi to the left and a volcanic ridge to the right. Looking towards NNE, 1 m horizontal resolution and 2.5x vertical exaggeration. Topography is shaded with illumination at 45° azimuth and 45° elevation.

5.3.4 Talus and debris flow deposits

Talus and debris flow deposits are present all around the lake floor of Kleifarvatn. They are visible below a certain platform which is at 7-8 m depth around almost the entire lake. They display medium backscatter intensities and are built up in steep slopes which gradually fade out, either into sediment basins or other flat areas. Debris flow deposits move further away from their origins than taluses, like the ones extending into the southern part of Kleifarvatn over some of the solfataras.

5.3.5 Landslides

Landslides are present in two areas on the lake floor in Kleifarvatn (Figure 27). One is originated in the southern part of Vatnshlíð and moved as far as 1 km from its source. It is by far the largest landslide mapped in Kleifarvatn. The other one, quite small, is located just northeast of Innri-Stapi in the northern part of the lake, possibly originated in the slopes of Sveifluháls.

5.3.6 Sand and sediment basin

Fine sediments located in shallow areas in embayments with sandy beaches and in basins on the lake floor were classified together on the geologic map of Kleifarvatn (Figure 27). The sand in shallow areas reflects lower medium backscatter (~-14 dB) and has very smooth topography although small ripples were noticed in some areas. The fine sediment in the basins displays low backscatter (~-20 dB) and has very smooth topography. No ripples were noticed in the sediment basins. The southwest corner of the large sediment basin is cut off by a 20-25 m high volcanic ridge (Figure 28).

6 Discussion

6.1 Öskjuvatn

Öskjuvatn caldera is one of the youngest calderas on Earth and has been studied extensively for the past 149 years (Carey, Houghton, & Thordarson, 2008a, 2008b; Þ. Einarsson, 1962; Hartley & Thordarson, 2012; Houghton, Thordarson, & Carey, 2010; Johnstrup, 1877; Ó. Jónsson, 1942). Johnstrup and Caroc (1877) described a chasm, elongated NW-SE in the southeast corner of the Askja caldera, which had several craters in its southern end. Hot water ran from these craters and into a pond which was 232 m below the Askja caldera floor. The Askja caldera floor is at 1100 m.a.s.l., the present day water level of Öskjuvatn is at 1053 m.a.s.l. and the depth down to the Great basin is ~205 m. That makes the Great basin 252 m below the Askja caldera floor so it can be concluded that the basin has subsided at least 20 m since 1876. It has also expanded to the south because according to Caroc‘s map it was almost circular and Thorvaldsfjall mountain reached much farther north than it does now. The centre of subsidence on Caroc’s map is further east than the current location of the Great basin indicating shifting of the focus of subsidence towards the west (Figure 30).

According to Houghton, Thordarson and Carey (2010) the 1875 eruption had several phases including a phreatoplinian phase and a Plinian phase. Based on isopachs and isopleths for the phase deposits and the composition of the deposits, they concluded that the vent location for the phreatoplinian phase was near the easternmost side of the present-day lake. On the other hand, the vent location for the Plinian phase was predicted to be to the south and west of the inferred source for the phreatoplinian phase. Based on the bathymetric map in Figure 14 the Eastern cone fits well with the vent position for the phreatoplinian phase. A crater to the southwest of the Eastern cone that fits well with the location predicted by Houghton et al. (2010) is found on the northern flank of Askur volcano. Looking at its morphology it‘s possible that this crater was active during the 1875 eruption and subsequently partly covered by the Askur volcano. This crater is visible on Caroc’s map just south of the growing lake in the foothills of Thorvaldsfjall (Figure 30). Both craters have powerful solfataras associated with them suggesting long-term activity. The craters were probably larger at the time when they were active but landslides, debris flow deposits and subsequent eruptions might have partly covered them.

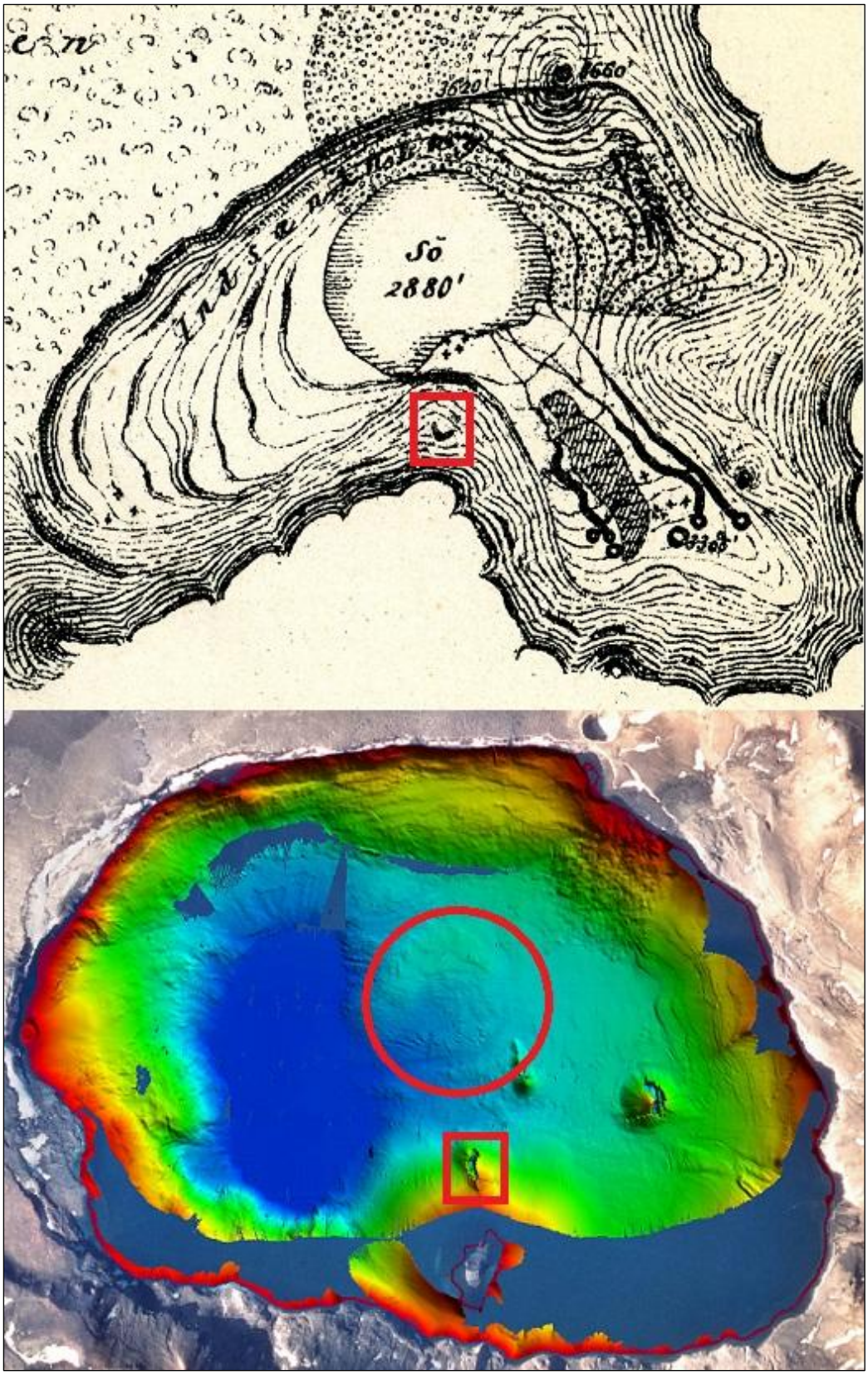

Figure 30. Caroc's map on the top and bathymetric map from the 2012 survey on the bottom. The red boxes indicate the same crater associated with a solfatara. The red circle on the bathymetric map shows the approximate location of the lake in Caroc's map. The explosion crater of Víti is located in the upper parts of both images.

Comparison of the contour map compiled by Rist (1975) (Figure 9) and the bathymetric map in Figure 14, reveal several differences. At the eastern boundary of the Eastern cone, a bend in the 140 m contour is present on the bathymetric map. Thus, the Eastern cone must have formed prior to the survey in 1963. The Western cone on the other hand is not visible on the contour map from Rist. The Great basin seems to have grown to the northeast, indicating ongoing subsidence in the caldera (Zeeuw-van Dalfsen et al., 2013). Another feature that is not visible on the contour map is the crater associated with a solfatara on the northern flank of Askur. As mentioned earlier, this crater is visible on Caroc's map.

Numerous faults were observed on the lake floor and almost all of them facing the centre of the lake. Normal faulting is the dominant type which, along with ring-type faults, are typical for caldera collapses (Gudmundsson, 1998). Step-like faulting in the eastern part of the lake is shown in Figure 31. The northern and northeastern parts of the lake show faulting of larger blocks with very small amount of sediment and other foreign material. Faults near the northwestern rim of Öskjuvatn are responsible for the enlargement of the Öskjuvatn caldera towards northwest. This continuous enlargement of the caldera towards

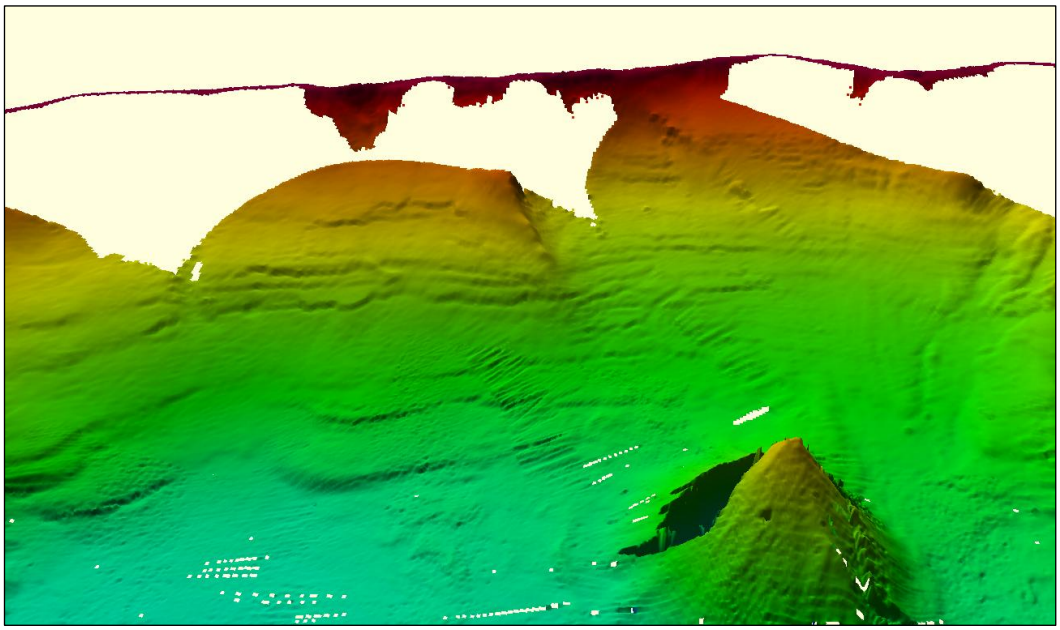

Figure 31. Faults observed in the eastern part of the lake floor of Öskjuvatn. The Eastern cone is in the lower left corner of the image. The image is shaded at 45° azimuth and 45° elevation with 2x vertical exaggeration

northwest provides more fresh outcrops in that area than in the eastern part, where the topography is much smoother. These outcrops are mainly composed of rocks from Askja caldera and welded deposits from the 1875 eruption (Carey et al., 2008a).

Two elongated structures in the southeastern corner of the research area probably represent lava from the oldest craters in the Öskjuvatn caldera. The craters are most likely located in the unsurveyed area in the southeastern part of the lake. The visible parts of the lavas are around 200 m long, similar in width and up to 5 meters thick. They display higher backscatter than the surroundings (Figure 32).

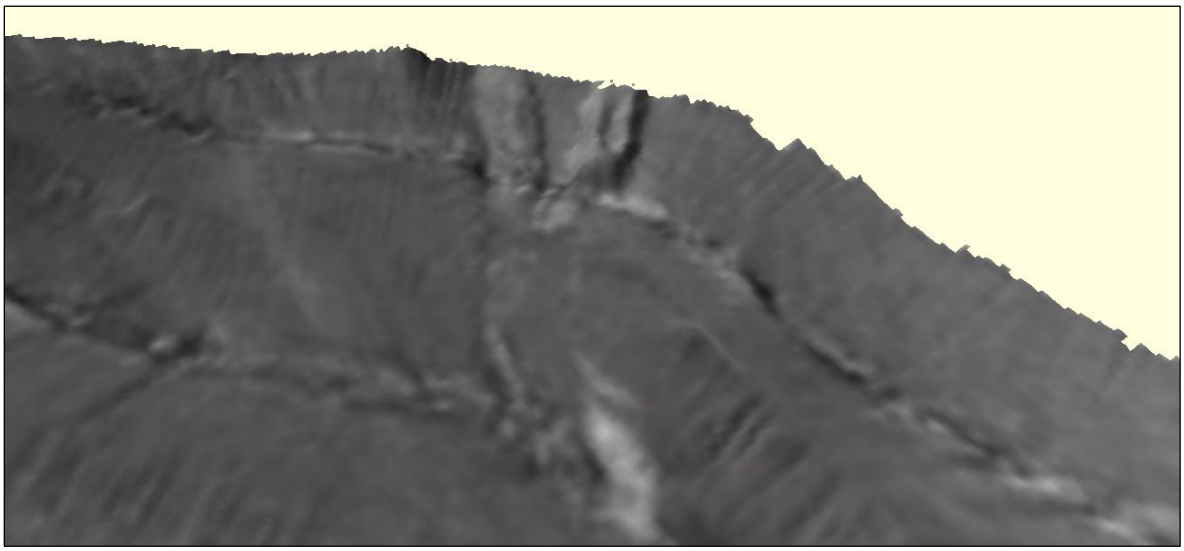

Figure 32. Lavas from the oldest craters in the Öskjuvatn caldera (central top). Image from the southeastern corner of the survey area, looking southeast. Backscatter data draped on 3D bathymetry with 2x vertical exaggeration.

A small explosion crater, around 130 m in diameter, was discovered at just 6 m depth near the western margin of the Öskjuvatn caldera. Because of its nature, i.e. multiple rims, its eruption must have occurred in a few phases. Tephra from this crater was laid ontop of previously existing topography down to the Great basin. The tephra overlies collapsed parts of the Ólafsgígar craters to the north and parts of the subaqueous parts of the Mývetningahraun lava to the south (Figure 33). Therefore it is impossible to accurately measure the subaqueous coverage of the Mývetningahraun lava. Because the tephra overlies both Mývetningahraun lava and collapsed parts of Ólafsgígar it is younger than 1922. According to image (e) in Figure 34 the western coastline formed a peninsula east into the lake which is not noted in previous or subsequent descriptions of the caldera (Ó. Jónsson, 1942). Therefore it is likely that this peninsula is an overestimate of the subaerial

coverage of Mývetningahraun lava where it reaches the lake. The triple explosion crater is considered to have formed in subaqueous conditions due to two main reasons, no subaerial tephra has been discovered and linked with it, and great amount of tephra flowed underwater and covered at least 0.6 km^2.

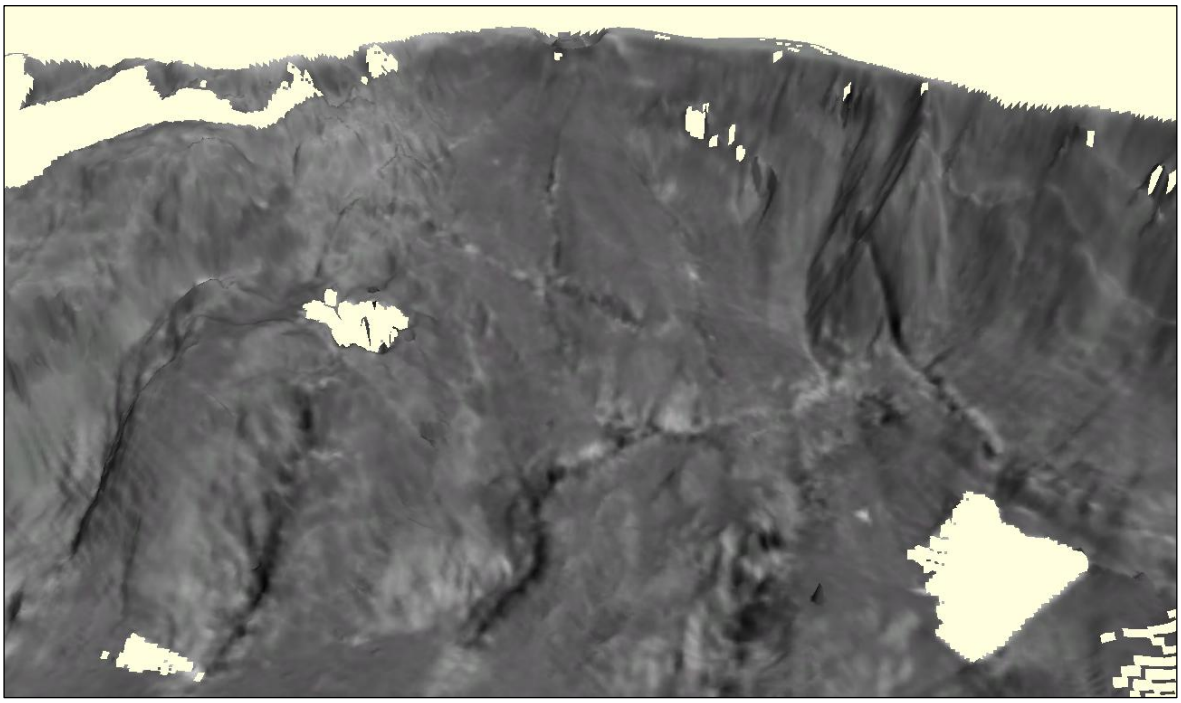

Figure 33. Explosion crater is located in the top central part and tephra from where it was dispersed downwards. Mývetningahraun lava enters the lake in the upper left corner and flows downwards. Ólafsgígarhraun lava enters the lake in the upper right. Backscatter data draped on 3D bathymetry with 2x vertical exaggeration.

Eruption volumes calculated in Table 5 show that estimates by Hartley and Thordarson (2012) of erupted volumes of lavas around Öskjuvatn were not very accurate. The new estimates do not add any substantial values to the total volume of erupted material but it increases the volume about 0.005 km^3. This change in total volume of erupted material subsequent to the 1875 eruption is only about 1% and drops to just over 0.5% if Nýjahraun lava is included (Hartley & Thordarson, 2012). The reason for this inaccuracy is lack of knowledge about their subaqueous coverage.

Prior to the bathymetric survey of 2012 the deepest part of Öskjuvatn was considered to be 217 m (Rist, 1975). With much better accuracy and greater coverage of the lake floor it was established that Öskjuvatn is at least 244.5 m deep, recorded in a solfatara in the southeast corner of the Great basin. This value should be viewed with caution because of rising air bubbles in the solfataras. They alter the paths of the acoustic waves and therefore

reduce the accuracy of depth measurements. The same story is for the other solfataras, the "holes" are somewhat artificial because of air bubbles in the water column. The greatest recorded depth outside any solfataras is 206 m in the Great basin. The whole basin is at 204-206 m depth and is very flat.

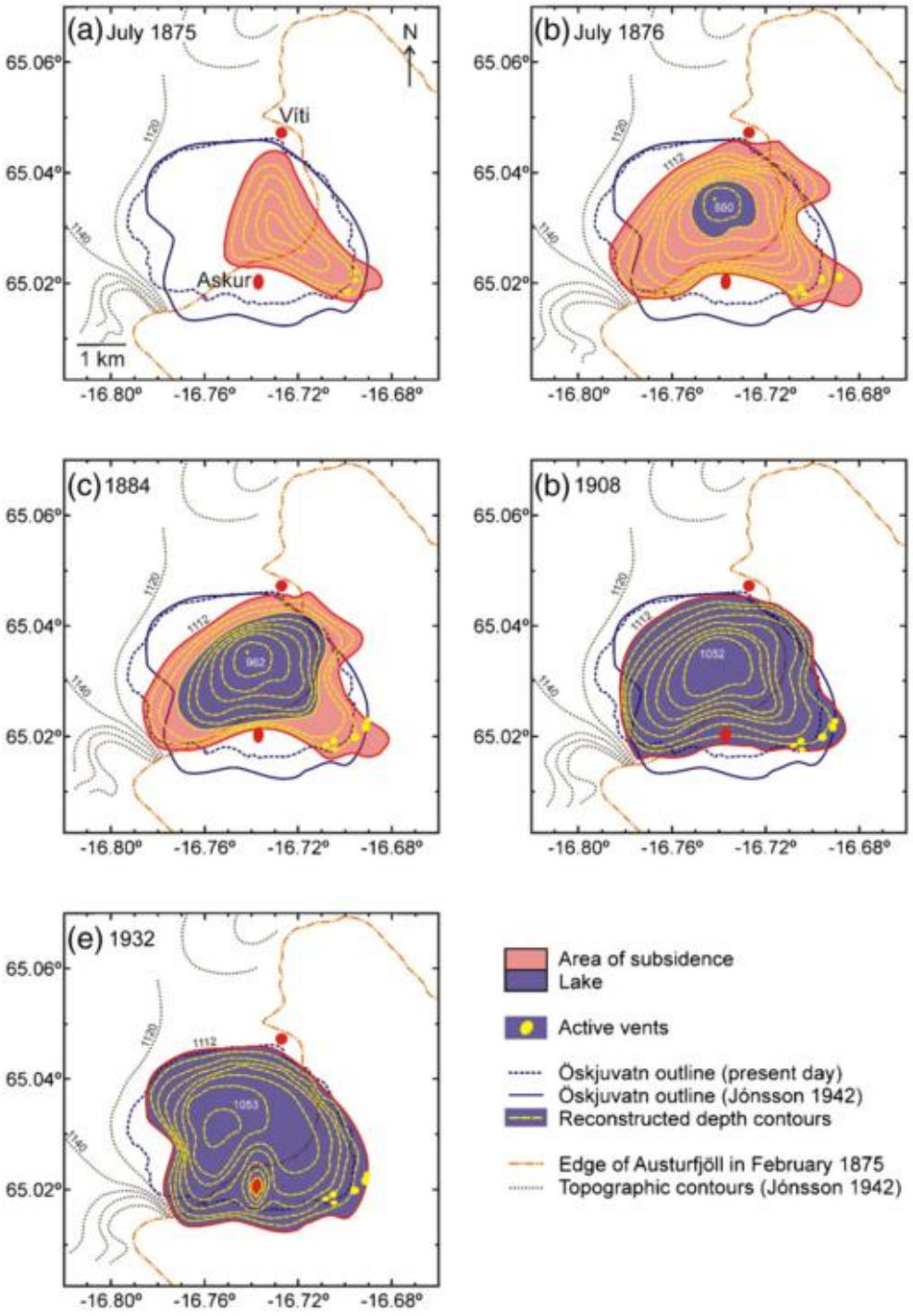

Figure 34. Development of Öskjuvatn caldera from Hartley & Thordarson (2012). Note the differnece between the present-day outline of the lake and outline drawn by Jónsson (1942).

6.2 Thingvallavatn

The large fault which marks the western boundary of Sandeyjardjúp basin (Figure 21 and Figure 23) was mapped by Thors (1992). It branches just north of Sandeyjardjúp basin, the western branch going very close to the shore in the northwestern corner of the lake. The continuation of this fault towards the northern shore of Thingvallavatn, and the location of the Almannagjá fault, could mean that the Almannagjá fault reaches almost through the entire lake. Hrafnagjá (Figure 11) is another prominent fault located on the eastern side of the Thingvellir graben which might be visible in the bathymetric data. It extends several kilometres along the Thingvellir graben and might well be the easternmost fault in Figure 21. Numerous other faults are visible across the lake floor of Thingvallavatn (Figure 11 and Figure 21), eastward dipping faults on the western side and westward dipping on the eastern side. The throw of these faults varies greatly between individual faults, from 0.5 m up to 45 m. Thors (1992) mapped the faults of Thingvallvatn based on their throw (Figure 11). According to his findings the majority of large faults in the current survey area is facing west. This harmonises very well with the multibeam bathymetric data. The faults in Thingvallavatn represent typical graben structure with normal faults on each side facing each other. The faults in Hestvík are a very good example of this arrangement.

Tephra dispersal from the Sandey eruption was mostly to the east of the island and could therefore be the major component of the bottom sediments east of Sandey (Sæmundsson, 1965, 1992; Thors, 1992). Backscatter intensity of the lake floor in the area northeast of Sandey shows a sudden increase in reflection towards the eastern shore, supporting the proposal of the tephra thinning to the east. Backscatter intensity varies somewhat in the area west of Sandeyjardjúp basin and south of the Thingvallahraun margin. A shallow gorge with high backscatter intensity is visible on top of Thingvallahraun lava just east of Heiðarbær. Sæmundsson (1965) proposed, based on alluvial deposits on land, that the Öxará river entered Thingvallavatn much further south than it does today. After the emplacement of Thingvallahraun lava it could have flowed on or near its western margin and entered the lake on its southern margin. Based on this proposal, the gorge near the southwestern margin of Thingvallahraun might be the temporary riverbed of Öxará.

The large block east of Svínanes (Figure 23) is not visible on the contour map by Rist (1975) but is mentioned by Thors (1992) as a possible source of volcanism. He also mentioned other small underwater peaks near Svínanes (marked “bedrock” in Figure 21)

which could be of the same origin. The large block and the bedrock/lavas northeast of Svínanes display medium to high backscatter intensity (Figure 35) indicating very thin sediment coverage. That might be results of wave erosion due to shallow conditions and young age. These features must have formed before or in the early stages of faulting in the area because of the nearly vertical fault on the eastern side of the large block. Faults were also discovered on the western side of the large block.

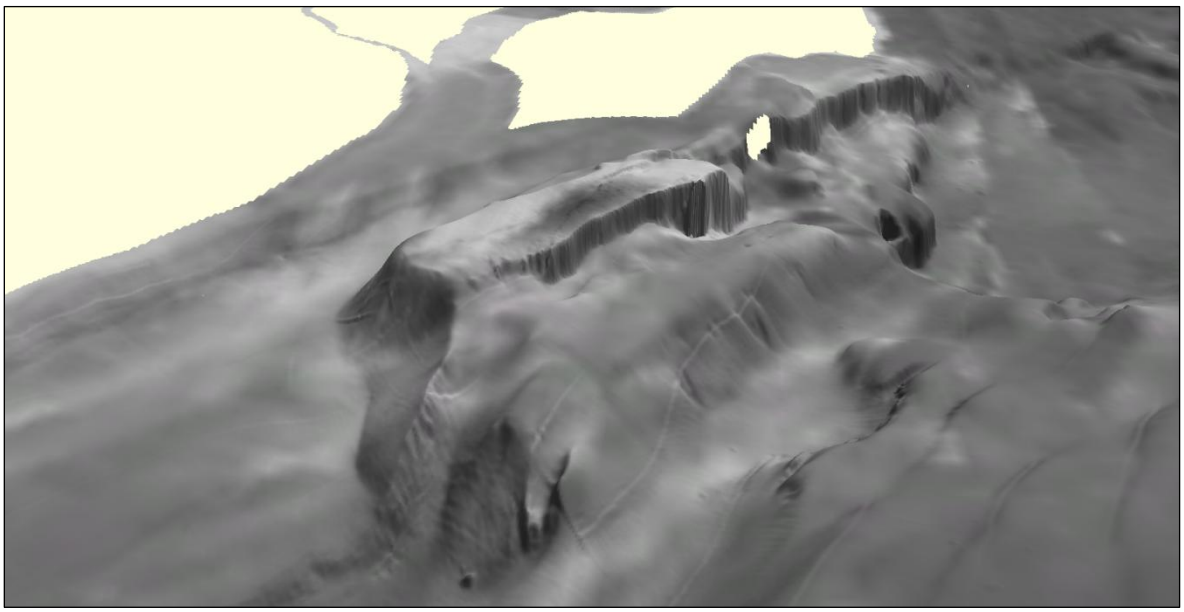

Figure 35. The large block (in the centre) east of Svínanes which is located in the white area to the left. Note the high backscatter intensity of most of the block. Backscatter data draped on 3D bathymetry with 2x vertical exaggeration.

Nesjavellir geothermal field is located just a few kilometres south-west of Thingvallavatn, in the northern foothills of the mountain Hengill. Based on its location and number of faults already mapped on the lake floor of Thingvallavatn the expectancy for geothermal activity in the lake was quite high. However, no solfataras were observed in the survey area which was very surprising. On the other hand, since the Nesjavellir geothermal field has been utilized for several decades, the pressure in the surrounding geothermal systems might have dropped leading to decreased geothermal activity in Thingvallavatn.

6.3 Kleifarvatn

The topography of the volcanic features on the lake floor is very clear thanks to high resolution of the bathymetric data which is up to 0.5 m, even in the deepest areas. The

greatest changes between the contour map by Rist (1975) and the new bathymetric map are the discovery of a volcanic ridge northeast of Lambatangi (Figure 36), improved topography of other volcanic features, locations of solfataras on the lake floor and locations of faults. The maps are compared in Figure 37. Only a small portion of the volcanic ridge northeast of Lambatangi is visible on the contour map. Thus it can be concluded that at least a part of it existed in 1964 when Kleifarvatn was surveyed for the

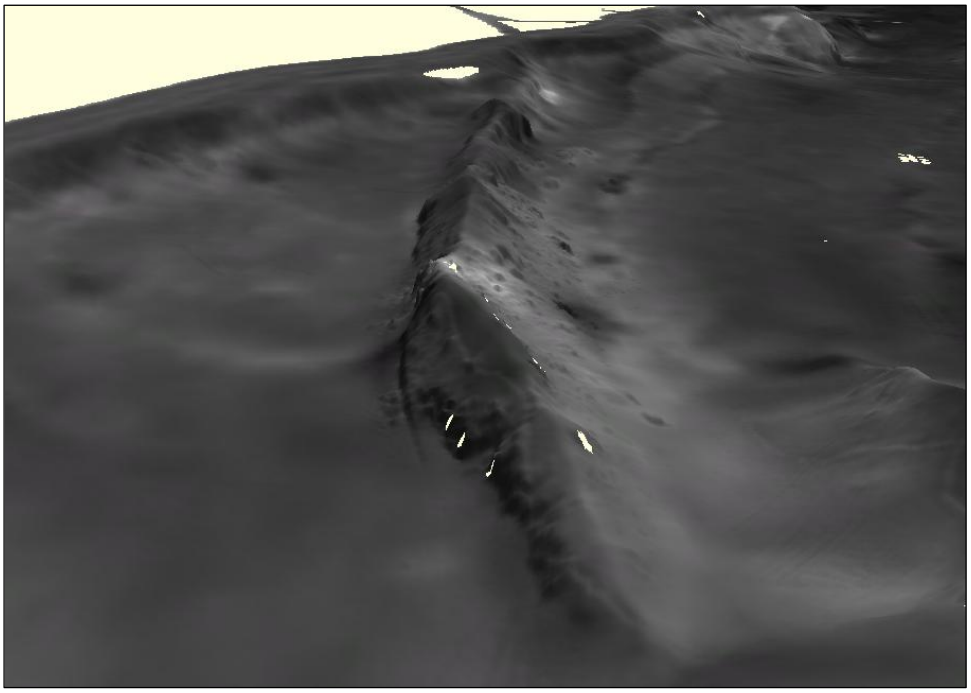

Figure 36. The N-S striking volcanic ridge northeast of Lambatangi. Looking towards north. Backscatter data draped on 3D bathymetry with no vertical exaggeration.

first time. Morales (1992) interpreted the contour map by Rist (1975) and concluded that the volcanic ridges on the lake floor presumably are composed of pillow lava. He also concluded that the volcanic ridge east of Syðri-Stapi probably is a segment of the Lambhagi hyaloclastite/pillow lava ridge. Based on the bathymetric data and backscatter intensity there is no reason to conclude otherwise. The flat-top hill near the northern shore of Kleifarvatn, northeast of Innri-Stapi, is most likely also made up of pillow lava like the other volcanic features. The N-S trending volcanic ridge northeast of Lambatangi and north of Geithöfði is possibly a segment of the Geithöfði ridge. The alignment and location of the volcanic ridge does not agree with the Lambatangi unit as proposed by Morales (1992). The alignment of the ridge is very unique because of regional alignment of faults

and volcanic structures in the area. However, N-S striking faults have been observed in several locations on the Reykjanes Peninsula (Clifton et al., 2003). It is therefore possible that one of this N-S striking faults fed magma to the surface and produced the ridge. Based on its structure, very narrow and sharp edges, it most likely formed either in subaqueous or subglacial conditions. A hole, at least 10 m deep, is located in the southeast corner of Kleifarvatn on the contour map by Rist. However, this hole is not visible on the new bathymetric map.

Numerous faults can be found on the Reykjanes Peninsula and the area around Kleifarvatn is no exception. It cannot be excluded that small fractures could have opened on the lake floor following the 2000 earthquake. No sharp faults can be seen on the lake floor but other faults, most likely older ones, are present in the lake (Figure 27). Most of these faults have a throw of 10-20 m or more which indicates that the same faults were active more than once throughout the formation of the lake (see large faults in Figure 29).

According to the geologic map of the Reykjanes Peninsula made by Jónsson (1978) evidence of geothermal activity were present near the southern shore of Kleifarvatn. Evidence of geothermal activity in the Krýsuvík area is also extensive. Thus during the survey of Kleifarvatn in 2012 the possibility of finding solfataras on the lake floor was very high (Figure 27). Interestingly, three solfataras are located on a straight line trending NNE-SSW, similar to most of the faults in the area. These solfataras could therefore all be located on a single fault. The solfataras just north of Geithöfði are most likely related to the Geithöfði volcanic ridge since they are located almost directly between Geithöfði and the N-S trending volcanic ridge in southwest Kleifarvatn.

The flat shoals extend from the shores and out to 7-8 m depth are composed of sand and other sedimentary particles from the shores (Figure 27). These shoals suggest that at some time in the lake's history the water level was a few meters lower than present. The last time the lake level dropped substantially was following an earthquake. Considering this, it seems likely that this has happened several times in the lake's history. It could even have stayed at that level for some time, allowing formation of a permanent sediment platform.

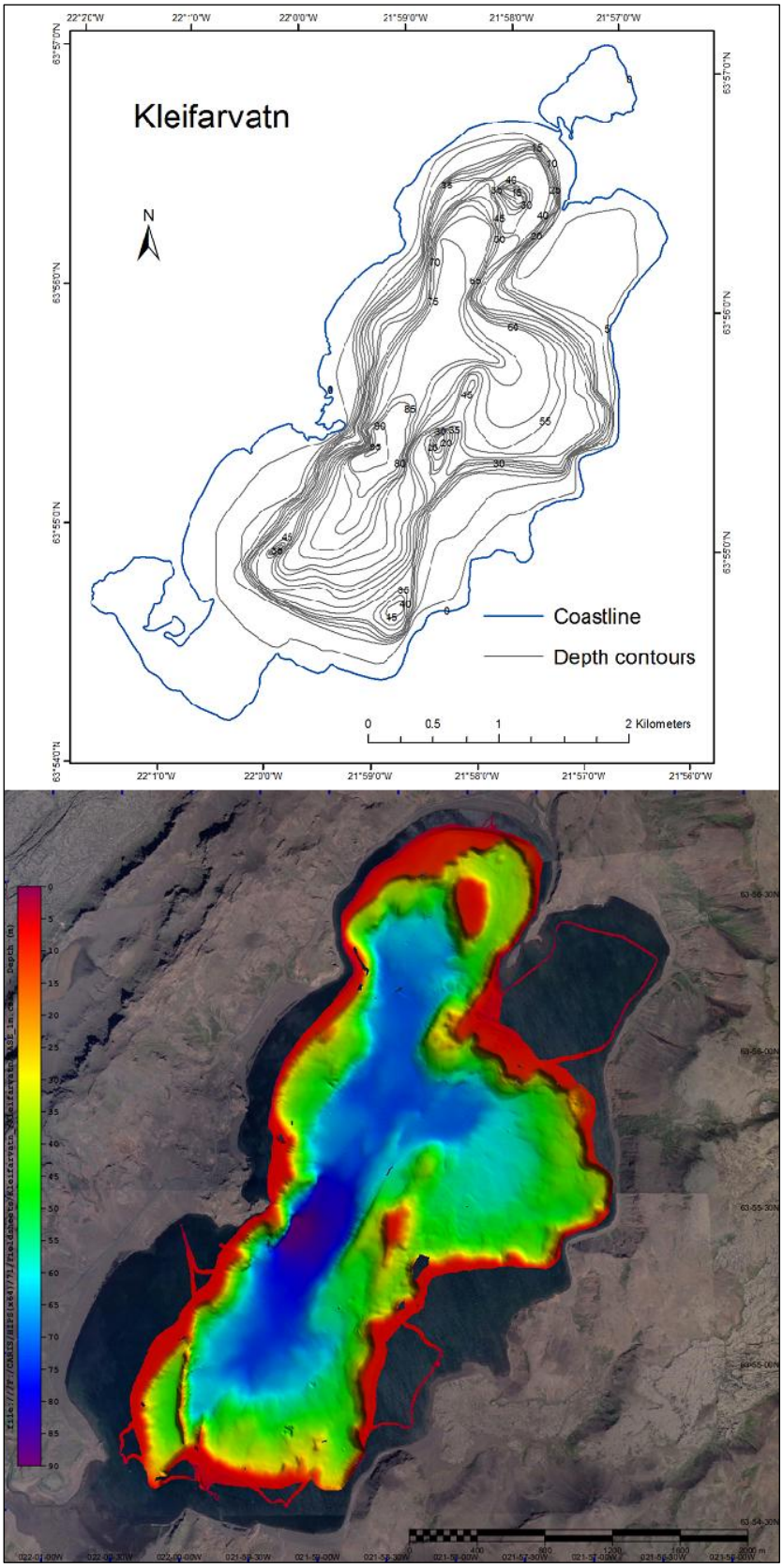

Figure 37. Contour map by Sigurjón Rist on the top and bathymetric map made after the multibeam survey in 2012 on the bottom. Vertical exaggeration is 2x on the bathymetric map.

7 Conclusions

Multibeam studies of Öskjuvatn, Thingvallavatn and Kleifarvatn revealed the topography of the lake floors with high resolution. Previous studies carried out by Sigurjón Rist in the 1950s and 1960s provided contour maps where the highest resolution was in the form of 5 m depth contours, in the case of Öskjuvatn the resolution was 20m depth contours (Rist, 1975). During those times, these maps were a true breakthrough, but technological developments since these maps were created allow for greater resolution. Comparison between the new bathymetric maps and the old contour maps show great improvement in accuracy, both depth and locations of subaqueous features, and general coverage. The comparison can also be used to detect any ongoing processes which alter the topography and morphology of the lake floors. The multibeam studies revealed some unknown features, e.g. scoria cones, an explosion crater, several solfataras and extensive lava flows in Öskjuvatn, N-S trending volcanic ridge in Kleifarvatn, and numerous faults and volcanic features in Thingvallavatn. The area which is of probably the most interest in Öskjuvatn is the southeastern part, east of Askur, which was unfortunately not surveyed due to bad weather conditions. The craters which erupted in January 1875 are most likely located in that area. Öskjuvatn will hopefully be surveyed again in the future in better weather conditions, which should reveal all the features on the lake floor.

A big advantage of these studies is that in a few years they can be repeated. The results from both studies could then be compared to see if there are any ongoing geological processes altering the topography of the lakes. This would be of special interest in lakes which are volcanologically active, like Öskjuvatn. In the case of Öskjuvatn, subsidence has been ongoing for the past 40 years and it would be interesting to repeat the multibeam study there in a few years to see if the ongoing subsidence also applies to the lake floor.

Multibeam studies like this one require great knowledge of the instruments used for the surveys and also alot of patience, especially in shallow lakes. The weather conditions are important, not only for the accuracy of the measurements but also for the wellness of the survey party. Therefore it is optimal to run multibeam surveys in the summer when wind speed is low and temperatures are high, not during wintertime with very low temperatures and very sudden weather changes.

References

Aðalsteinsson, H., Jónasson, P. M., & Rist, S. (1992). Physical characteristics of Thingvallavatn, Iceland. *Oikos*, *64*, 121–135.

Aðalsteinsson, H., Rist, S., Hermannsson, S., & Pálsson, S. (1989). *Stöðuvötn á Íslandi: Skrá um vötn stærri en 0,1 km2*. Reykjavík.

Arnórsson, S., Björnsson, A., Gíslason, G., & Guðmundsson, G. (1975). *Systematic exploration of the Krísuvík high-temperature area, Reykjanes-peninsula, Iceland* (pp. 1–20).

Bacon, C. R., Gardner, J. V, Mayer, L. A., Buktenica, M. W., Dartnell, P., Ramsey, W., … Ramsey, D. W. (2002). Morphology , volcanism , and mass wasting in Crater Lake , Oregon. *Geological Society of America Bulletin*, *114*(6), 657–692.

Bacon, C. R., & Lanphere, M. a. (2006). Eruptive history and geochronology of Mount Mazama and the Crater Lake region, Oregon. *Geological Society of America Bulletin*, *118*(11-12), 1331–1359.

Brennan, C. W. (2009). Basic Acoustic Theory. R2Sonic LLC.

Briem, V. (1877). Frjettir frá Íslandi 1876 - Menntun. *Frjettir Frá Íslandi*, *5*(1), 46–48.

Bull, J. M., Minshull, T. a., Mitchell, N. C., Thors, K., Dix, J. K., & Best, a. I. (2003). Fault and magmatic interaction within Iceland's western rift over the last 9 kyr. *Geophysical Journal International*, *154*(1), F1–F8.

Carey, R. J., Houghton, B. F., & Thordarson, T. (2008a). Contrasting styles of welding observed in the proximal Askja 1875 eruption deposits I: Local welding. *Journal of Volcanology and Geothermal Research*, *171*(1-2), 1–19.

Carey, R. J., Houghton, B. F., & Thordarson, T. (2008b). Contrasting styles of welding observed in the proximal Askja 1875 eruption deposits I: Regional welding. *Journal of Volcanology and Geothermal Research*, *171*(1-2), 1–19.

Caris. Caris Hips and Sips 8.1 - User Guide (2013). Canada.

Clifton, A. E., Pagli, C., Jónsdóttir, J. F., Eythorsdóttir, K., & Vogfjörð, K. (2003). Surface effects of triggered fault slip on Reykjanes Peninsula, SW Iceland. *Tectonophysics*, *369*(3-4), 145–154.

Einarsson, P. (2008). Plate boundaries, rifts and transforms in Iceland. *Jökull*, *58*, 35–58.

Einarsson, Þ. (1962). Askja og Oskjugosið 1961. *Náttúrufræðingurinn*, *32*(1), 1–18.

Fonseca, L., & Calder, B. (2005). Geocoder : An Efficient Backscatter Map Constructor. In *US Hydrographic Conference* (pp. 1–9). New Hampshire: University of New Hampshire.

Fonseca, L., & Calder, B. (2007). Clustering Acoustic Backscatter in the Angular Response Space. In *US Hydrographic Conference* (pp. 1–12). New Hampshire.

Gudmundsson, A. (1998). Formation and development of normal-fault calderas and the initiation of large explosive eruptions. *Bulletin of Volcanology*, *60*(3), 160–170.

Gunnarsson, S. (1875). Vikuröskufall í Múlasýslum á 2. í páskum, 29. marz 1875 (Pumice fall in the Múlasýslur, 2nd day of Easter, 29 March, 1875). Letter written on 24 April 1875. *Norðanfari*, *14*(27-28), 58–59.

Hartley, M. E., & Thordarson, T. (2012). Formation of Öskjuvatn caldera at Askja, North Iceland: Mechanism of caldera collapse and implications for the lateral flow hypothesis. *Journal of Volcanology and Geothermal Research*, *227-228*, 85–101.

Hjartardóttir, Á. R. (2008). *The fissure swarm of the Askja central volcano*. University of Iceland.

Houghton, B. F., Thordarson, T., & Carey, R. J. (2010). Tephra dispersal and eruption dynamics of wet and dry phases of the 1875 eruption of Askja Volcano, Iceland. *Bulletin of Volcanology*, *72*(3), 259–278.

Iceland, N. L. S. of. (2011). IS 50V database (version 3.1).

Instruments, L.-3 C. S. (2000). Multibeam Sonar Theory of Operation. Washington.

Ísafold. (1875, March). Eldgosið. *Ísafold*, 35–37.

Johnstrup, F. (1877). Om de i Aaret 1875 forefaldne vulkanske Udbrud paa Island tilligemed nogle indledende geografiske Bemærkninger. *Geografisk Tidsskrift*, *1*, 50–66.

Jónsson, J. (1978). *Geological map of the Reykjanes peninsula*. Reykjavík.

Jónsson, Ó. (1942). Öskjuvatn. *Náttúrufræðingurinn*, *12*(2), 56–72.

Khubaeva, O. (2007). *Geothermal mapping in the Krýsuvík geothermal system* (pp. 145–156). Reykjavik.

Kjartansson, G. (1964). Aldur nokkurra hrauna á Suðurlandi. *Náttúrufræðingurinn*, *34*, 101–113.

Kongsberg. (2006). EM 3002 Multibeam echo sounder: The new generation high performance shallow water multibeam. Horten: Kongsberg.

Lock, G. (1881). Askja , the Largest Volcano of Iceland; With a Short Description of the Ódádahraun of Iceland. *Royal Geographical Society*, *3*(8), 471–483.

Mawejje, P. (2007). *Geothermal exploration and geological mapping at Seltún in Krýsuvík geothermal field, Reykjanes peninsula, SW-Iceland* (pp. 257–276). Reykjavík.

Medialdea, T., Somoza, L., León, R., Farrán, M., Ercilla, G., Maestro, A., … Alonso, B. (2008). Multibeam backscatter as a tool for sea-floor characterization and identification of oil spills in the Galicia Bank. *Marine Geology*, *249*(1-2), 93–107.

Morales, J. R. V. (1992). *Geology and geothermal considerations of Krisuvik valley, Reykjanes Peninsula, Iceland*. Reykjavík: Orkustofnun.

Morgan, E. D. (1882). Excursion to Askja, August 1881. *Proceedings of the Royal Geographical Society and Monthly Record of Geography*, *4*(3), 140–148.

Moustier, C. D. E., & Matsumoto, H. (1993). Seafloor Acoustic Remote Sensing with Multibeam and Bathymetric Sidescan Sonar Systems. *Marine Geophysical Researches*, *15*(1), 27–42.

Nelson, C. H. (1967). Sediments of Crater Lake , Oregon. *Geological Society of America Bulletin*, *78*(7), 833–848.

Nelson, C. H., Bacon, C. R., Robinson, S. W., Adam, D. P., Bradbury, J. P., Barber, J. H., … Vagenas, G. (1994). The volcanic, sedimentologic, and paleolimnologic history of the Crater Lake caldera floor, Oregon: Evidence for small caldera evolution. *Geological Society of America Bulletin*, *106*, 684–704.

Reck, H. (1910). *Das vulkanische Horstgebirge Dyngjufjöll mit den Einbruchskalderen der Askja und des Knebelsees sowie dem Rudloffkrater in Zentralisland*. Berlin: K. Akademie der Wissenschaften.

Rist, S. (1975). *Stöðuvötn, OS-ROD7519*. Reykjavík.

Russell, W. S. C. (1917). Askja, a Volcano in the Interior of Iceland. *Geographical Review*, *3*(3), 212–221.

Sæmundsson, K. (1965). Úr sögu Þingvallavatns. *Náttúrufræðingurinn*, *35*(3), 103–141.

Sæmundsson, K. (1982). Öskjur á virkum eldfjallasvæðum á Íslandi. In H. Þórarinsdóttir, Ó. H. Óskarsson, S. Steinþórsson, & Þ. Einarsson (Eds.), *Eldur er í norðri*. Reykjavik: Sögufélag Reykjavikur.

Sæmundsson, K. (1992). Geology of the Thingvallavatn area. *Oikos*, *64*, 40–68.

Sæmundsson, K. (1995). *Hengill geological map (bedrock) 1:50.000*. Reykjavík: Orkustofnun, Hitaveita Reykjavíkur and Landmælingar Íslands.

Sæmundsson, K., & Karson, J. A. (2006). *Stratigraphy and Tectonics of the Húsavík – Western Tjörnes Area*. Reykjavik.

Sæmundsson, K., & Sigmundsson, F. (2012). Norðurgosbelti. In J. Sólnes, F. Sigmundsson, & B. Bessason (Eds.), *Náttúruvá á Íslandi: Eldgos og jarðskjálftar* (pp. 315–357). Reykjavik: Háskólaútgáfan.

Sigurðsson, J. (1875, March). Skýrsla um eldgosið í Þingeyjarsýslu. *Norðanfari*, 26.

Sigvaldason, G. (2002). Volcanic and tectonic processes coinciding with glaciation and crustal rebound: an early Holocene rhyolitic eruption in the Dyngjufjöll volcanic centre and the formation of the Askja caldera, north Iceland. *Bulletin of Volcanology*, *64*(3-4), 192–205.

Thoroddsen, T. (1905). *Landskjálftar á Íslandi*. Copenhagen: Prentsmiðja SL Möllers.

Thors, K. (1992). Bedrock, sediments, and faults in Thingvallavatn. *Oikos*, *64*, 69–79.

Watts, W. L. (1876). *Across the Vatna Jökull; or, Scenes in Iceland*. London: Longmans & Co.

Williams, H. (1961). The floor of Crater Lake, Oregon. *American Journal of Science*, *259*, 81–83.

Zeeuw-van Dalfsen, E., Rymer, H., Sturkell, E., Pedersen, R., Hooper, A., Sigmundsson, F., & Ófeigsson, B. (2013). Geodetic data shed light on ongoing caldera subsidence at Askja, Iceland. *Bulletin of Volcanology*, *75*(5), 1–13.